

Institut für Molekular- und Zellbiologie, Hochschule Mannheim  
Direktor: Prof. Dr. rer. nat. Mathias Hafner

**How *in vitro* alterations in cellular energy pathways  
can overcome obstacles in drug research**

**Inauguraldissertation**

zur Erlangung des Doctor scientiarum humanarum (Dr. sc. hum.)  
der  
Medizinischen Fakultät Mannheim  
der Ruprecht-Karls-Universität  
zu  
Heidelberg

vorgelegt von  
**Swen Seeland**  
aus  
Gengenbach  
2012

Dekan: Prof. Dr. rer. nat. Dr. med. Dr. h.c. Uwe Bicker

Referent: Prof. Dr. rer. nat. Mathias Hafner

*Für Christina, Lucas, Elias, Johannes*

*und meine Eltern*

# TABLE OF CONTENTS

	Page
ABBREVIATIONS.....	1
1 INTRODUCTION .....	3
1.1 General .....	3
1.2 Drug discovery and development .....	3
1.2.1 Drug discovery.....	4
1.2.2 Drug development.....	5
1.3 Drug interactions.....	6
1.3.1 ABC-Transporters and their famous member: P-glycoprotein (ABCB1) .....	9
1.3.2 Identification of P-glycoprotein substrates: A challenge .....	10
1.4 Target characterisation in drug discovery.....	11
1.4.1 Purinergic P2X7 receptor mediates metabolic alterations .....	12
1.5 Toxicology in drug research.....	14
1.5.1 Drug-induced liver injury (DILI) .....	16
1.6 Bioenergetic pathways, or, how a meal provides energy for $10^{14}$ cells.....	19
1.7 The multiparametric cytosensor system.....	20
2 AIMS .....	23
2.1 Real-time identification of P-glycoprotein substrates .....	23
2.2 Does the P2X7 receptor mediate effects on cellular metabolism upon ATP treatment?.....	24
2.3 Identification of drug-induced adverse liver effects on human HepG2 cells.....	24
3 MATERIAL AND METHODS .....	26
3.1 Materials.....	26
3.2 Cell culture.....	28
3.2.1 LLC-PK1 and L-MDR1 cells .....	30
3.2.2 HUVEC cells.....	31
3.2.3 Human mononuclear blood cells.....	31
3.2.4 P2X7 overexpressing HEK293 cells .....	32
3.2.5 Mouse microglia BV2 cells.....	33
3.2.6 Primary Wistar rat cortical cells .....	33

3.2.7	Human hepatocarcinoma-derived HepG2 cells .....	34
3.3	Methods .....	35
3.3.1	Real-time monitoring of cell physiological parameters .....	35
3.3.2	Western blot detection of P-glycoprotein.....	38
3.3.3	Metabolic activity of human mononuclear blood cells .....	40
3.3.4	Dynamic mass redistribution assay .....	41
3.3.5	YoPro1 uptake analysis.....	42
3.3.6	Fluo-4-AM calcium measurements .....	43
3.3.7	Electrophysiology .....	43
3.3.8	MTT cell viability assay .....	44
3.3.9	Metabolic activity of human hepatocarcinoma-derived cells, HepG2 .....	44
3.3.10	Data recording, analysis and statistics .....	46
4	RESULTS.....	47
4.1	Identification of P-glycoprotein substrates .....	47
4.1.1	P-glycoprotein levels in LLC-PK1 and L-MDR1 cells.....	47
4.1.2	Real-time identification of P-glycoprotein substrates.....	48
4.2	Purinergic P2X7 receptor mediates metabolic changes upon ATP treatment.....	54
4.3	Detection of drug-induced liver toxic effects using HepG2 cell .....	65
5	DISCUSSION.....	79
5.1	Real-time identification of P-glycoprotein substrates .....	79
5.2	Purinergic P2X7 receptor mediates metabolic changes upon ATP treatment.....	84
5.3	Characterisation of drug-induced liver effects in HepG2 cells.....	88
6	CONCLUSION .....	99
7	ABSTRACT.....	103
8	BIBLIOGRAPHY.....	108
9	PUBLICATIONS ARISING FROM THIS THESIS .....	120
10	ACKNOWLEDGEMENTS .....	121

## ABBREVIATIONS

µg	microgram
µL	microliter
µM	micromolar
µm	micrometer
ABCB1	ATP-binding cassette transporter B1
ADME	absorption, distribution, metabolism and elimination
ADP	adenosine-5`-diphosphate
AM	acetoxymethyl ester
ATP	adenosine-5`-triphosphate
BV2	immortalized mouse (strain: C57BL/6) microglia cells
Bz-ATP	2`, 3`-O-(4-benzoylbenzoyl)-adenosin-5`triphosphate
cDNA	complementary deoxyribonucleic acid
CO <sub>2</sub>	carbon dioxide
Da	Dalton
DDI	drug-drug interaction
DILI	drug-induced liver injury
DMEM	Dulbecco`s modified Eagle medium
DMPK	Drug Metabolism and Pharmacokinetics
DMSO	dimethyl sulfoxide
DNA	deoxyribonucleic acid
EBM	endothelial basal medium
EC <sub>50</sub>	half maximal effective concentration
EDTA	ethylenediaminetetraacetic acid (disodium salt)
EGM	endothelial growth medium
FADH	flavin adenine dinucleotide (reduced form)
FBS	fetal bovine serum
g	gravitation constant
GSH	γ-L-glutamyl-L-cysteinylglycine (or: glutathione)
h	hour
HBSS	Hanks` balanced salt solution
HCl	hydrochloric acid
HEK293	human embryonic kidney cell line
HEK-hP2X7	human P2X7 overexpressing HEK293 cells
Hepes	4-(2-hydroxyethyl)-1-piperazineethanesulfonic acid
HepG2	human hepatocarcinoma-derived cell line
HPLC	high performance liquid chromatography
i.e.	<i>id est</i>
IC <sub>50</sub>	half maximal inhibitory concentration
IgG-HRP	immunoglobulin G-coupled with horseradish peroxidase
IL-1b or IL-1β	interleukin-1β

---

IU	international unit
k	kilo
$K_M$	Michaelis-Menten constant
LC-MS	liquid chromatography coupled to mass spectrometry
LLC-PK1	porcine kidney epithelial cell line
L-MDR1	porcine kidney epithelial cell line transfected with human mdr1 gene
M	molar
$m/z$	mass over charge ratio
MDR1	multi drug resistance gene-1
MDR1-G1	mouse monoclonal antibody raised against amino acids 1040-1208 of human mdr1 protein
MEM	modified Eagle medium
mg	milligram
min	minute
mL	millilitre
mM	millimolar
MTT	3-(4, 5-dimethyl-2-thiazolyl)-2, 5-diphenyl-2H-tetrazolium bromide
NADH	nicotinamide adenine dinucleotide (reduced form)
NAPQI	N-acetyl-p-benzoquinone imine
NC	nitrocellulose
nM	nanomolar
nm	nanometer
P2X7	purinergic ligand gated ion channel
PBS	phosphate buffered saline
P-gp	permeability glycoprotein
pH	negative logarithm of the hydrogen ion concentration
RNA	ribonucleic acid
ROS	reactive oxygen species
rpm	rotations per minute
s	second
SDS-PAGE	sodium dodecyl sulphate-polyacrylamide gel electrophoresis
SEM	standard error of the mean
UK	United Kingdom
US	United States of America
UV	ultraviolet
V	volt
v/v	volume/volume
$V_{max}$	maximum rate
wt	wild type
w/v	weight/volume
YoPro1	4-[(3-methyl-2(3H)-benzoxazolylidene)methyl]-1-[3-(trimethylammonio)propyl]-, diiodide

# 1 INTRODUCTION

## 1.1 General

This dissertation yields a means to support drug research based on the monitoring of cellular energy pathways. Moreover, the newly achieved approach presented here resolves key mechanistic issues from various sections of drug discovery and development, thus representing a beneficial and supportive tool for the pharmaceutical industry.

## 1.2 Drug discovery and development

The basic mission of the pharmaceutical research industry is to understand disease and to provide safe and effective drugs for patients.

Drug discovery and development are two distinguished processes that contribute to the drug research pipeline. The whole story of drug research starts with the drug discovery process.

Once a lead compound is identified, it enters the drug development process (Figure 1).

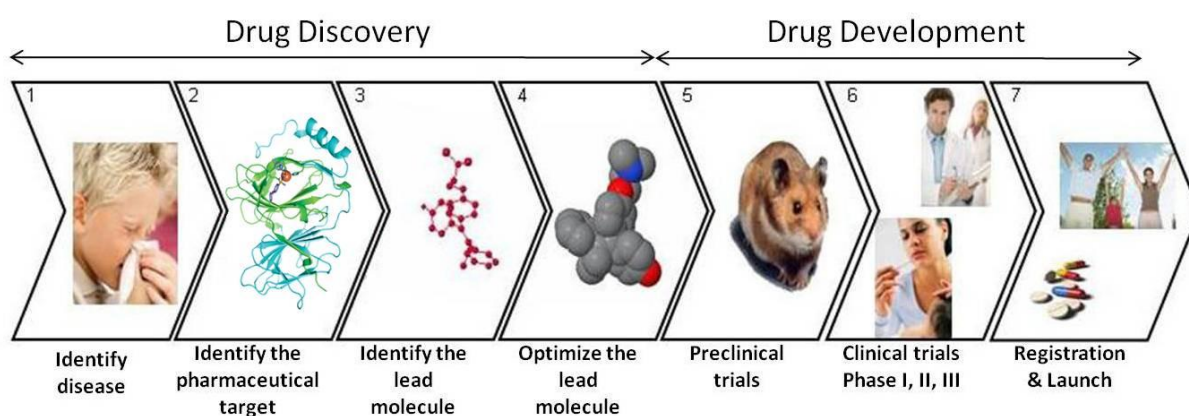


**Figure 1.** Drug discovery and development is a long process that starts with the selection of a disease and the pharmaceutical target identification. Following a multitude of processes in drug discovery, the compound enters preclinical trials and subsequently the clinical phases (Phase I, II, III) before it can be launched on the market.



### 1.2.1 Drug discovery

The initial issues in drug discovery involve choosing a disease, selecting a disease-specific target, and finding a suitable assay to determine the activity of molecules with respect to the selected target. In the past, most drugs were discovered by identifying ingredients from traditional remedies or plants. Today's drug discovery is supported by enormous knowledge of the mechanisms of diseases, and how these diseases are controlled. With this information and a deeper insight, the scientist can search for molecules that modulate targets in a selective manner. Selectivity can play a pivotal role in the development of fewer side effects, but has also proved beneficial for new and unexpected indications for drugs (1). In any case, the drug discovery track is difficult and similar to the proverbial search for the needle in a haystack. However, once a molecule is successful in the screening process, the next step in drug discovery is the identification of a lead compound, which is a molecule that exhibit activity towards the target, but is not yet good enough to be the drug itself. Combinatorial chemistry (involves rapid synthesis and computer simulations) provides a large number of slightly modified molecules for compound lead identification and optimisation. These synthesised analogues are analysed in large screening studies to show their potential activity with respect to the target. Simultaneously the first safety experiments (cytotoxicity assays, cytochrome P450 inhibition, covalent binding to cell proteins, metabolic stability, plasma protein binding) were investigated to assess the potential risk of the compounds and to support lead compound optimisation. Once a pharmacophore is identified, the optimisation of the molecule can focus more on the feature of the pharmacophore responsible for the activity towards the target. Irrespective of all the advantages of the new technologies, drug discovery is still a long, expensive, and inefficient process (Figure 2) requiring more and more support technologies to yield a more economical and successful process (2).

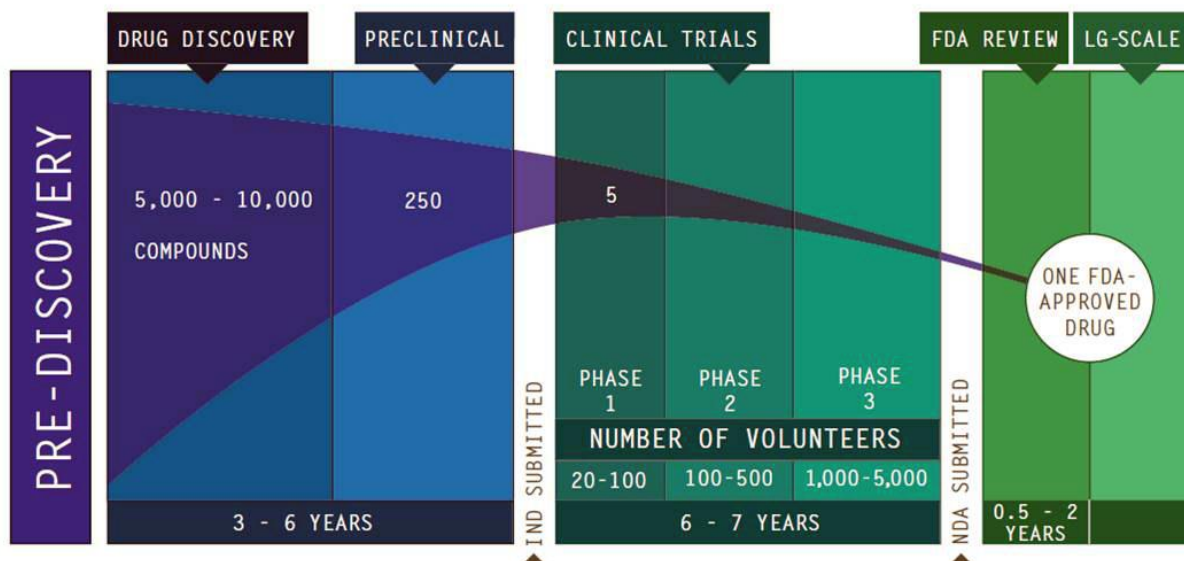


**Figure 2. Stages of the drug development process.** This chart represents the attrition rate of compounds as they travel through the drug development process over time. Starting with 10`000 candidates, only one will finally make it to market (from: [www.PhrMA.org](http://www.PhrMA.org), January 2012, Washington, US).

### 1.2.2 Drug development

Drug discovery and development are more of interdependent than rigorously separated processes. Preliminary tests in the developmental stage, before lead compound selection, can help eliminate poor drug candidates in the early process and thereby save limited resources. However, once a lead compound has been selected in the drug discovery process, the new drug candidate enters the drug development process. Drug development consists of two different disciplines: preclinical research and clinical trials (Figure 1). Prior to "first in man", the preclinical department provides required data (e.g. toxicity, pharmacokinetics and -dynamics, metabolism, enzyme induction, drug transport, etc.) for the new drug candidate to the regulatory authorities for the clinical Phase I trial. In addition to the safety profile of the drug, the preclinical department recommends the first human dose for the clinical trial, estimated from several toxicology, efficacy, and supporting experiments. To follow regulatory requirements, a number of tests are available to determine the toxicity of the new drug candidate before it enters the first clinical trial in humans. Section 1.5 - Toxicology

in drug research – depicts in more detail the requirements of toxicity studies in drug research. Briefly, many cell-based *in vitro* and *in vivo* experiments are performed to examine the safety of the new drug candidate and the collection of all data is required for the next steps. Finally, all data gathered from the studies are collected in an Investigational New Drug application (IND) and then submitted to the regulatory authorities for approval of the clinical trials. It is worth mentioning that the costs to bring a new drug to market are above 500 million dollars (3, 4), the process taking an average of 10 to 15 years, with a success rate of only 0.01%. This means that, of every 10`000 compounds that enter the research and development pipeline, ultimately only one drug receives approval (Figure 2) (5). Taking this in perspective, to say the least the implementation of new technologies that can support the drug research process in an economical manner will be appreciated.

### **1.3 Drug interactions**

The terms drug interactions refers to circumstances in which the efficacy of a drug is altered, be it an increased or decreased thereof, or a completely different effect occurs. Several kinds of drug interactions are known; i.e. the interaction of two administered drugs (drug-drug interactions, DDI), or the interaction of an administered drug with ingredients in food. Epidemiology shows that, among adults older than 55, at least 4% take medication and supplements, putting them at risk of DDI (6-8). That is why DDIs remain a decisive issue in drug research. The earlier the DDI can be detected, the greater the probability that this deleterious effect can be changed by the design of the molecule. In the pipeline of drug research, several mechanistic approaches are implemented to assess the DDIs potential of a drug candidate (e.g. enzyme inhibition and induction, transport substrate and inhibition identification, etc.). Drug interaction has a crucial influence on the pharmacokinetic and

---

pharmacodynamic of drugs. Regarding the pharmacodynamic, the effect of the drug on a disease can be potentiated or simply lost. The pharmacokinetic of a drug can be subdivided into absorption, distribution, metabolism, and excretion (ADME) processes of the drug molecule in the body. This ADME process can be significantly altered by a DDI, e.g. by inhibition or induction of metabolising enzymes or by inhibition of transport proteins (e.g. ABC-transporters, solute carrier, etc.) (9). Drug transporters mediate the uptake or efflux of a broad variety of endogenous compounds, metabolites, or drugs (10, 11). The transporters are well distributed in the body and are found highly expressed in tissues where they play pivotal roles. P-glycoprotein (P-gp, ABCB1), the most famous member, is found at high levels at the blood-brain barrier endothelia, protecting the brain from brain-critical substances, but also at the level of the small intestine, where it can deny drug entry into the systemic circulation. Drug-drug interactions with transporters occur when translocation of a drug is disturbed by a second drug. This alteration by a second drug can function via inhibition or induction (12-14). In recent years, scores of DDI studies with drug transporters have been investigated and concern with molecules interacting with drug transporters has become ever more important (15-21). It is a great aspiration in drug research to design drugs that show no undesirable interactions with drug transporters. The importance of the function of drug efflux pumps is well established with the neurotoxic pesticide ivermectin. Ivermectin itself is a substrate for P-gp and consequently is not able to cross the blood-brain barrier and enter the brain, as shown in Figure 3. In cases where ivermectin is co-administered with a drug that has P-gp inhibition potential, ivermectin can cross the blood-brain barrier and enter the brain with fatal neurotoxic consequences (22). This observation was confirmed in mouse models lacking the expression of P-gp ( $mdr1a^{-}/b^{-}$ ) and resulted in markedly elevated brain levels of ivermectin (23). Overall, ABC-transporters serve as protective shields by preventing

uptake or facilitating clearance of toxic substances. A guide on drug-interaction studies was provided by the regulatory authorities to cover the most frequent and known DDIs (24). Existing techniques are used regularly in drug research, but often come up against the limits of their potentials in the prediction of DDIs. For all of the above reasons, I decided to test the possibility of real-time, label-free substrate identification of the drug efflux pump, P-gp.

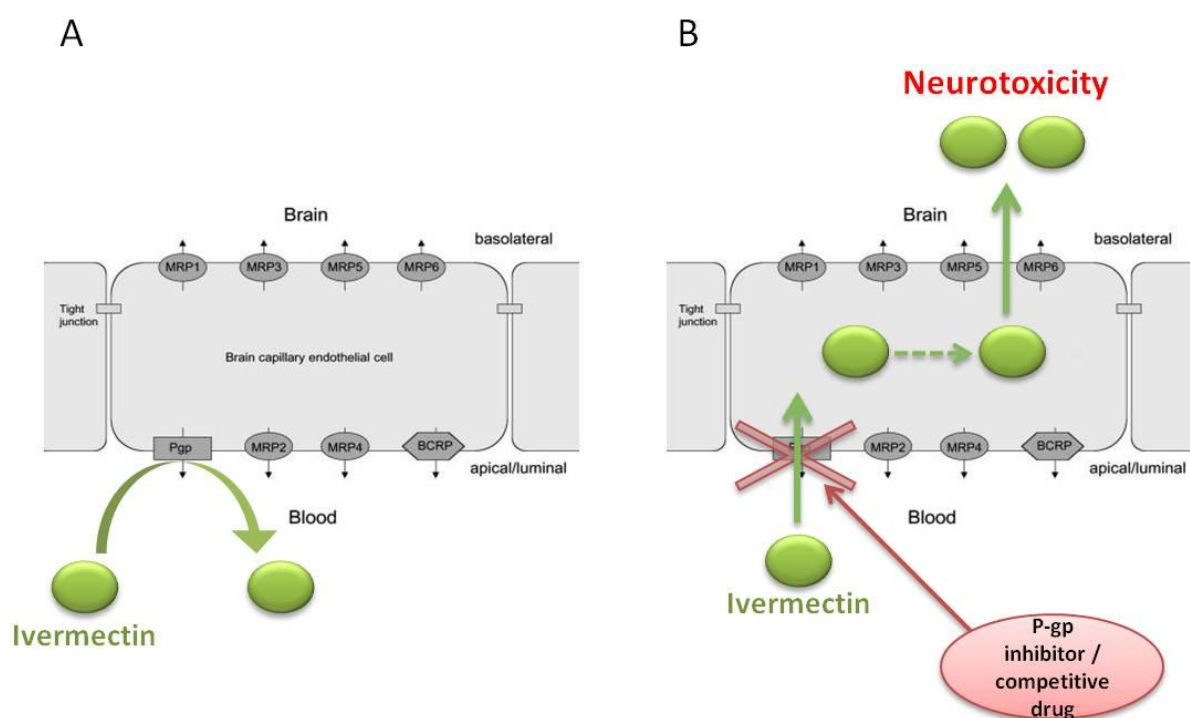


**Figure 3.** Putative localisation of drug efflux proteins on the plasma membrane of brain capillary endothelial cells that form the blood–brain barrier. The proposed direction of transport is indicated by black arrows. Only efflux transporters that are localised on the apical (luminal) side of the brain capillary endothelium would be in a position to restrict brain uptake of xenobiotics. (A) Indicates the protective function of P-glycoprotein (Pgp) at the level of the blood–brain barrier using ivermectin as an example of a P-gp substrate. Ivermectin cannot enter the brain, owing to the active efflux of P-gp from the brain capillary cell. (B) Co-administration of a P-gp inhibitor or a competing drug can block the protective function and ivermectin can penetrate the brain capillary cells and thus enter the brain, with dramatic neurotoxic consequences. It should be noted that this figure represents only a simplified scheme of drug-efflux transporter distribution at the blood–brain barrier. There are various other transporters localised in brain capillary endothelial cells (25), which are not illustrated here because their potential role, if any, in drug efflux is not clear. In consideration of the fact that ivermectin penetration is on the basolateral side, involvement of MRP1 (multi-drug resistance protein-1) as well as passive diffusion was analysed (26).

---

### 1.3.1 ABC-Transporters and their famous member: P-glycoprotein (ABCB1)

ATP-binding cassette (ABC) transporters are one of the largest families of multidomain integral membrane proteins that use ATP hydrolysis energy to translocate molecules across cell membranes. They are found in all species including man (27). These efflux pumps recognise a wide range of chemically diverse endogenous and exogenous compounds and act as gatekeepers, contributing to cell defence (28, 29). They are involved in biomedical phenomena such as the multidrug-resistance of cancer cells or the poor bioavailability of drugs (30, 31). One of the best-characterised ABC-transporters is P-gp, the gene product of the human multi-drug resistance (MDR1) gene and the first member of subfamily B of the ABC-transporters (ABCB1). P-gp is highly expressed in human tissues that have a protective function and is found on the luminal surface of cell barriers, including the kidney proximal tubule, small intestine, colon, testis, adrenal cortex, and the blood-brain barrier (17). The expression pattern of P-gp suggests a protective function of P-gp towards potentially toxic xenobiotics. P-gp is a 170 kDa protein consisting of two homologous drug-binding transmembrane domains (32) and a cytosolic nucleotide-binding domain with ATPase activity (33). P-gp recognises and couples its substrates in the cytosolic membrane leaflet (32) and translocates them from the cytosolic membrane leaflet out of the cell or to the outer membrane leaflet, which prevents substrate uptake into the cytosol (34). Transporting the drug consumes two ATP molecules; one ATP is required to induce the drug-releasing conformation, the second to reset P-gp to the drug-binding conformation (35, 36). The rate of ATP hydrolysis in the transport process correlates linearly with the rate of effective transport (37, 38) and can therefore be used to monitor P-gp activity.

---

### 1.3.2 Identification of P-glycoprotein substrates: A challenge

P-gp has a broad substrate range and modulates the pharmacokinetics of many, chemically unrelated drugs (39). As a consequence, efficient screening methods are needed to identify substrates or inhibitors of P-gp during the drug discovery and development process (40). High-throughput fluorescent assays exist to identify P-gp modulators, including the rhodamine123- (41) or the calcein-AM (42) assay. However, identification of substrates of P-gp remains a challenge: predictive cellular assays such as the transcellular transport assay (43) or any *in vivo* experimentation relies on sensitive, compound-specific, and expensive analytical procedures such as the use of radiolabeled test compounds or quantitative mass spectroscopy. In contrast, generic biochemical assays such as the ATPase release assay (44) make use of membrane preparations of P-gp-expressing cells. However, these assays are not necessarily representative of the *in vivo* situation, because membrane integrity is disturbed and the orientation of P-gp binding sites towards the intracellular or extracellular space is lost during the preparation of cell homogenates. Schwab *et al.* (2003) showed that the assays mentioned above and generally used in drug development demonstrate limitations in terms of the reliable identification of P-gp substrates; ten of 28 P-gp substrates were not identified by analysis as substrates in either one or more of these assays (40). Because it is well understood, that P-gp requires energy in the form of ATP for the translocation of drugs out of the cell (Figure 4), this consumed ATP must be regenerated intracellularly, which results in a higher consumption of oxygen and a release of acidic metabolic products. A system that can monitor such alterations should be able to identify P-gp modulators in an effective and elegant way.

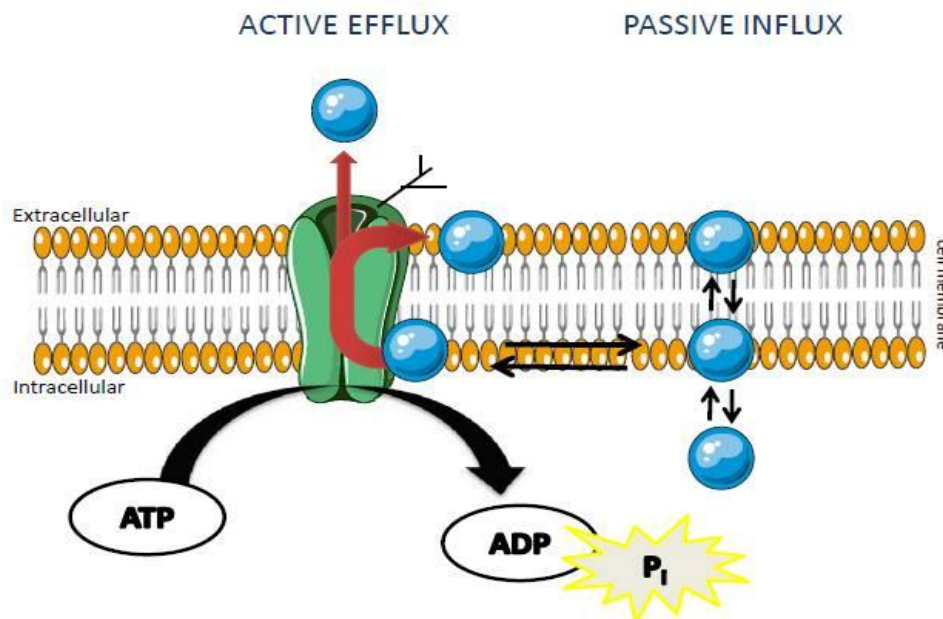


Figure 4. P-glycoprotein binds its substrates in the cytosolic leaflet of the plasma membrane and translocates them into the outer membrane leaflet or into the extracellular compartment. The active transport utilises ATP for translocation (P<sub>i</sub>: phosphate).

#### 1.4 Target characterisation in drug discovery

Finding new medications based on knowledge of biological targets require an intensive ligand design process (45). The number of new entities approved by the Food and Drug Administration (FDA) in the last few years remains stable, with only 18 to 26 newly approved drugs per year (46). The reasons for the stagnated number are multifactorial (47, 48). However, it is recognised that a crucial step in drug discovery is the initial identification of a disease relevant target and target characterisation, and this seems to be one of the main bottlenecks (49-51). In particular, drug discovery repeatedly struggles with the limitations associated with the existing cell-based *in vitro* models for the characterisation of new targets. To circumvent such limitations in drug discovery, implementation of new technologies plays a pivotal role in successful characterisation of new disease relevant targets. Therefore, one of the sub-projects of this thesis was to characterise the purinergic P2X7 receptor.



---

### 1.4.1 Purinergic P2X7 receptor mediates metabolic alterations

Ubiquitous adenosine triphosphate (ATP) influences innumerable cellular metabolic mechanisms (52, 53), provides energy for transporters that translocate molecules against concentration gradients, facilitates muscle contraction, and drives protein synthesis and degradation. It thereby underpins vital chemical (e.g. oxidative phosphorylation) (52), mechanical (e.g. motor proteins) (53, 54) and biochemical (e.g. glycolysis) processes in the cell (55, 56). Intracellular concentrations of ATP range from 1.0 to 10 mM (57), while extracellular ATP concentrations are typically very low under physiological conditions, being strictly regulated by the presence of ATPases (58). There are, however, conditions under which local extracellular ATP concentrations do reach high levels (58, 59). For example, ATP has been reported to be released at the synapses of neurons, where it acts as a neurotransmitter (60, 61). In addition, intracellular ATP is released into the extracellular environment in cases of cell destruction, necrosis, or hypoxia (62). In such cases, high extracellular ATP levels trigger immune system responses that lead to pro-inflammatory states and immune modulation of macrophages/monocytes, lymphocytes, mast cells and endothelial cells (63-65), in addition to initiating cell death in leukocytes and endothelial cells (66-68). These effects are thought to be induced, in part, by the purinergic receptor P2X7, which is activated by ATP only at concentrations above 500  $\mu$ M (69, 70). This concentration is more than ten times higher than that required for ATP to activate other P2X or P2Y receptors (71, 72). Activation of the P2X7 receptor initiates a series of cellular responses that include depolarisation, secondary messenger activation of phospholipase C, and a rise in intracellular  $\text{Ca}^{2+}$  concentrations that stimulates caspase-1, cytokine release, and activation of p38 mitogen-activated protein kinase (73, 74). Sustained exposure (> 1 min) to ATP highlights the unique ability of the P2X7 receptor to form a large, non-

selective pore (Figure 5) (75). The opening of the pore, which is permeable to molecules up to a molecular mass of 900 Daltons, results in complete depolarisation of the membrane potential (ion flux), cell swelling, and finally cell death (76-78). Interestingly, the activation of caspase-1 and mitogen-activated protein kinase pathways has been linked to P2X7 pore formation (79, 80). Moreover, pore formation has also been proposed as regulating physiological processes such as cell fusion and phagocytosis (81, 82). However, little is known to date of how extracellular ATP influences the regulation of metabolic pathways in a cell, and whether this occurs via the P2X7 receptor.

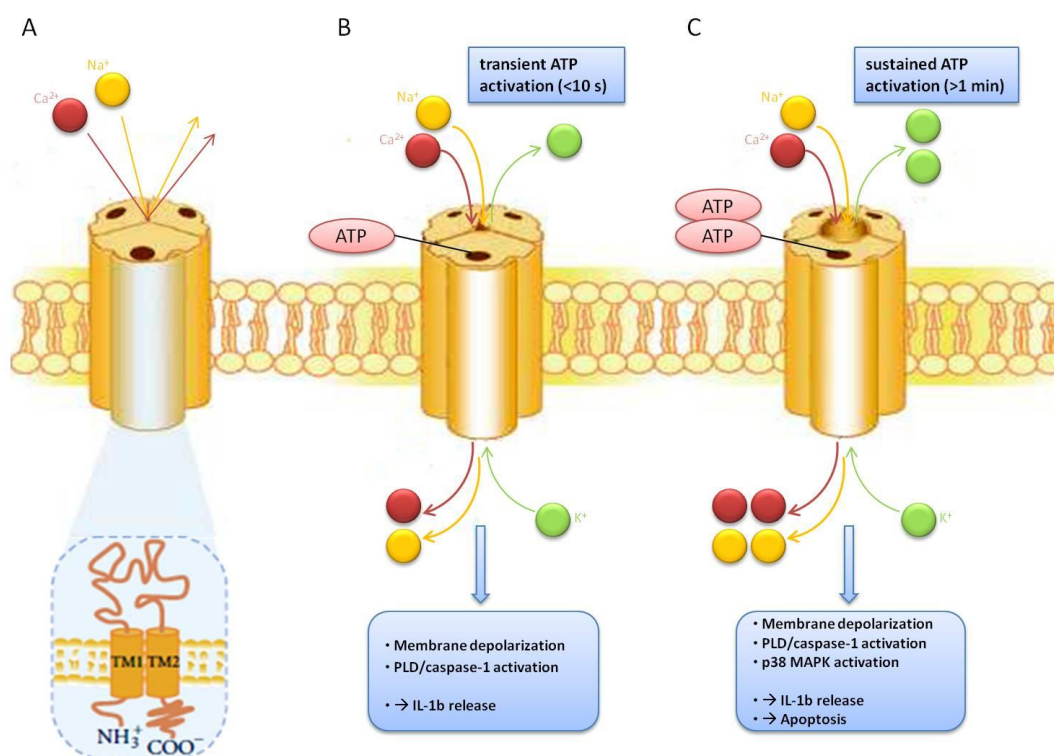


**Figure 5. Function and signalling pathways of the P2X7 receptor. (A)** The P2X7 receptor is a homomeric cation channel. Each of the three subunits possesses two transmembrane domains (TM1 and TM2) (83), an extracellular loop with an ATP binding site and intracellular carboxyl (COO<sup>-</sup>) and amino termini (NH<sub>3</sub><sup>+</sup>). **(B)** Brief (< 10 s) activation of P2X7 with high concentrations of ATP (> 100 μM) lead to rapid, reversible channel opening with ion flux, followed by depolarisation (73). Acute receptor activation also initiates second messenger processes, resulting in phospholipase D (PLD) and caspase-1 activation. **(C)** Sustained activation of P2X7 receptor (> 1 min) induce large pore formation (> 4 nm), which triggers the enhanced influx of cations and molecules up to 900 Da (75). The rise of intracellular calcium and efflux of potassium activates the caspase-1 pathway and thus a conversion of pro-IL-1b (pro-interleukin-1β) into IL-1b (interleukin-1β) and release from the cell. Stimulation of the P2X7 receptor also leads to an activation of p38 mitogen-activated protein kinase (MAPK) (74). Prolonged activation of the P2X7 receptor leads to complete depolarisation of the membrane potential (ion flux), cell swelling, and finally cell death (76, 78, 84).

---

## 1.5 Toxicology in drug research

Findings from human graves indicate the use of therapeutic agents as early as the Neolithic age and with the poor knowledge of the used agents, it was indeed a *risqué* to ingest substances that were potentially poisonous. A chemical entity itself does not constitute a poison; the entity must achieve a sufficiently `high` dose, which was attempted by Paracelsus as early as the sixteenth century. As depicted in the ratio of the median lethal dose ( $LD_{50}$ ) to the median effective dose ( $ED_{50}$ ), the therapeutic index has to be assessed very carefully. The goal of the pharmaceutical industry is obviously to develop safe drugs with high efficacy in therapy, which can narrow down the therapeutic index and has to assess carefully.

Before entering the development process, drug candidates have first to be screened in different *in vitro* assays (i.e. biochemical and cellular assays), and the chemical structure of a potential drug optimised. Subsequently the most promising development candidates are investigated in more complex *in vitro* assays and pharmacological *in vivo* models. The latter consist mainly of rodents and possibly non-rodents. These *in vivo* models are concomitantly used to assess plasma concentration profiles and possible adverse effects. Compounds for development are selected based on the before mentioned battery of assays. These compounds are subsequently assessed in toxicology and safety pharmacology studies in order to enable "entry into man" (clinical Phase I) of the preclinical candidate. Non-clinical safety studies to conduct human clinical trials and to obtain marketing authorisation for pharmaceuticals are described in the ICH (International Conference on Harmonisation) M3 guideline (European Medicine Agency<sup>®</sup>, Canary Wharf, London, UK). Toxicology assessment consists of *in vitro* and *in vivo* studies covering genotoxicology/carcinogenicity, general (or repeated) toxicology, reproduction toxicology and safety pharmacology. The

read-out from the toxicology studies can indicate adverse effects, which will require additional experiments for the elucidation of the observed effects. Briefly, the genotoxicology studies consider the gene mutation potential of a drug and, in general, support all single dose clinical development trials. To support the multiple dose trials, an additional assessment capable of detecting chromosomal damage in the mammalian system should be completed. Carcinogenicity studies are commonly relevant for marketing. General toxicology studies, which are required, consist of repeated drug application to two mammalian species (one non-rodent) for several weeks up to month, related to the duration, therapeutic indication, and scope of the proposed clinical trial. The reproduction toxicology is performed again in two mammalian species (one non-rodent) in *in vivo* experiments and concerns the safety of pregnant humans. Before the availability of the results, all clinical trials are exclusively performed in male humans. The last set of toxicology studies is safety pharmacology. The core of safety pharmacology studies includes the assessment of effects on the cardiovascular, central nervous and respiratory system. The compiled resulting data show whether more investigations have to be undertaken to issue the safety profile of the drug. The most critical organs in terms of adverse effects are the organs excessively exposed to the drug or its metabolites. In the first instance, this adverse effect occurs mainly in the liver and the kidneys, as well as in the heart and lungs. Adverse effects that not be overcome, are usually a deathblow to the drug candidate. In general, adverse effects results represent the point at which mechanistic toxicologists become active. In a specific set of experiments, the toxicologist tries to reveal the mechanism and hazardousness of the observed adverse effect. If the mechanism can be clarified and ranked as reversible, monitorable, rodent specific and/or acceptable (e.g. by a safety margin), the development process can be continued. It cannot be denied that toxicology measurements

are enormously relevant parts of the drug discovery and development process and can greatly influence the progress of a potential drug candidate. However, it should be mentioned that toxicology is not a single discipline in the drug research process. For example, the preclinical department (DMPK) supports toxicology studies through a number of important results that it issues, to accumulate better knowledge of drug candidates and thus improved insight into adverse effect. However, an observation of an adverse effect in organs (e.g. liver), especially in the range of the considered therapeutic dose, is a serious event in the preclinical process and requires further investigation for the identification of the underlying mechanisms. Common sets of techniques are available, but do not represent a panacea for the analysis of toxicology findings. In any case, any additional information that permits a deeper insight into the toxicological mechanism can help to determine the progress of a drug candidate and can probably save resources.

### **1.5.1 Drug-induced liver injury (DILI)**

Drug-induced liver injury (DILI) is an important health problem that can necessitate discontinuation of an essential drug, hospitalisation with intensive care, or even liver transplantation (85). In 80% of all cases, DILI is caused by direct, dose-dependent toxicity by an administered drug or its metabolites. Alternatively, immunologically mediated idiosyncratic toxicity may lead to liver injury (86, 87). Idiosyncratic hepatotoxicity can lead to a drug being withdrawn from the market, even after launching and clinical trials. A prime example of such a drug was Rezulin (Troglitazone), which was withdrawn in 2000 due to the risk of severe idiosyncratic hepatotoxicity (88, 89). Drugs that exhibit chemical (direct) hepatotoxicity have predictable dose-response curves and well characterised mechanisms of toxicity. Examples include the promotion of dysfunction in physiological pathways and finally

cell death by direct insult by chemically reactive compounds, induction of an apoptotic process, or infliction of cellular stress (90). The latter phenomenon is often observed in the context of oxidative or metabolic stress, where inhibition of the mitochondrial respiratory chain results in a release of reactive oxygen species (ROS) to an excessive level and depletion of ATP (91-93). Furthermore, certain drugs influence mitochondrial activity by inhibiting fatty acid  $\beta$ -oxidation (91), impairing mitochondrial DNA replication (94) or opening the mitochondrial permeability transition pore, which is unavoidably associated with cell death (95). All of the physiological dysfunctions mentioned above ultimately lead to hepatic tissue damage. If energy is available in the form of ATP, injured cells enter programmed cell death (apoptosis). If ATP sources are exhausted, cells follow the necrosis pathway, enhancing hepatic inflammation (96).

As shown in Figure 6, the vast majority of hepatic portal blood is composed of blood from the gastrointestinal viscera (from the lower part of the oesophagus to the upper part of rectum) and to a smaller extent from the spleen (92). The portal vein system is responsible for directing blood and absorbed drugs to the liver in a concentrated form. Therefore, the liver plays a pivotal role in drug metabolism and detoxification and is consequently vulnerable to injury.

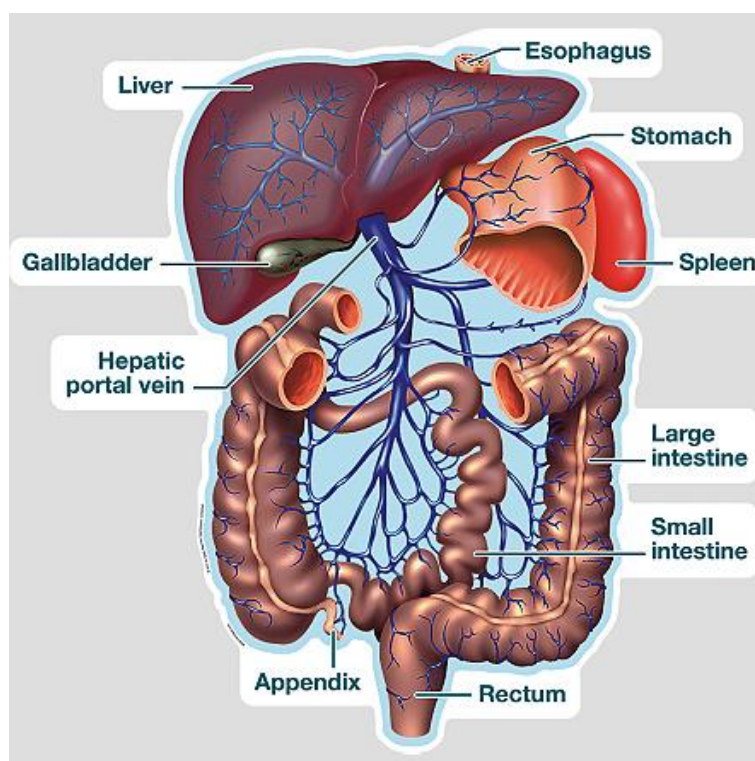


**Figure 6.** The hepatic portal system is comprised of veins from almost every part of the digestive tract, even from the lower oesophagus and the upper rectum. In this view, some organs have been removed to reveal the blood vessels. (from: Robert, A.: *Anatomie und Physiologie*, Dorling Kindersley Verlag 2011)

In phase I metabolism, initially the hepatic cytochrome P450 system transforms mainly lipophilic drugs into water-soluble metabolites for excretion in bile or urine (97). These oxidative metabolism pathways are followed by a phase II metabolism pathway (98, 99). Phase II metabolism reactions are usually conjugation reactions to glucuronic acid, sulphate or glutathione and the resulting hydrophilic metabolites are excreted into plasma or bile via transporters located at the hepatocytes membrane. In order to avoid hepatotoxicity, the generation of phase I products should not exceed the capacity of the liver to detoxify them. For example, such an incapacity can arise with abuse of alcohol and ingestion of acetaminophen, even a customarily tolerable dose of acetaminophen can, under these conditions, result in severe liver injury (100).

Resulting hepatic dysfunction is generally paralleled by a rise in biochemical liver markers such as alanine aminotransferase, alkaline phosphatase and/or bilirubin (101). These initial

indicators of hepatotoxicity, when observed during the drug discovery and development process, call for alert and necessitate mechanistic follow-up studies. Such studies are ideally based on the use of additional biomarkers as predictors and are time consuming and costly if performed in experimental animals (102). However, in view of the poor correlation between clinical findings of DILI and standard preclinical animal studies, such efforts remain a challenge and are a source of concern for investigators and regulatory authorities. Ongoing efforts are therefore directed towards the development of predictive *in silico* or *in vitro* models to gain better insight into mechanisms leading to DILI and to uncover potential risks in the drug research (103). One strategy to gain improved insight into toxicity is the use of cytosensor systems, where a silica-based sensor system allows online monitoring of metabolic activity in target cells in the presence of potentially toxic chemicals (104). Because drug-induced liver adverse effects are of great interest, I therefore decided to identify drug-induced liver adverse effects *in vitro* to support mechanistic toxicology studies and thus drug research.

## **1.6 Bioenergetic pathways, or, how a meal provides energy for $10^{14}$ cells**

All cellular work, all of the activities of life, requires energy either from ATP or from other energy related molecules. For this, cells store energy mainly in the form of chemical bonds (52, 55, 56). The intracellular metabolic pathways are a series of chemical reactions in the cell to break down substrates and synthesise new, energetic molecules. These pathways are important to maintain the homeostasis of an organism (52, 105). Several distinct but linked metabolic pathways are used by cells to transfer the energy released by breakdown of fuel molecules into ATP and other small molecules (e.g. NADH, FADH) that are used for further energy generation. Cellular respiration is the process in the cell that converts the energy



from nutrients into ATP, using molecular oxygen ( $O_2$ ) as an electron acceptor, and is divided into four different but tightly linked parts; i.e. glycolysis, oxidative decarboxylation of pyruvate, Krebs cycles and finally oxidative phosphorylation (52, 55, 56). Regarding the whole cellular respiration process from glycolysis to oxidative phosphorylation, a net of 38 ATP molecules are produced from one molecule of glucose, whereas 38 ATP molecules is only a theoretical value. De facto, in reality this is reduced due to several minor influences such as slightly leaky inner mitochondrial membranes or the consumption of energy by transporting and providing substrates (pyruvate, phosphate, ADP) for the ATP synthesis (106). The energy generating process is very susceptible to modification and the real value of generated ATP is closer to 28 – 30 ATP molecules (107), but it is nonetheless an effective process to generate energy. However, exogenous variations can influence these sensitive processes significantly, thus recording  $O_2$  consumption and excretion of acidic metabolic products ( $CO_2$  and lactate) from these processes can be used as responsive parameters to detect minute alterations in cellular metabolism and respiration.

### **1.7 The multiparametric cytosensor system**

Because the goal of this thesis was to develop a new technology for the pharmaceutical industry based on bioenergetic pathways, I used a multiparametric cytosensor system capable of monitoring the energy pathways of cells. Two similar systems for the identification of these parameters were used (Figure 7), i.e. the Bionas®1500, a single sensor chip system, and the Bionas®2500, which measures six cell-coated chips simultaneously. The multiparametric cytosensor system allows simultaneous measurement of several metabolic parameters of the specific cells grown on the silica-sensor chip. The core of the system

consists of the silica-sensor chip SC1000 (Figure 8), including the sensors for the real-time monitoring of the cell physiological parameters.

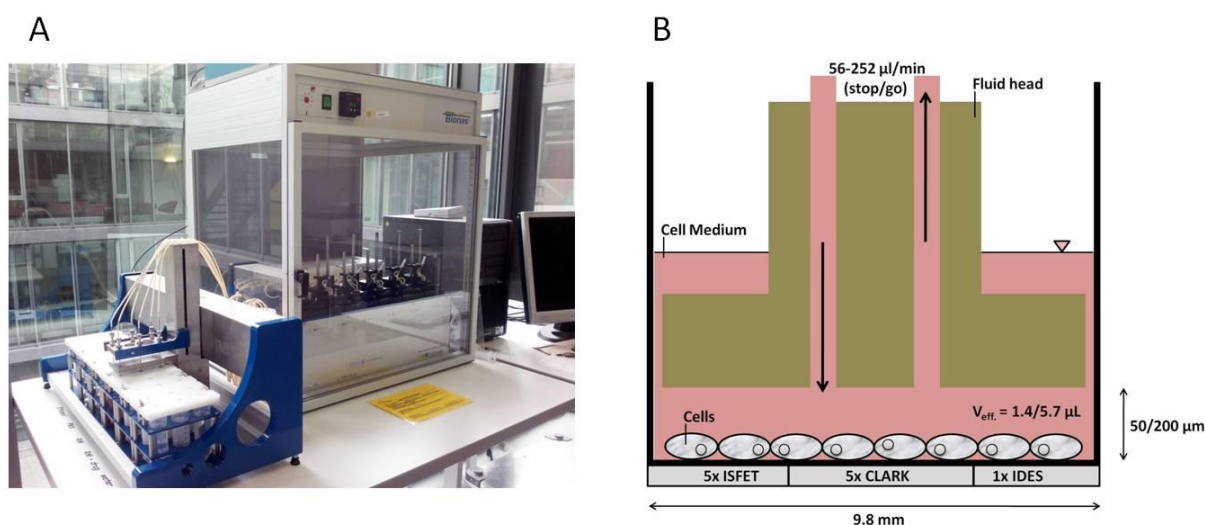


**Figure 7. (A) Photographic illustration of the Bionas<sup>®</sup>2500 system. (B) Schematic diagram of the flow system and dimensions for the sensor chip analysis, indicating the inlet and outlet (arrows) of the assay medium and the small incubation chamber with an effective volume of 1.4 μL or 5.7 μL, respectively. The sensor chip SC1000 forms the bottom of the reaction chamber, including the three different sensors.**

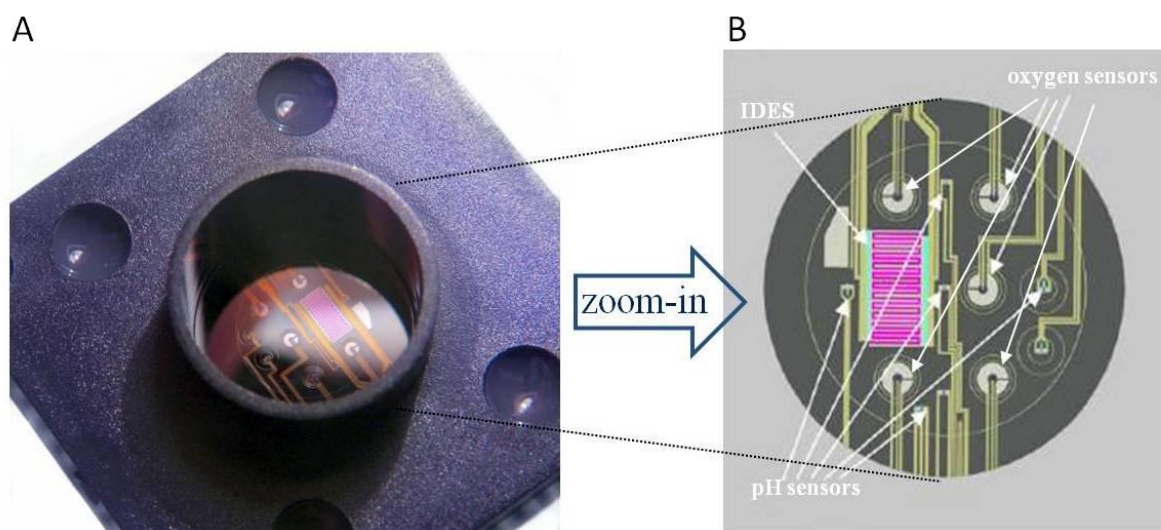


**Figure 8. (A) Photographic representation of the silica-sensor chip SC1000. The silica-sensor chip has a surface area of 75 mm<sup>2</sup>. (B) The zoom-view depicts the integrated sensors, include one interdigitated electrode structures (IDES) for the measurement of cellular impedance, five ion sensitive field effect transistor (ISFET) sensors for the measurement of pH, and five Clark-type sensors for the measurements of oxygen concentration (pictures reproduced with permission of Bionas Ltd., Rostock, Germany)**

The supply of the assay medium to the sensor chip was carried out in stop and go phases. During these “stop phases”, metabolic breakdown products of the cells (lactate and carbonate) were released into the assay medium and were allowed to accumulate, resulting in alterations of extracellular pH (reflecting metabolic/glycolytic activity) (Figure 9A) (108). Simultaneously, the change in oxygen concentration is recorded, which is an indication of cellular respiration activity (Figure 9B). Initial rates of extracellular acidification and respiration were calculated by changes in the slope in the stop phases and a linear regression analysis. The system records one raw data point every 10 s in the stop and go phases of an experiment. Impedance measurements were carried out continuously over the whole experiment to monitor cell adhesion and thus cell morphology, viability and membrane functionality (109).

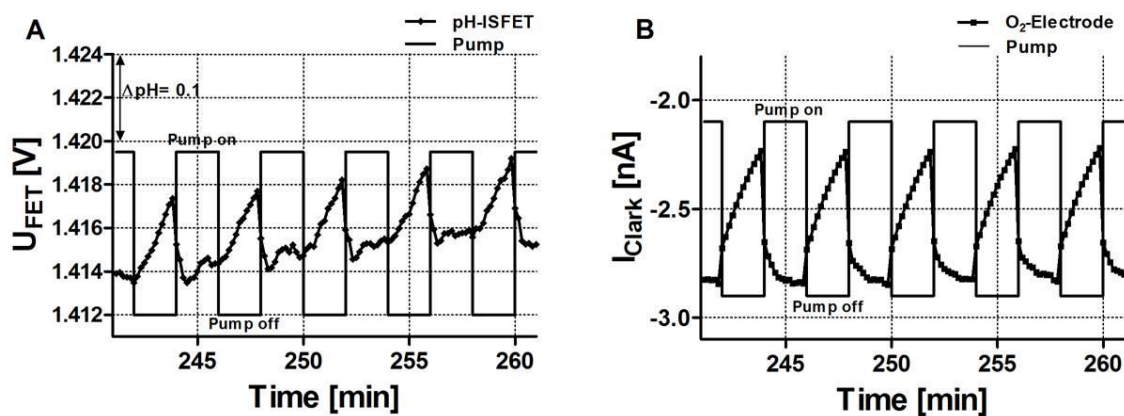


Figure 9. Representative raw data from an example of a multiparametric cytosensor system experiment. Cellular respiration of L-MDR1 cells is shown during several 2 min stop (pump off) and 2 min go (pump on) cycles (solid lines). Recorded data (square symbols) are plotted against time and include measurement of extracellular acidification (A) and oxygen concentration (B). The pH is proportional to a measured voltage ( $U$ ) and the oxygen concentration is proportional to a measured current ( $I$ ). Extracellular acidification (A) and cellular respiration (B) rates were calculated from the initial slope of each stop phase by a linear regression.

## 2 AIMS

Because cellular activities require energy, the goal of this thesis was to develop a new technology for drug research based on the monitoring of cellular energy pathways. For this approach, different questions from three sections of drug discovery and development were explored and effective ways were sought to answer questions by utilising the cellular energy pathways.

### 2.1 Real-time identification of P-glycoprotein substrates

As described in section 1.3.2, the common techniques to identify substrates for P-gp *in vitro* suffer from several limitations and concerns in reliability (40-44). In view of these limitations, the aim of the project was to implement a new, label-free method to identify substrates of P-gp on-line in living cells by monitoring changes in cellular energy pathways. A further goal was to validate this assay as an effective and generic tool for the reliable identification of these P-gp substrates. Concerning the energy pathways, the regeneration of consumed ATP via cellular processes is coupled with the formation of carbon dioxide and lactate, which are released into the extracellular milieu as carbonic acid and lactic acid (108). Besides acidification, oxygen is consumed during ATP regeneration, resulting in a decrease in oxygen concentration in the extracellular environment. These two processes, i.e. oxygen consumption and extracellular acidification, are indicators of ATP regeneration and thus P-gp activity. Using a MDR1-overexpressing cell line, the objective was to develop a label-free and real-time analysis system for the identification of P-gp substrates in living cells.

---

## **2.2 Does the P2X7 receptor mediate effects on cellular metabolism upon ATP treatment?**

To investigate the effects of extracellular ATP on cell metabolism, I also used the multiparametric, cell-based sensor system to simultaneously monitor metabolic-related extracellular acidification rate (pH changes), cellular respiration (oxygen consumption), and cellular morphology and adhesion (impedance measurements) (108). In an initial set of experiments, the release of hydrogen peroxide from mononuclear blood cells exposed to exogenously applied ATP was explored, as a marker for metabolic activity. Results from these experiments were suspected of being linked with the purinergic P2X7 receptor.

To investigate the role of extracellular ATP on cell metabolism associated with the purinergic P2X7 receptor, I further took advantage of a recombinant cell line expressing the P2X7 receptor at high levels. This P2X7 cell line was used to analyse alterations in cell metabolism, mitochondrial respiration, and changes in cell shape upon the application of exogenously applied ATP.

I subsequently verified the role of the P2X7 receptor by using of a specific P2X7 agonist (Bz-ATP) and a selective P2X7 receptor antagonist. The effect of the antagonist on cell metabolism was investigated in terms of its ability to block P2X7 receptor-mediated ion flux, intracellular Ca<sup>2+</sup> increase, and YoPro1 uptake.

## **2.3 Identification of drug-induced adverse liver effects on human HepG2 cells**

I used the multiparametric, chip-based cytosensor system to determine physiological changes in a cell line overexpressing the drug efflux transporter P-gp (110) (section 2.1) and for the identification of metabolic changes after exogenous application of ATP to cells overexpressing the purinergic P2X7 receptor (section 2.2). In light of the sensitivity of such a

cytosensor system to deviations in the physiological parameters, the question arises as to whether this approach might be adapted to monitor the early onset of drug-induced hepatocellular damage *in vitro*.

In view of the above, the aim of this thesis project was to implement and validate a cell-based multiparametric cytosensor system to characterise DILI. For this approach, eight prototypic drugs known to be hepatotoxic in therapeutic use were investigated with respect to their toxicological potential on human hepatocarcinoma-derived HepG2 cells. The distinct differences in the mechanisms of hepatotoxicity and liver pathology were thoroughly considered during the selection of these eight drugs. The HepG2 cell line is frequently used as a model of liver cells (111, 112). In an additional control experiment, the metabolic activity of HepG2 cells was assessed and results derived from the mass spectrometry analysis were compared to previously published data (113-115). Emphasis was placed on the assessment of mitochondrial respiration, metabolic activity and/or morphological changes and cell adhesion as major markers of toxicity. Based on the nature of cellular response, different types of effects, including necrosis-like-, apoptosis-like cell death, and metabolic or oxidative stress, were discriminated.

### **3 MATERIAL AND METHODS**

#### **3.1 Materials**

All chemicals were obtained in the highest available purity from Sigma-Aldrich (Buchs, Switzerland) and LGM Pharma (Boca Raton, Florida, US) unless otherwise indicated. Reference chemicals and drugs used in the studies are listed in Table 1. An overview of the cell culture media, supplements, and adjuvant used is given in Table 2. The P2X7 receptor antagonist, amiodarone, cyclosporine A, doxorubicin, isoniazide, and methotrexate were used as stock solutions in dimethyl sulfoxide (DMSO). Organic solvents concentrations did not exceed 1.0% (v/v) in any of the experiments. The MTT (3-(4, 5-dimethylthiazol-2-yl)-2, 5-diphenyltetrazolium bromide) stock solution was prepared in phosphate buffered saline at a concentration of 5 mg/mL, and was then sterile-filtered and stored at 4 °C in the dark. Aside from common laboratory material, all materials used, cell lines, buffers, and solutions are mentioned in the related chapter.

**Table 1. An overview of the compounds (i.e. drugs, antagonists, and agonists) investigated in the projects**

Project	Compound	Molecular weight	Solvent for stock solution	Concentrations used in experiments with the sensor system
P-glycoprotein (ABCB1)	Caffeine	194.2	Water	10 $\mu$ M
	Daunorubicin HCl	564.0	DMSO	1.0 $\mu$ M
	Elacridar	563.6	DMSO	0.1 $\mu$ M
	Fexofenadine HCl	538.1	DMSO	1.0 $\mu$ M
	Loperamide HCl	513.5	DMSO	10 $\mu$ M
	Propranolol HCl	295.8	Water	10 $\mu$ M
	Quinidine HCl	378.9	Water	10 $\mu$ M
	Verapamil HCl	491.1	Water	1.0, 5.0, 15, 50 $\mu$ M
P2X7 receptor	ATP <sup>a</sup>	507.2	Water	0.005 - 5.0 mM
	Bz-ATP <sup>a</sup>	715.4	Water	1.0, 10, 50, 100 $\mu$ M
	P2X7 receptor antagonist	455.5	DMSO	10 $\mu$ M
Liver Toxicology	Acetaminophen	151.2	Water	0.01, 0.1, 1.0, 5.0, 10 mM
	Amiodarone HCl	681.8	DMSO	1.0, 5.0, 10, 15, 30 $\mu$ M
	Cyclosporin A	1'202.6	DMSO	1.0, 3.0, 10, 30, 60 $\mu$ M
	Doxorubicin HCl	580.0	Water	1.0, 5.0, 10, 25 $\mu$ M
	Isoniazide	137.1	Water	0.1, 0.5, 1.0, 3.0, 5.0 mM
	Methotrexate hydrate	454.4	DMSO	1.0, 10, 50, 100, 200 $\mu$ M
	D-Sorbitol	182.2	Water	0.001, 0.01, 0.1, 1.0, 5.0 mM
	Terfenadine	471.7	DMSO	5.0, 25 $\mu$ M
	Valproic acid sodium salt	166.2	Water	0.5, 1.0, 3.0, 5.0, 10 mM

<sup>a</sup> Stock solution adjusted to pH 7.4 using sodium hydroxide.



### 3.2 Cell culture

Cell culture work was carried out under standard biosafety level 2 conditions (116). Cell handling was performed in a microbiological safety cabinet (Skan, Allschwil, Switzerland) to reduce risk of contamination. All freshly prepared primary cells and cell lines grow as adherent cells in standard 75 cm<sup>2</sup> tissue culture flasks (TPP AG, Trasadingen, Switzerland). With the exception of the primary rat cortical cells, all cells used were passaged by trypsination twice a week using a dilution factor ratio of 1:5 to 1:20. For this procedure, cells were rinsed with 15 mL pre-warmed PBS, followed by cell detachment with 0.25% trypsin-EDTA and dilution in the appropriate culture medium. Cell viability was analysed by a Vi-Cell XR cell viability analyser (Beckman Coulter, Krefeld, Germany), using a trypan blue exclusion test. Cells showing cell viability below 80% were rejected for use in experiments. The amount of cells used for experiments was calculated based on the viable cells. For optimal cell attachment, some cells require surface coating with poly-L-lysine, poly-D-lysine or fibronectin prior to experiments, according to the manufactures protocols. Briefly, surfaces were disinfected using 70% (v/v) aqueous ethanol, rinsed twice with PBS, and incubated for 3 h with the coating agents at 37 °C in a humidified atmosphere containing 5% CO<sub>2</sub>. Coating agents were removed and surfaces were rinsed with PBS prior to the cell suspension being dispensed.

**Table 2. An overview of the media, supplements, and adjuvants used in the cell culture.**

Media, Supplements, Adjuvants	Catalogue number	Supplier
DMEM containing GlutaMAX™	21885	Life technologies™, Basel, Switzerland
Neurobasal™ medium	21103	
Medium 199 containing GlutaMAX™	41150	
MEM containing GlutaMAX™	21090	
MEM (10x)	21430	
Medium 199 (10x)	21180	
GlutaMAX™ Supplement (200 mM)	35050	
L-Glutamine 200 mM (100x)	25030	
Geneticin (G418), selective antibiotics (50 mg/mL)	10131	
Penicillin/streptomycin solution (10 kUnits/mL penicillin and 10 mg/mL streptomycin)	15140	
Sodium pyruvate (100 mM)	11360	
Hanks`balanced salt solution (HBSS) (10x)	14065	
Hepes buffer solution (1 M)	15630	
Non-essential amino acids (100x)	11140	
B-27 supplement (50x)	17504	
Trypsin-EDTA (0.25% Trypsin, 1 mM EDTA)	25200	
Fluo-4-AM™, (1.0 mM solution in DMSO)	F14202	
Heat-inactivated foetal bovine serum	A15-104	PAA Laboratories, Pasching, Austria
Foetal calf serum	2-01F30-1	BioConcept, Allschwil, Switzerland
Penicillin/streptomycin solution (10 kUnits/mL penicillin and 10 mg/mL streptomycin) for mouse microglia BV2 cells	4-01F00-H	
Colchicine (10 µg/mL)	L6211	Biochrom AG, Berlin, Germany

**Table 2 (continued). An overview of the media, supplements, and adjuvants used in the cell culture.**

Media, Supplements, Adjuvants	Catalogue number	Supplier
Poly-D-Lysine (0.01%)	P6407	Sigma, Buchs, Switzerland
Poly-L-Lysine (0.01%)	P4707	
Phosphate buffered saline (PBS), without Ca <sup>2+</sup> and Mg <sup>2+</sup>	D8537	
Fibronectin from bovine plasma (1.0 mg/mL)	F1141	
Papain (20 Units/mg protein)	LK003178	Worthington, Lakewood, NJ, US
EBM <sup>®</sup> medium	CC-3121	Lonza Ltd., Walkersville, MD, US
EGM <sup>®</sup> SingleQuots	CC-4133	
Bovine brain extract (BBE) (9.0 mg/mL)	CC-4098	
Hydrocortisone (1.0 mg/mL)	CC-4036C	
Gentamicin/amphotericin solution (30 mg/mL gentamicin, 15 µg/mL amphotericin-B)	CC-4081C	
Human embryonic growth factor (3.0 mg/mL)	CC-4107C	

### 3.2.1 LLC-PK1 and L-MDR1 cells

The human P-gp overexpressing cell line L-MDR1 derived from the porcine kidney epithelial cell line LLC-PK1 was obtained under license from The Netherlands Cancer Institute (Amsterdam, The Netherlands). Cells were maintained under standard cell culture conditions (section 3.2) and described previously (39, 40). Cells were cultivated at passage numbers 12 – 26 in 75 cm<sup>2</sup> cell culture flasks at 37 °C in Medium 199 with 2.0 mM GlutaMAX supplemented with 50 IU/mL penicillin, 50 µg/mL streptomycin and 10% (v/v) foetal bovine serum in a humidified atmosphere containing 5% CO<sub>2</sub>. L-MDR1 cells were subcultured in the presence of 150 ng/mL colchicine to maintain P-gp expression levels. Colchicine was omitted from medium 12 h prior to use in the experiments to avoid the development of other drug resistance mechanisms that could modify the action of P-gp (117). It has been shown that,

once in culture and induced, cells express constant levels of P-gp for up to at least 15 passages (118).

### **3.2.2 HUVEC cells**

Human umbilical vein endothelial cells were obtained from Lonza (CC-2517, Walkersville, MD, US) and maintained under standard cell culture conditions. Cells were maintained in EBM® medium with Clonetics EGM® SingleQuots supplemented with 2.0% (v/v) heat-inactivated foetal bovine serum, 1.0 µg/mL hydrocortisone, 36 µg/mL bovine brain extract, 3.0 ng/mL human embryonic growth factor, 30 µg/mL gentamicin, 15 ng/mL amphotericin-B, 50 IU/mL penicillin and 50 µg/mL streptomycin at 37 °C in a humidified atmosphere containing 5% CO<sub>2</sub>.

### **3.2.3 Human mononuclear blood cells**

For the preparation of fresh mononuclear cells (lymphocytes, monocytes and macrophages), 30 mL human blood containing 10% (v/v) citrate as anticoagulant were taken and mononuclear cells were isolated using a polymorphprep™ (Axis-Shield, Oslo, Norway) density centrifugation kit according to the manufacturer's protocol. Briefly, in a 50 mL reaction tube, 15 mL of human blood were layered on 17 mL of the polymorphprep™ buffer (Axis-Shield, Oslo, Norway) and centrifuged at 500 *g* for 30 min at 22 °C. After gradient centrifugation, different bands of blood cells appear. The mononuclear cell band was transferred to a new 50 mL reaction tube and diluted with one equivalent of 0.45% (v/v) aqueous sodium chloride solution to restore physiological osmolarity. The solution was again centrifuged at 450 *g* for 18 min at 20 °C and the supernatant removed. Subsequently, the

cell pellet was reconstituted in 0.9% (v/v) aqueous sodium chloride solution and again centrifuged at 400 g for 10 min at 20 °C. Supernatant was removed and remaining red blood cells were hypertonically lysed by adding 9.0 mL demineralised water for 17 s and then centrifuged at 300 g for 10 min at 20 °C. The cell pellet after the last centrifugation step was reconstituted in 20 mL PBS and cell viability and concentration analysed by a Vi-cell XR cell viability analyser. Cell concentration was adjusted to  $2 \times 10^6$  cells/mL and a 250  $\mu$ L-aliquot of this cell suspension was dispensed into a 96-well plate and immediately used for experiments.

#### **3.2.4 P2X7 overexpressing HEK293 cells**

The human P2X7 (HEK-hP2X7) cell line generation was performed in the laboratories of Actelion Ltd. (Allschwil, Switzerland) according to established molecular cloning protocols. Specifically, RNA was extracted from human whole blood using the Qiagen RNeasy®kit (Qiagen, Hombrechtikon, Switzerland) according to the manufacturer's instructions. Subsequently cDNA was generated (Superscript®II, Life technologies, Basel, Switzerland) and the human P2X7 gene (genebank ref. BC011913) was amplified and ligated into a pcDNA3.1 (+) vector. HEK293 cells (ATCC CRL–1573, Manassas, VA, US) were transfected with the pcDNA3.1 (+)hP2X7 plasmid using lipofectamine™2000 transfection reagent (Life Technologies, Basel, Switzerland) according to the manufacturer's instructions. Following a 24 h-exposure to DNA, cells were trypsinised and re-seeded at low density in the presence of 0.25 mg/mL geneticin (G418). Geneticin resistant cells were then selected during two consecutive rounds of cloning by serial limiting dilution with visual inspection. Individual clones were screened for P2X7 expression by applying ATP and recording the resulting uptake of YoPro1. A specific cell clone was chosen based on RNA and protein expression.

Cells were cultivated at passage numbers 1 – 30 in 75 cm<sup>2</sup> cell culture flasks at 37 °C in DMEM with 2.0 mM L-glutamine, supplemented with 50 IU/mL penicillin, 50 µg/mL streptomycin and 10% (v/v) heat-inactivated foetal calf serum in a humidified atmosphere containing 5% CO<sub>2</sub>. HEK-hP2X7 cells were cultured in the presence of 0.25 mg/mL geneticin (G418) to maintain P2X7 expression levels. It has been shown that, once in culture and induced, cells express constant levels of P2X7 for up to at least 30 passages.

### **3.2.5 Mouse microglia BV2 cells**

A mouse microglia BV2 cell line for patch-clamp experiments was cultured under standard cell culture conditions. The cells were maintained in 75 cm<sup>2</sup> cell culture flasks at 37 °C in DMEM with 2.0 mM GlutaMAX supplemented with 50 IU/mL penicillin, 50 µg/mL streptomycin and 10% (v/v) foetal calf serum in a humidified atmosphere containing 5% CO<sub>2</sub>.

### **3.2.6 Primary Wistar rat cortical cells**

Freshly prepared cortical cultures originated from Wistar rat embryos 18 days post-gestation. After enzymatic cell dissociation with papain, the cells were resuspended and diluted to 3 x 10<sup>5</sup> cells/mL in neurobasal medium supplemented with 0.5 mM L-glutamine, 2.0% (v/v) B27, 50 IU/mL penicillin and 50 µg/mL streptomycin. Fifty µL-aliquots of this suspension were dispensed into poly-D-lysine-coated 384-well micro BioCoat™ plates (Becton Dickinson, Basel, Switzerland) and incubated at 37 °C for a period of about 8 days in a humidified atmosphere containing 5% CO<sub>2</sub>.

### **3.2.7 Human hepatocarcinoma-derived HepG2 cells**

The human epithelial hepatocarcinoma-derived cell line HepG2 was obtained from the American Type Culture Collection (ATCC HB-8065, Rockville, MD, US) and was maintained under standard cell culture conditions (see section 3.2) and as described previously (119). Briefly, the HepG2 cells were cultivated at passage numbers 3 - 15 in 75 cm<sup>2</sup> cell culture flasks at 37 °C in MEM with 2.0 mM GlutaMAX, supplemented with 1.0 mM sodium pyruvate, 1.0% (v/v) non-essential amino acids, 50 IU/mL penicillin, 50 µg/mL streptomycin and 10% (v/v) heat-inactivated foetal bovine serum in a humidified atmosphere containing 5% CO<sub>2</sub>.

### 3.3 Methods

#### 3.3.1 Real-time monitoring of cell physiological parameters

For the real-time measurements of physiological parameters, two cell-based sensor systems were used. The Bionas®1500 hosted one cell-coated chip for analysis, whereas the Bionas®2500 was able to measure six cell-coated chips simultaneously (Figure 7). The systems were used as described previously (110) with project related modifications (Table 3).

**Table 3. Conditions of the assays using the multiparametric cytosensor system**

Project	Bionas system	Cells per sensor chip [ x 10 <sup>5</sup> ]	Chip coating	Effective chamber volume [μL]	Flow rate [μL/min]	Stop cycle [min]	Go cycle [min]	Compound exposure time [min]	Cell line / assay medium composition
P-glycoprotein (ABCB1)	1500	0.75 - 1.5		5.7	252	2	2	20	<b>LLC-PK1; L-MDR1</b> Medium 199 (21180), 2.0% FBS, 0.3 mM GlutaMAX, 50 IU penicillin, 50 μg/mL streptomycin
P2X7 receptor	1500	2.0	Fibronectin	1.4	63	4	3	21	<b>HEK293; HEK-hP2X7</b> MEM (21430), 0.1% FBS, 25 IU penicillin, 25 μg/mL streptomycin
Liver Toxicology	2500	2.0		5.7	56	3	3	1`140	<b>HepG2</b> MEM (21430), 0.1% FBS, 1 mM sodium pyruvate, 1% NEAA, 25 IU penicillin, 25 μg/mL streptomycin

Prior to experiments, cells were detached by trypsination for approx. 4 min and cell viability analysed by a Vi-Cell XR analyser. Cells were then diluted in culture medium to reach the required cell amount by adding 0.35 mL of these cell suspensions to the pre-warmed sensor chips and incubating for at least 16 h prior to use. The core of the system consists of the



---

silica-sensor chip SC1000 (Figure 8) containing ion sensitive field effect transistor and Clark-type sensors for the measurement of dynamic changes of acidification and oxygen consumption. Cell adhesion was monitored by means of impedance measurements using an interdigitated electrode structures circuit. The effective volumes of the reaction chamber (i.e. the volume of the space between the surface of the sensor chip and the chamber lid) were either 1.4  $\mu\text{L}$  or 5.7  $\mu\text{L}$  (Table 3) and were determined by the distance (50  $\mu\text{m}$  or 200  $\mu\text{m}$ ) between the flow head and the sensors chip surface (Figure 7). Cells were seeded directly onto the silica-sensor chip with or without prior surface coating according to the type of cells used in the experiments (Table 3). During analysis, assay medium (Table 3) was delivered to the cells at a constant flow rate (Table 3). The supply of assay medium was interrupted periodically, as described previously (110). These stop/go cycles were carried out throughout the entire experiment (divided into periods of medium exchange and periods without medium flow), during which the parameters were recorded. The duration of the stop and go cycles were project dependent and are defined in Table 3. During these “stop phases”, metabolic breakdown products of the cells (lactate and carbonate) were released into the assay medium and were allowed to accumulate, resulting in a change in extracellular pH (108). Extracellular oxygen concentrations were monitored in parallel. Initial rates of extracellular acidification and respiration were calculated by changes to the slope in the stop phases and a linear regression analysis. Recorded data were normalised to a reference value, which represented the baseline signal of a cell-coated chip prior to treatment with the compound. Impedance measurements were carried out continuously to monitor cell adhesion and thus cell morphology, viability, and membrane functionality (109). As a control, 0.2% Triton X-100 was added to the cells at the end of each experiment to induce cell membrane destruction and thus detachment of cells from the surface of the sensor chip.

The signals that were generated under these conditions were used to provide a reference signal from the cell-free sensor surface (0% baseline value) (109). These relative signals relate to a 0% control value of an empty sensor chip and to a 100% reference value representing the baseline signal of a cell-coated chip prior to compound treatment.

The initialisation procedure of the sensor system prior to each experiment was carried out routinely, whereat the supply lines of the system were conditioned in a three-step procedure: disinfection with 70% (v/v) aqueous ethanol, flushing with an excess of PBS and rinsing with low-buffered assay medium. For the measurements, an assay medium with low buffer capacity was required (Table 3). Assay media were prepared from ten-fold concentrated stock media and the concentration of penicillin and streptomycin was halved, due to the reduced foetal bovine serum content and therefore more unbound antibiotics in the medium. The concentration of foetal bovine serum in the assay media did not exceed 2.0% (v/v) to keep the buffer capacity of the FBS as low as possible. The assay media contained neither HEPES nor  $\text{NaHCO}_3$  and were adjusted to pH 7.4 using sodium hydroxide. Before use, the integrity of the cell monolayer covering the surface of the microsensor chip was verified using a Motic DM-39C reflected-light microscope (Motic Group Ltd., Hong Kong, China). Cell monolayers with a cellular confluence below 80% were rejected for use.

Signals from the metabolic sensor chip were then recorded after a stabilisation phase of at least 3 h to acquire a constant baseline signal-to-noise ratio from the different sensors. Subsequently, treatment of compounds dissolved in assay medium (adjusted to pH 7.4 with sodium hydroxide) or drug-free running medium (control) was initiated. For those compounds for which stock solutions were prepared in other media, an equal amount of DMSO was added to the assay medium for initial stabilisation phase to avoid the detection of effects from DMSO. All compounds and their individual concentrations in the

---

multiparametric cytosensor system assays are listed in Table 1. Raw data were recorded by all sensors at intervals of 10 s to obtain one raw data point per ten seconds. From these data points, initial rates of acidification and cellular respiration were derived by linear regression. Compound treatment phases were followed by compound wash-out periods for detection of regeneration processes. After the experiment, impedance values were recorded following solubilisation of cells by 0.2% (v/v) Triton X-100. This control is used to compare cell monolayer integrity during the experiment with a reference value obtained from a cell-free sensor chip at the end of the experiment. This value represents, by definition, the 0% reference control value.

### **3.3.2 Western blot detection of P-glycoprotein**

A Western blot analysis was carried out to confirm the presence of P-gp in L-MDR1 and its absence in parental LLC-PK1 cells. LLC-PK1 (passage no. 25) and L-MDR1 (passage no. 14) cells were harvested by trypsination (5 min) at approx. 80% confluence, viability was determined by a Vi-cell XR analyser, and diluted in PBS to reach a final cell concentration of  $6 \times 10^5$  cells/mL. The cell suspension was transferred in a pre-cooled 2 mL S-homogeniser (Sartorius, Göttingen, Germany), placed on ice, and homogenised for fifteen cycles. The separation of the cell proteins was achieved by sodium dodecylsulphate-polyacrylamide gel electrophoresis (SDS-PAGE). For the SDS-PAGE analysis, 12  $\mu$ L of the homogenised cell suspension was mixed with 3  $\mu$ L loading buffer (2.3% sodium dodecylsulphate, 72.5 mM Tris(hydroxymethyl)-amminomethane (pH 6.8), 17.3% glycerol, 10 mg/mL bromophenol blue) and incubated for 5 min at 95 °C for protein denaturation. The samples were subsequently transferred to a NuPAGE® 4 - 12% Bis-Tris precast gel (Life technologies, Basel, Switzerland) for protein electrophoresis. The SDS-PAGE was carried out in MOPS

---

(4-morpholinepropanesulfonic acid) buffer (Life technologies, Basel, Switzerland) using the XCell-SureLock™ aperture (Life technologies, Basel, Switzerland) according to the manufactures protocol. In addition to the samples, 5  $\mu$ L of the Precision-Plus™ protein standard (BioRad Laboratories, Hercules, California, US) was added as a molecular weight marker. A current of 170 V was applied for approx. 1 h to the SDS-PAGE for electrophoretic protein separation. Subsequently the proteins were transferred to a Protran® nitrocellulose (NC) membrane (0.45  $\mu$ m pore size, Schleicher & Schuell, Dassel, Germany) by means of an iBlot®Dry blotting system (Life technologies, Basel, Switzerland) according to the manufactures instruction protocol. All regions of the NC membrane, that did not containing proteins were saturated by incubation of the NC membrane with blocking milk (10% skim milk powder, 1.0% bovine serum albumin, 150 mM NaCl, 10 mM Tris-HCl (pH 7.4) and 0.3% Tween 20) over night at 4 °C. The primary mouse monoclonal MDR1-G1 (sc-13131, SantaCruz Biotechnology, Santa Cruz, CA, US) and the anti- $\beta$ -actin (A1978, Sigma, Buchs, Switzerland) antibodies were added to the blocking buffer (1:1`000 each, v/v) and incubated at room temperature under gentle agitation for 1 h. After three washings with western-wash buffer (3.0 g/L bovine serum albumin, 150 mM NaCl, 10 mM Tris-HCl (pH 7.4), 0.05% Triton X-100) for 10 min each step, the secondary antibody (goat-anti-mouse IgG-HRP, cat. no. sc-2005, SantaCruz Biotechnology, Santa Cruz, California, US) was added (1:5`000, v/v) to the blocking milk and then applied to the NC membrane. After 1 h incubation under gentle agitation and room temperature the NC membrane was washed three times with Western-wash buffer, as described above. For the analysis of the proteins, the NC membrane was incubated for 1 min with a 1:1 (v/v) mixture of the Western-lightning-ECL™ chemiluminescence reagents (NEL101 and NEL102, PerkinElmer, Wellesley, MA, US) and transferred to a photosensitive Kodak BioMax™ Light film (Kodak, Rochester, NJ, US). The

---

film was exposed to the NC membrane for 1 min at room temperature and then developed by the Curix 60 tabletop processor (Agfa, Mortsel, Belgium).

### **3.3.3 Metabolic activity of human mononuclear blood cells**

Production of cellular hydrogen peroxide ( $H_2O_2$ ) was analysed by the Amplex<sup>®</sup>Red assay obtained from Life technologies (Basel, Switzerland) after application of the P2X7 agonists (ATP or Bz-ATP) to human mononuclear blood cells. Oxidation of glucose by glucose oxidase resulted in the generation of hydrogen peroxide, which is coupled to the conversion of the Amplex<sup>®</sup>Red reagent to fluorescent resorufin in the presence of horseradish peroxidase. Briefly,  $5 \times 10^5$  human mononuclear blood cells (section 3.2.3) were placed in the wells of a 96-well plate and incubated with 50  $\mu$ M Amplex<sup>®</sup>Red and 0.1 U/mL horseradish peroxidase for 0.5 h at 37 °C in Krebs Ringer phosphate solution (145 mM NaCl, 5.7 mM sodium phosphate, 4.9 mM KCl, 0.5 mM  $CaCl_2$ , 1.2 mM  $MgSO_4$ , and 5.5 mM glucose), protected from light. After adding ATP (0 – 4.0 mM) or Bz-ATP (0 – 400  $\mu$ M) to the cells, the fluorescence was quantified by means of a microplate reader (Synergy MX, BioTek<sup>®</sup>, Luzern, Switzerland) at excitation and absorbance wavelengths at 550 nm and 600 nm, respectively. Background fluorescence, determined using a reaction without mononuclear cells, was subtracted from each value. From these preliminary results, the optimal ATP concentration was determined as 1.0 mM and this was used again for the determination of hydrogen peroxide release, in the presence of the selective P2X7 receptor antagonist (0 - 25  $\mu$ M).

### 3.3.4 Dynamic mass redistribution assay

The Corning Epic<sup>®</sup> system (Corning Inc., Tewksbury, MA, US) was used, consisting of a temperature controlled unit, an optical detection unit, and an on-board robotic liquid handling device. The Epic<sup>®</sup> system measures changes within the cell monolayer in the index of refraction, which can be ligand-induced upon mass redistribution. HUVEC cells (section 3.2.2) were detached by trypsination for approx. 5 min and analysed by a Vi-cell XR cell viability analyser. Cells were then diluted in culture medium to reach a final concentration of  $4 \times 10^5$  cells/mL medium. A 30  $\mu$ L-aliquot of this cell suspension was transferred to a fibronectin-coated 384-well Epic<sup>®</sup> microplate containing 10  $\mu$ L HUVEC medium (section 3.2.2) and incubated at 37 °C for 20 h in a humidified atmosphere containing 5% CO<sub>2</sub> to achieve a confluent monolayer. Each microplate well bottom contained a resonant waveguide grating biosensor. Prior to the experiment, the medium was replaced by 30  $\mu$ L HBSS buffer supplemented with 20 mM HEPES and 0.06% (w/v) bovine serum albumin and kept for 2 h in the Epic<sup>®</sup> reader at a constant temperature of 26 °C for equilibration. The sensor microplate was then analysed and an initial baseline curve was recorded. Subsequently, the ATP solution in the assay buffer was dispensed into the microplate at a concentration range of 0 to 5.0 mM and the dynamic mass redistribution was monitored for 4`000 s. Control experiments were performed in the absence of ATP under otherwise identical conditions. In these controls, the volumes of the ATP-containing solutions were replaced by assay buffer.

### 3.3.5 YoPro1 uptake analysis

Uptake of membrane-impermeable fluorescent dyes, such as YoPro1, is a hallmark of early downstream signalling by the P2X7 receptor and was used as a means of identifying the P2X7 receptor antagonists in human embryonic kidney cells expressing the P2X7 receptor at high levels (120, 121).

HEK-hP2X7 cells (section 3.2.4) were detached by trypsination (0.5 ml per 75 cm<sup>2</sup> dish), which lasted two minutes and were analysed by a Vi-cell XR cell viability analyser. Cells were then diluted in medium (section 3.2.4) without geneticin to a final concentration of  $2 \times 10^5$  cells/mL and a 50  $\mu$ L-aliquot of this cell suspension was transferred to a poly-L-lysine pre-coated black-wall, clear-bottom 384-well-plate and incubated 48 h at 37 °C in a humidified atmosphere containing 5% CO<sub>2</sub>. Medium was removed from cells and assay buffer containing 0.5  $\mu$ M YoPro1 was added into the wells. Solutions of the antagonist were prepared by serial dilutions of a 10 mM DMSO solution into PBS. Each concentration was represented in duplicate. For IC<sub>50</sub> measurements, ten concentrations were measured (10  $\mu$ M being the highest concentration followed by nine serial dilution steps 1:3, v/v). The cells were incubated with the selective P2X7 receptor antagonist and ATP at a final concentration of 250  $\mu$ M for 90 min. During this period, four time points were taken. Each time point comprised the average of several measurements made within a few seconds. Fluorescence was measured in the FLIPR®-Tetra (fluorescent imaging plate reader; Molecular Device, Sunnyvale, CA, US) using the filters appropriate for YoPro1 fluorescence (excitation 485, emission 530). The FLIPR®-Tetra was equipped with Molecular Devices Screen Works system control software to define and run experimental protocols. The affinity of the antagonist was determined at the EC<sub>50</sub> concentration of the agonist (250  $\mu$ M ATP for HEK293 cells

---

overexpressing human recombinant P2X7 receptor). For IC<sub>50</sub> measurements, the maximum intensity is plotted against the concentration of the antagonist to determine IC<sub>50</sub> values.

### 3.3.6 Fluo-4-AM calcium measurements

Calcium transients were determined using a Tetra high-throughput fluorescence imaging plate reader (Molecular Devices, Sunnyvale, CA, US) at room temperature. Wistar rat primary cortical cells (section 3.2.6), at day eight in culture, were loaded with 1.0 μM Fluo-4-AM in HBSS (pH 7.4) containing 20 mM HEPES. Cells were washed once with HBSS 10 min before recording. After a 15 min pre-incubation with 0.01 - 10 μM of the selective P2X7 receptor antagonist, the P2X7 agonist Bz-ATP was applied to the cells at a final concentration of 250 μM. In control incubations, Bz-ATP was replaced by DMSO in equal amounts used in the Bz-ATP incubations. Data points were collected every one second and analysed using the plate reader specific software (Molecular Devices, version 2.0.0.24, Sunnyvale, CA, US) and IGOR software (IGOR Pro, version 6.12A, Oregon, US).

### 3.3.7 Electrophysiology

For patch-clamp experiments, mouse microglia BV2 cells (section 3.2.5) were analysed in the whole cell patch-clamp configuration (122). Patch electrodes were filled with intracellular buffer containing 120 mM KF, 20 mM KCl, 1.0 mM EGTA (ethylene glycol-bis(aminoethyl ether)-tetraacetic acid) and 10 mM HEPES adjusted to pH 7.2 with potassium hydroxide. Recordings were done at room temperature in external buffer containing 147 mM NaCl, 2.0 mM KCl, 0.3 mM CaCl<sub>2</sub>, 10 mM HEPES and 12 mM D-glucose adjusted to pH 7.4 with sodium hydroxide. At a constant holding potential of -70 millivolt, 100 μM Bz-ATP were



---

applied in the absence or presence of different concentrations of the selective P2X7 receptor antagonist by a computer-controlled application system. Agonist-induced steady-state currents were corrected for leakage, and concentration-response curves were fitted to averaged current amplitudes derived from 3 – 4 cells.

### **3.3.8 MTT cell viability assay**

HepG2 cells were seeded in 96-well plates at a density of  $5 \times 10^4$  cells/well and were cultured as described above (section 3.2.7). Twenty-four hours after seeding, medium was removed and 100  $\mu$ L aliquots of cell culture medium containing the test compounds were added to each well in triplicate. Control cells were incubated in the presence of 1.0% (v/v) DMSO (100% viability control). After 24 h, cell culture medium was replaced by 100  $\mu$ L cell culture medium containing 10% (v/v) MTT stock solution. Cells were incubated for additional 2 h at 37 °C. In a final step, the cell culture medium was discarded and reduced MTT, which is present as water-insoluble formazan dye crystals, was dissolved by adding 20  $\mu$ L of 3.0% (v/v) sodium dodecylsulphate solution in water, and 100  $\mu$ L of a 40 mM hydrochloric acid in isopropanol. Optical density was measured at 550 nm using a Spectramax<sup>®</sup> M2 plate reader (Molecular Devices, Sunnyvale, CA, US).

### **3.3.9 Metabolic activity of human hepatocarcinoma-derived cells, HepG2**

Acetaminophen and amiodarone were incubated with human hepatocarcinoma-derived HepG2 cells (section 3.2.7) to confirm activity in phase I and phase II metabolism. Since the metabolic pathways and the metabolites of these two compounds in the liver were already

---

elucidated, these compounds were used as prime examples to confirm metabolic activity of HepG2 cells.

For the determination of metabolic activity of HepG2 cell, 19 h-incubations with amiodarone and acetaminophen were performed. HepG2 cells were detached by trypsination for 5 min and analysed by a Vi-Cell XR cell viability analyser. Cells were then diluted in culture medium to a nominal density of  $1.25 \times 10^6$  viable cells/mL and 400  $\mu$ L aliquots of this suspension were dispensed into 24-well plates and incubated at 37 °C for a period of about 20 h in a humidified atmosphere containing 5% CO<sub>2</sub> for cell attachment.

At the end of the pre-incubation period, the medium was removed from each well and replaced by 200  $\mu$ L of pre-warmed (37 °C) incubation medium containing amiodarone or acetaminophen at final concentrations of 20  $\mu$ M. Triplicate wells were sampled after 19 h of incubation by addition of 200  $\mu$ L of ice-cold acetonitrile and transfer of the entire well content into 2 mL cryovials. Samples were stored frozen at -20 °C pending analysis. Prior LC-MS analysis, samples were centrifuged at 20`800 *g* for 5 min at 4 °C and supernatant were submitted to LC-MS analysis without further treatment. Control incubations in the absence of cells were performed in parallel.

The analytical system consisted of two Shimadzu HPLC pumps LC-20AD XR (Shimadzu, Reinach, Switzerland) equipped with a membrane degasser (DGU-20A), a Shimadzu system controller CBM-20A, a Thermo Scientific (San Jose, CA, US) photodiode array detector ACCELA™, a Shimadzu autosampler model SIL-30AC, and a LTQ-Orbitrap Velo Pro™ (Thermo Electron, San Jose, CA, US).

The chromatographic separation of amiodarone and acetaminophen and their metabolites were achieved on a Phenomenex Luna®C18(2) column (250 x 4.6 mm, 5  $\mu$ m, 100 Å) at 30 °C with a flow rate of 1.0 mL/min. Mobile phases consisted of 0.1% (v/v) formic acid in water

(phase A) and acetonitrile (phase B). The autosampler temperature was set to 4 °C. The applied gradient for the separation of the test compounds and their metabolites is described below:

Time [min]	0	20	25	26	35
Phase B [%]	5	95	95	5	stop

For the analysis of parent drug and metabolites, a full scan, high resolution LTQ-Orbitrap Velo Pro™ was used (Thermo Electron, San Jose, CA, US). The analysis was performed in positive ion mode and a mass range of 100 to 1`000 *m/z*. High resolution reconstructed ion chromatograms of potential metabolites were generated using mass tolerance of 10 parts per million (ppm) and Xcalibur® software package (Version 2.1.0, Thermo Electron, San Jose, CA, US). Photodiode array detection (PDA) was used in parallel in the wavelength range of 200 to 300 nm.

### 3.3.10 Data recording, analysis and statistics

The evaluations as well as the kinetics and statistical calculations were performed using GraphPad Prism® software (Version 5.04, GraphPad Software Inc., La Jolla, CA, US), Bionas® data analyser software (Versions 1.22 and 1.66, Bionas GmbH, Rostock, Germany), OriginPro® (Version 7.5, OriginLab®, Northampton, MA, US) and Microsoft® Office Excel 2007. Each experiment was performed at least in triplicates. Results are expressed as the mean ± SEM or means with 63% or 95% confidence interval (CI). Statistical significances were estimated by unpaired t-tests and designated to *\*p < 0.05*, *\*\*p < 0.01*, and *\*\*\*p < 0.001*.

---

## 4 RESULTS

### 4.1 Identification of P-glycoprotein substrates

In this part of the thesis, the multiparametric cytosensor system (Figure 7) was used for real-time identification of P-gp substrates in human P-gp overexpressing LLC-PK1 cells (L-MDR1). The cells used in the study were preliminarily analysed to assess the expression level of P-gp using Western blot analysis technique.

#### 4.1.1 P-glycoprotein levels in LLC-PK1 and L-MDR1 cells

The level of P-gp in parental LLC-PK1 and human MDR1-transfected cells (L-MDR1) was determined by Western blot detection. LLC-PK1 cells in culture at passage 25 and L-MDR1 cells in culture at passage 14 were used to assess the levels of P-gp. Cell concentrations of both cell lines were adjusted to  $6 \times 10^6$  cells/mL and subsequently homogenised. Identical aliquots of the resulting suspensions were transferred for protein separation by electrophoresis, followed by an electrical transfer of the proteins to a NC membrane. The NC membrane was incubated simultaneously with two specific monoclonal antibodies for the identification of P-gp (170 kDa) and total  $\beta$ -actin (42 kDa) levels. Beta-actin was used as a loading control and helped to determine whether the samples were loaded equally across all lanes and served to display the effective transfer of protein during Western blotting. Beta-actin is a suitable loading control due to its general expression across all eukaryotic cell types (123). Comparing the intensity of the loading control (Figure 10), the  $\beta$ -actin bands in both lanes indicate equal levels of  $\beta$ -actin in LLC-PK1 and L-MDR1 cells. An intense signal at 170 kDa was detected, indicating the presence of high levels of P-gp in the L-MDR1 cells. In

contrast to the L-MDR1 cells, no band at 170 kDa was detected in the lane with LLC-PK1 cell. The presence of high P-gp levels in L-MDR1 cells, and the absence of P-gp in LLC-PK1 cells was confirmed by the Western blot, and I therefore went on to use the cells in the multiparametric cytosensor system. Parental LLC-PK1 cells were assessed to be P-gp deficient and used as a control cell line in all further experiments of this project.

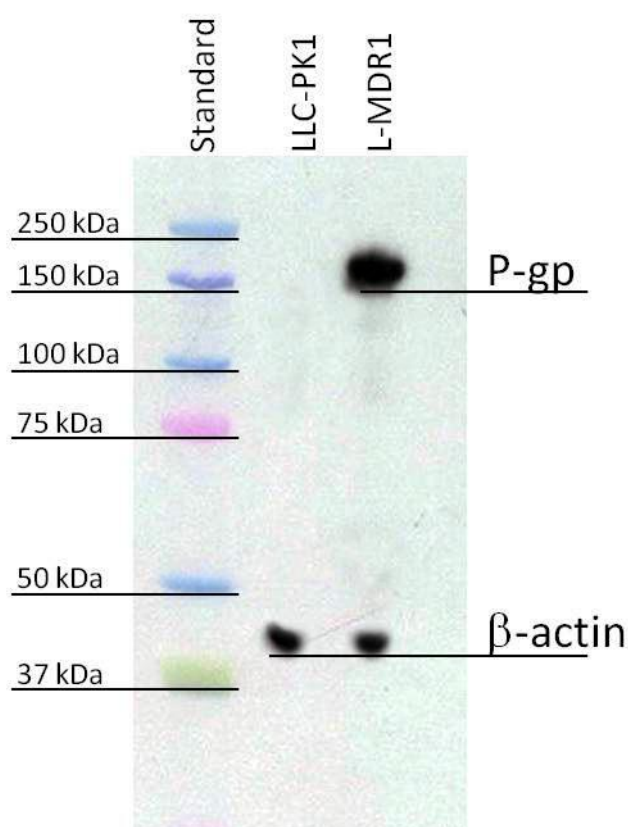


**Figure 10.** Western blot analysis of P-gp (170 kDa) levels in parental LLC-PK1 cells and human MDR1 transfected L-MDR1 cells. A 12  $\mu\text{L}$  aliquot of a cell suspension containing  $6 \times 10^6$  cells/mL was added to each lane for protein separation. After electrophoretic blotting of the proteins over to nitrocellulose membrane, P-gp was detected by a monoclonal antibody MDR1-G1 and visualised by staining with a secondary goat-anti-mouse IgG-HRP antibody, which is responsible for chemiluminescence. The  $\beta$ -actin staining was used as a loading control for better comparison of the analysed total protein levels. Position and size of the molecular weight marker are indicated.

#### 4.1.2 Real-time identification of P-glycoprotein substrates

The multiparametric cytosensor system was used as an analytical tool for the real-time monitoring of changes in extracellular acidification (pH-changes), cell respiration (oxygen

concentration) and cell adhesion (cell impedance). The sensor system assay was optimised with respect to maximal stimulation amplitudes to allow for a sensitive and reliable recording of signals. Important assay parameters included the use of an assay medium with a low buffer capacity supplemented with 2.0% (v/v) foetal bovine serum albumin. Optimal cell densities were in the range of 0.75 to  $1.5 \times 10^5$  attached cells per chip and the effective volume of the reaction chamber (i.e. the effective volume of the 200  $\mu\text{m}$  space between the surface of the sensor chip and the chamber lid) was 5.7  $\mu\text{L}$ .

During measurements, the flow of assay medium was periodically interrupted for two minutes. After each measuring period, the incubation chamber was flushed for another two minutes with assay medium before a new measuring cycle was initiated. Cell viability was measured during the entire experiment and deviations were in the range of  $\pm 20\%$  over a run time of 1`500 min for all experiments of this project. A representative pattern of the cellular viability in all experiments of this study is given in Figure 11.

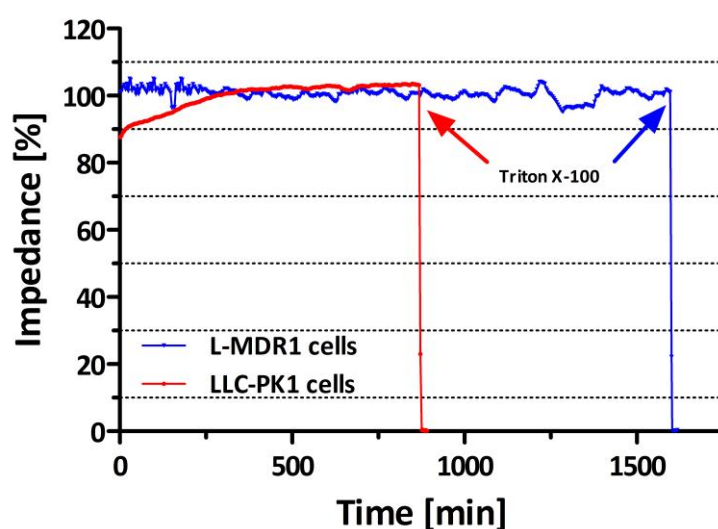


**Figure 11.** Representative pattern of impedance curves recorded with L-MDR1 cells (blue) and LLC-PK1 cells (red) up to 1`600 min compiled from two different experiments. The arrows indicate the release of death cells from the chip after Triton X-100 treatment.

In a first set of experiments, activity of P-gp was monitored in the presence of verapamil (a P-gp substrate (40, 124)) and the negative control caffeine (non-P-gp substrate (125)). Experiments were initiated as soon as a stable baseline metabolic rate was attained (100% threshold in Figure 12). Extracellular acidification rates, as well as respiration rates were identified and correlated with P-gp activation (Figure 12, phase 1 of the experiment). After a regeneration phase of approx. 100 min P-gp activity was inhibited by adding 100 nM elacridar (Figure 12, phase 2). Subsequent addition of again 10  $\mu$ M verapamil (Figure 12, phase 3) showed no further stimulatory effects, neither in extracellular acidification nor in respiration rates. Elacridar alone decreased the basal levels of extracellular acidification and respiration rates of almost 25% (Figure 12, phase 2) with subsequent stabilisation at the reduced basal activity level. At the end of the experiment (Figure 12), reference 0% signal-levels of the cell-free microsensor chip were achieved by the addition of 0.2% (v/v) Triton X-100. Cell viability was recorded during the entire experiment and was in the range of the acceptable deviations.

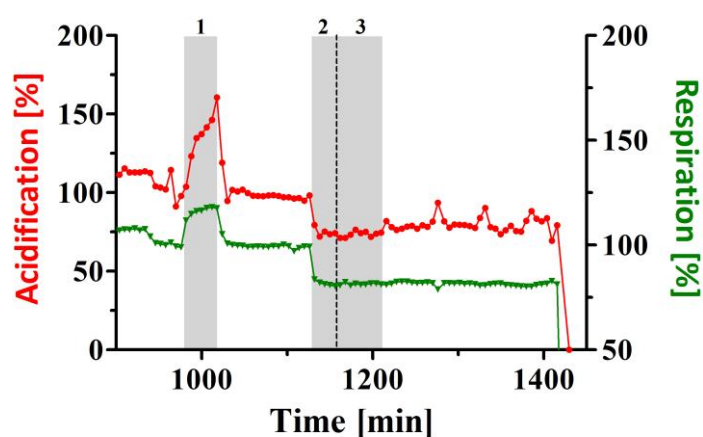


**Figure 12.** Stimulation of P-gp overexpressing L-MDR1 cells in the presence and absence of the P-gp inhibitor elacridar. Phase 1: stimulation of L-MDR1 cells with 10  $\mu$ M verapamil results in an increase in the extracellular acidification rate (red, circles) and an increase in the oxygen consumption rate (green, triangles). Phase 2: addition of 100 nM elacridar after a wash-out phase. Phase 3: addition of 10  $\mu$ M verapamil in the presence of 100 nM elacridar. At the end of the experiment: Triton X-100 (0.2%, v/v) treatment to obtain the 0% reference value of the empty sensor chip. Depicted is a representative pattern of  $n = 3$  experiments.

Different concentrations of verapamil (1.0 - 50  $\mu\text{M}$ ) were analysed using L-MDR1 cells (Figure 13, solid symbols) and the Michaelis-Menten kinetics were calculated. Stimulation of P-gp by verapamil showed saturation at high concentrations and was characterised by a  $K_M$  value of  $0.92 \pm 0.12 \mu\text{M}$  (calculated based on extracellular acidification rates (red), mean  $\pm$  SEM,  $n = 4$ ) and  $4.9 \pm 2.7 \mu\text{M}$  (calculated based on respiration rates (green), mean  $\pm$  SEM,  $n = 4$ ).  $V_{\text{max}}$  values for extracellular acidification rates ( $57.4 \pm 1.6\%$  as compared to 0% control, mean  $\pm$  SEM,  $n = 4$ ) were twice as high as the corresponding  $V_{\text{max}}$  values for respiration rates ( $25.4 \pm 5.2\%$  as compared to 0% control, mean  $\pm$  SEM,  $n = 4$ ). At substrate concentrations of 50  $\mu\text{M}$  verapamil, a sudden drop in extracellular acidification rates as well as in respiration rates was observed.

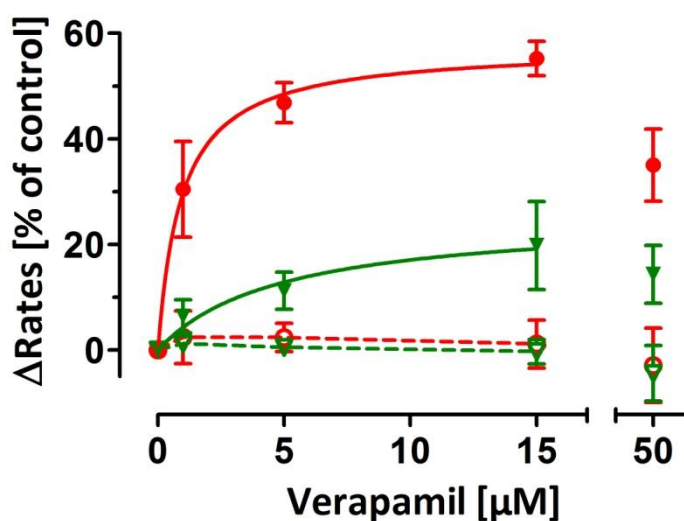


Figure 13. Stimulation of P-gp in the presence of different concentrations of verapamil. Extracellular acidification (red, circles) and oxygen consumption (green, triangles) in P-gp overexpressing L-MDR1 cells (solid symbols) and parental, LLC-PK1 (open symbols, dotted lines) cells measured as a function of increasing concentrations of verapamil. Solid lines: curve fitting using a Michaelis–Menten type kinetics model. Signals obtained at a verapamil concentration of 50  $\mu\text{M}$  were rejected for kinetic calculations, due to substrate inhibition effects. Level of significance between L-MDR1 and parental LLC-PK1 controls:  $***p < 0.001$ ,  $n = 4$ .

Cell viability was measured during the entire experiment and deviations were in the range of  $\pm 13\%$  over an experimental run time of 1`500 min. In a separate set of control experiments (Figure 13, open symbols), P-gp-deficient LLC-PK1 cells were incubated in the presence of



verapamil and did not show any stimulation effects in either extracellular acidification rates or respiration rates.

Figure 14 showed the identification of P-gp substrates using the extracellular acidification parameter because this shows higher sensitivity. Seven market drugs were analysed with respect to their potential to modulate P-gp activity. Activation of P-gp was expressed as the ratio between acidification rates measured during and immediately before stimulation of L-MDR1 cells (delta acidification rates). Propranolol, caffeine, quinidine, verapamil, and loperamide were used at a substrate concentration of 10  $\mu\text{M}$ , while daunorubicin and fexofenadine concentrations were reduced to 1.0  $\mu\text{M}$ . Both, propranolol and caffeine, known not to interact with P-gp, were used as negative controls. Compared with the two negative controls, all P-gp substrates were identified with statistical significance. Cellular impedance and thus cellular viability were not affected by the test compounds in the concentration ranges used.

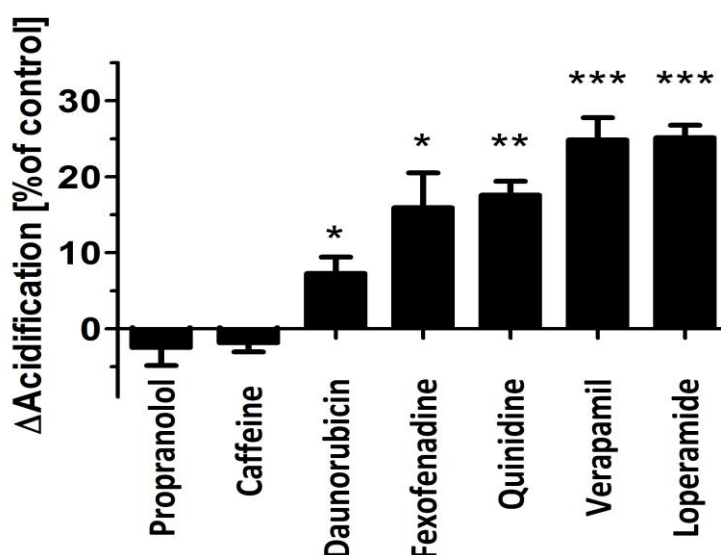


Figure 14. Identification of P-gp substrates using the multiparametric cytosensor system in combination with P-gp expressing L-MDR1 cells. Extracellular acidification rates were determined in the presence and absence of test compound (10  $\mu\text{M}$  final substrate concentration with the exception of 1.0  $\mu\text{M}$  of daunorubicin and fexofenadine). Ratios of acidification rates before and during stimulation ( $\Delta$  Acidification) are shown. Data are means  $\pm$  SEM,  $n > 3$ . Levels of statistical significant difference between acidification rates in unstimulated or stimulated cells are \* $p < 0.05$ , \*\* $p < 0.01$  or \*\*\* $p < 0.001$ .

Figure 15 showed the control experiments in LLC-PK1 cells with a set of test compounds. No effects of these test compounds were detected under the same experimental conditions.

Cell viability was again within the limit of acceptable deviations.

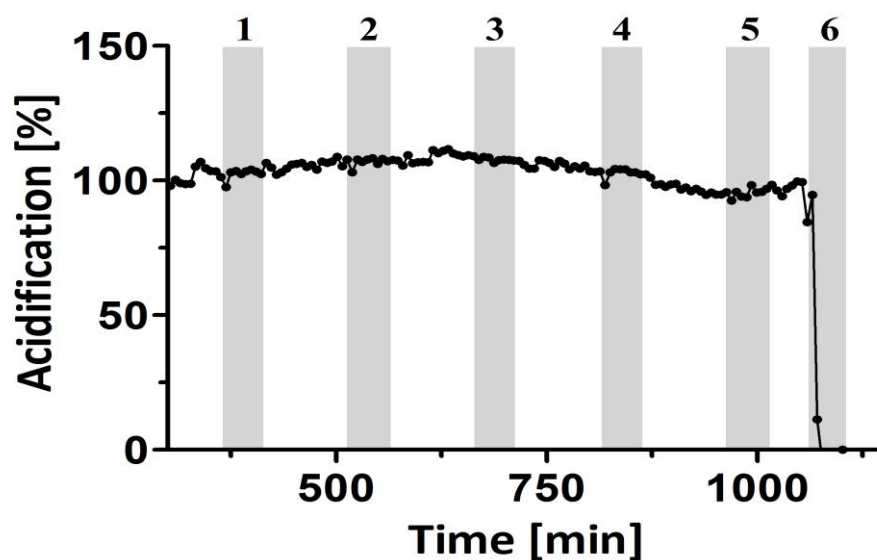


Figure 15. Control experiments demonstrating absence of stimulatory effects in parental LLC-PK1 cells. Caffeine (phase 1), verapamil (phase 2), loperamide (phase 3), quinidine (phase 4) and paclitaxel (phase 5) did not induce extracellular acidification in P-gp deficient LLC-PK1 cells. All compounds were tested at a substrate concentration of 10  $\mu$ M. Triton X-100 (0.2%, v/v) treatment (phase 6) at the end of the experiment was used to obtain the 0% reference value of the cell-free sensor chip. Depicted is a representative pattern.

#### 4.2 Purinergic P2X7 receptor mediates metabolic changes upon ATP treatment

*Metabolic activity of human mononuclear blood- and HUVEC cells after treatment with extracellular ATP was assessed.*

Many metabolic processes in cells lead to the formation of hydrogen peroxide, which can be used as a marker for metabolic activity (126). Therefore, I investigated the effect of exogenously applied ATP on the release of hydrogen peroxide from mononuclear cells, freshly prepared from human donor blood. Cells were treated with ATP and supernatant was analysed after 20 min. ATP induced a strong, concentration-dependent increase in hydrogen peroxide release with a half-maximal effective concentration of  $558 \pm 5.0 \mu\text{M}$  (mean  $\pm$  SEM,  $n = 3$ ), as depicted in Figure 16.

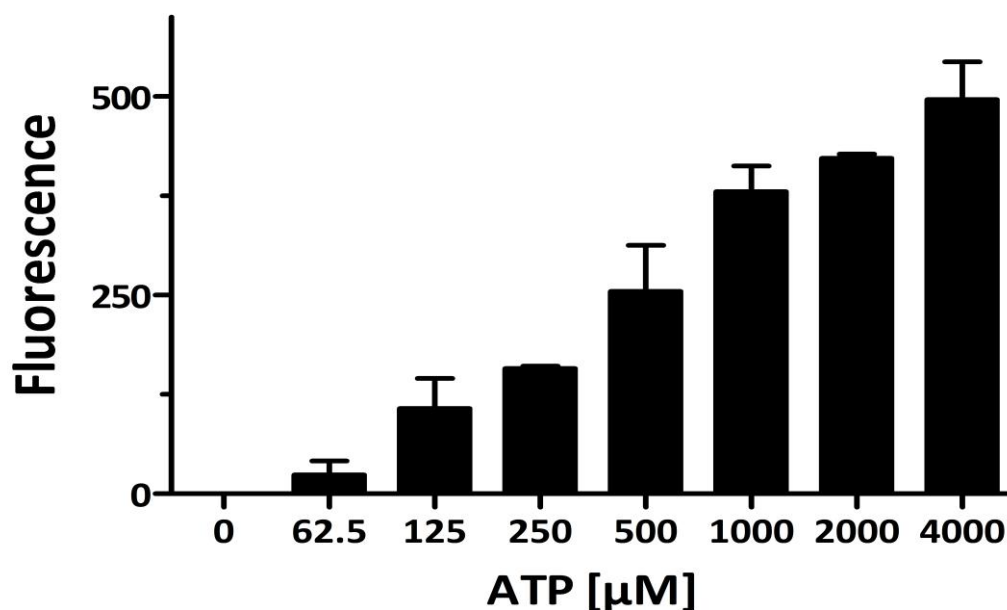
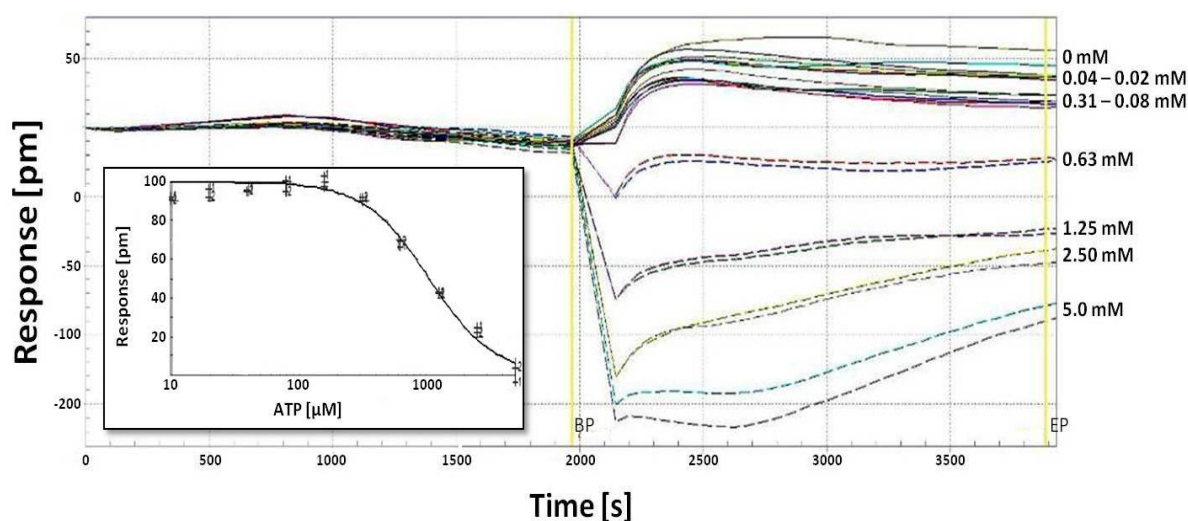


Figure 16. Rate of hydrogen peroxide formation in human mononuclear blood cells. The formation of hydrogen peroxide was analysed in mononuclear blood cells upon exogenously applied ATP, as a marker for metabolic activity in cells. Human mononuclear blood cells were exposed to ATP at the concentration range of 0 to 4.0 mM. Fluorescence was measured with a fluorescence microplate reader using excitation at 550 nm and fluorescence absorbance at 600 nm. Background fluorescence, determined for a control reaction with no  $\text{H}_2\text{O}_2$ , was subtracted from each value. The half-maximal effective concentration was  $\text{EC}_{50} = 558 \pm 5.0 \mu\text{M}$  ( $n = 3$ ).

Extracellular ATP mediates its effect by activating ionotropic or metabotropic receptors. Usually, activity of metabotropic receptors is linked to changes in cellular metabolism, thus the name 'metabotropic'. However, in this case, the concentration response curve for ATP induction of hydrogen peroxide release, with the  $EC_{50}$  value above  $500 \mu\text{M}$ , did not fit with the ATP sensitivity of the twelve known metabotropic P2Y receptors. Only P2X7 receptors have such low sensitivity to extracellular ATP (71). It is probable that non-linear mechanisms between receptor activation and hydrogen peroxide release could explain such an observation. Nevertheless, when the effect of extracellular ATP was tested on dynamic mass redistribution in HUVEC cells, a similar concentration-response correlation with an  $EC_{50}$  of  $933 \pm 110 \mu\text{M}$  (mean  $\pm$  SEM of three experiments with  $n = 2$  replicates) (Figure 17) was observed.



**Figure 17.** The mass redistribution of human umbilical vein endothelial cells (HUVEC) was assessed in the Epic system to identify changes upon treatment with exogenously applied ATP. Cells showed significant concentration-dependent effects in the Epic, indicating strong morphological changes with an  $EC_{50} = 933 \pm 110 \mu\text{M}$  (mean  $\pm$  SEM of three experiments with  $n = 2$  replicates). The larger figure showed one of the three representative raw data sets. The smaller figure depicts the calculation of the  $EC_{50}$  derived from the raw data.

I therefore tested whether the selective and potent P2X7 receptor antagonist was able to block the ATP-induced effect on human mononuclear blood cells.

The P2X7 receptor antagonist elicited a moderate inhibition of the hydrogen peroxide formation in human mononuclear blood cells with a half-maximal inhibition ( $IC_{50}$ ) of  $3.0 \pm 0.5 \mu\text{M}$  (mean  $\pm$  SEM,  $n = 3$ ), indicating that P2X7 receptors at least partially mediate the observed metabolic effects (Figure 18).

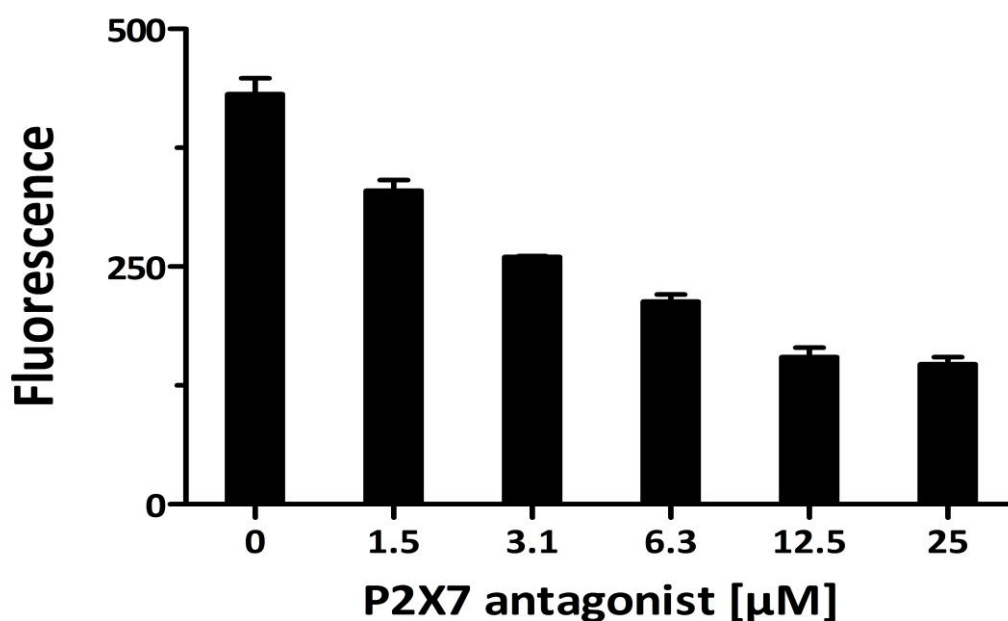


**Figure 18.** P2X7 receptor antagonist effect on hydrogen peroxide levels in human mononuclear blood cells. Inhibition of ATP-induced hydrogen peroxide release by the selective P2X7 receptor antagonist. The P2X7 receptor antagonist was used from 0 to 25  $\mu\text{M}$  and the  $IC_{50}$  was  $3.0 \pm 0.5 \mu\text{M}$  (mean  $\pm$  SEM,  $n = 3$ ).

In addition, Bz-ATP, which selectively activates the P2X4- and P2X7 receptors (71), was able to mimic the results of observations with ATP in the hydrogen peroxide release assay (Figure 19), corroborating my hypothesis that P2X7 receptors at least partially link extracellular ATP with intracellular metabolic pathways. The  $EC_{50}$  could not be calculated, because the hydrogen peroxide release did not reach a plateau at the highest concentrations of Bz-ATP used, showing room for increasing metabolic levels.

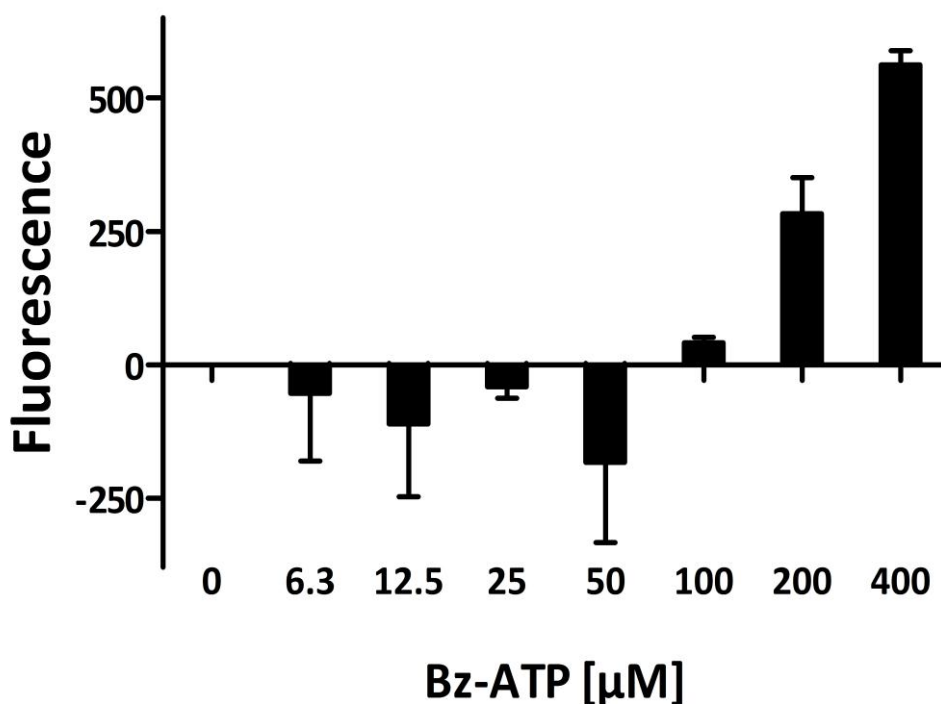


**Figure 19.** The formation of hydrogen peroxide was analysed in human mononuclear blood cells upon treatment with P2X7-specific extracellular Bz-ATP, as a marker for increased metabolic activity in cells. Human mononuclear blood cells were exposed to Bz-ATP in the concentration range of 0 to 400  $\mu\text{M}$ . Fluorescence was measured with a fluorescence microplate reader using excitation at 550 nm and fluorescence absorbance at 600 nm. Background fluorescence, determined for a control reaction without  $\text{H}_2\text{O}_2$ , was subtracted from each value ( $n = 3$ ).

I subsequently went on to study more specifically how P2X7 receptors influence cellular metabolism using the label-free multiparametric sensor system. I used the Bionas<sup>®</sup>1500 to analyse changes in oxygen concentration, extracellular acidification, and cell impedance. Enhanced metabolic activity of cells requires increased oxygen consumption for regeneration of energy, which is detectable during the stop phases by a decrease in oxygen concentration. Moreover, toxicity associated with mitochondrial inhibition or uncoupling of the proton circuit is detectable by the alteration of oxygen consumption. The sensor system was optimised with respect to maximal stimulation amplitudes, as described previously (110). This allows for sensitive and reliable recording of the signals. Optimal cell density was

---

$2 \times 10^5$  attached cells per fibronectin-coated chip and an effective incubation chamber volume of  $1.4 \mu\text{L}$  (i.e. the effective volume of the  $50 \mu\text{m}$  space between the surface of the sensor chip and the chamber lid). Viability of cells was monitored continuously by measurement of cellular impedance. Continuous deviations in the range of about  $\pm 1.2\%$  per hour from initial values were considered acceptable and were attributed to cell proliferation or cell release from the chip.

*The multiparametric cell-based sensor system detects metabolic alterations upon Bz-ATP treatment.*

Both human P2X7-overexpressing HEK293 cells (HEK-hP2X7) and parental HEK293 cells with no expression of P2X7 were monitored for alterations in physiological cell parameters to assess the influence of exogenously applied Bz-ATP to intracellular metabolic pathways. The results obtained with HEK-hP2X7 cells were compared to those of parental HEK293 cells (127). HEK-hP2X7 cells immediately responded to Bz-ATP treatment in a concentration-dependent manner. In agreement with previous findings (128), cell morphology changed, with a maximum effect being reached at  $100 \mu\text{M}$  Bz-ATP (13% above control with parental HEK293 cells) (Figure 20A). In comparison to HEK-hP2X7, parental cells HEK293 showed only negligible effects on the impedance sensor, predominantly at lower concentrations of Bz-ATP. One-hundred  $\mu\text{M}$  Bz-ATP applied to parental cells showed reduced amplitude. Furthermore, in HEK-hP2X7 cells the metabolic activity (Figure 20C) and cellular respiration (Figure 20B) increased in a concentration-dependent manner upon Bz-ATP treatment. An obvious effect was observed in metabolic and respiratory activity on HEK-hP2X7 cells at the highest Bz-ATP concentration ( $100 \mu\text{M}$ ). Compared to parental HEK293 cells, a reduction of 23% in cellular respiration was observed at  $100 \mu\text{M}$  Bz-ATP, while metabolic activity was

increased by 24% relative to parental HEK293 cells. This particular effect at 100  $\mu\text{M}$  Bz-ATP with HEK-hP2X7 cells was absent in parental HEK293 cells (Figure 20B, C).

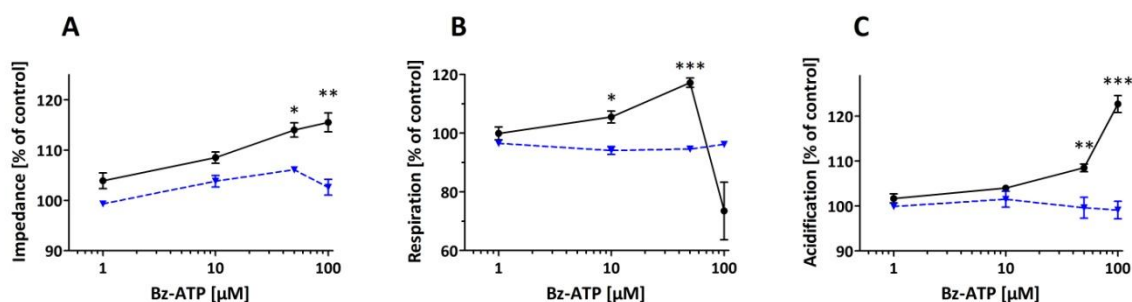


**Figure 20.** Concentration-dependant stimulation effects of HEK-hP2X7 cells (black, solid lines) and parental HEK293 cells (blue, dotted lines) upon treatment with the P2X7 specific agonist Bz-ATP analysed by the sensor system. (A) Compared to parental HEK293 cells, the human P2X7 overexpressing HEK293 cells showed a more significant increase in cellular impedance up to 100  $\mu\text{M}$  Bz-ATP, while parental HEK293 cells initiate a reduction of impedance effects at concentrations above 50  $\mu\text{M}$ . (B) Cellular respiration showed a concentration-dependent increase in HEK-hP2X7 at concentrations equal to and below 50  $\mu\text{M}$  Bz-ATP compared to parental HEK293 cells. Bz-ATP treatment at 100  $\mu\text{M}$  demonstrates the toxicological effect of Bz-ATP by strong inhibition of the respiratory activity. This effect is most likely a consequence of pore dilatation and  $\text{Ca}^{2+}$ -influx. Respiration of the parental HEK293 cells was almost stable at all concentrations of Bz-ATP. (C) The metabolic activity of the HEK-hP2X7 cells was again activated upon Bz-ATP treatment. A remarkable amplitude is depicted at 100  $\mu\text{M}$  Bz-ATP and is a domino effect, due to a lack of ATP generation via oxidative phosphorylation. Statistical significance: \* $p < 0.05$ , \*\* $p < 0.01$ , \*\*\* $p < 0.001$ ,  $n = 4$ .

The morphological changes upon Bz-ATP treatment are an indication of ligand binding to the human P2X7 receptor (128). Therefore, the calculation of an  $\text{EC}_{50}$  was carried out in HEK-hP2X7 cells (Figure 21). Activation of P2X7 by Bz-ATP showed saturation at high concentrations and was characterised by an  $\text{EC}_{50}$  value of  $9.6 \pm 0.8 \mu\text{M}$  (mean  $\pm$  SEM,  $n = 5$ ).



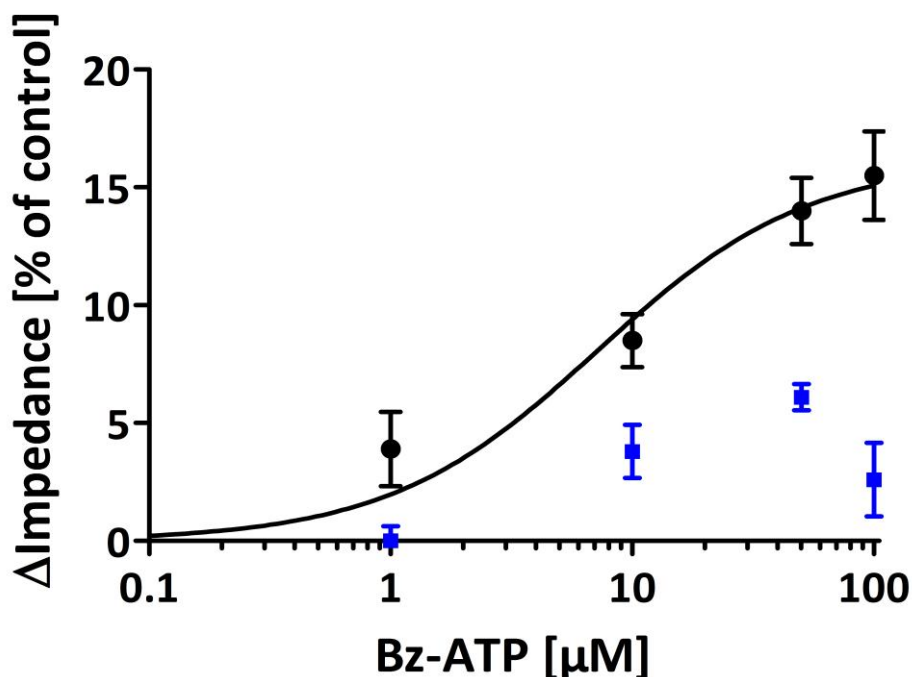
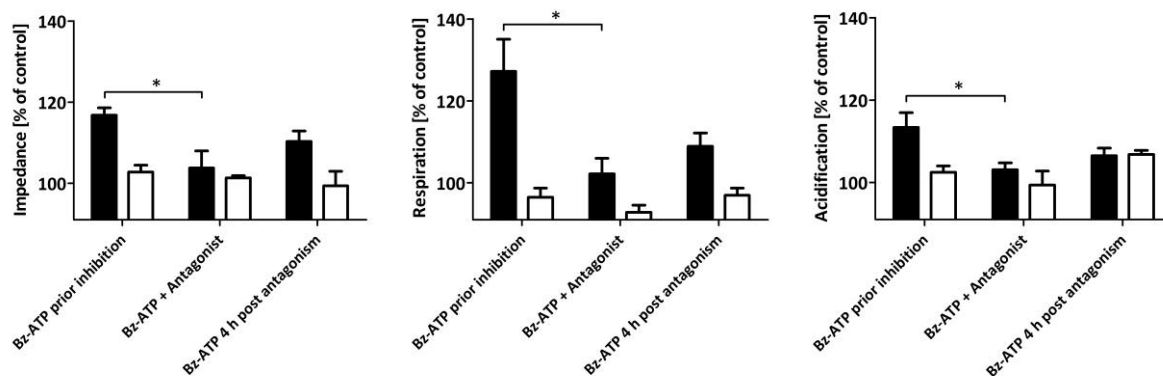


Figure 21. Stimulation of P2X7 in the presence of different concentrations of Bz-ATP. Morphological changes in HEK-hP2X7- (black circles) and parental HEK293 (blue squares) cells were measured as a function of increasing Bz-ATP concentrations. The solid line shows the curve fitting using an enzyme kinetic model. Strong morphological changes were observed with an  $EC_{50}$  of  $9.6 \pm 0.8 \mu\text{M}$  (mean  $\pm$  SEM,  $n = 5$ ). The level of significance between HEK-hP2X7 and parental HEK293 controls for concentrations above  $1.0 \mu\text{M}$  was  $**p < 0.01$ ,  $n = 5$ .

The results of the multiparametric cytosensor system (Figure 20) confirm the correlation between exogenously applied Bz-ATP and the triggering of intracellular metabolic pathways via the P2X7 receptor. Therefore, the inhibition of these alterations in order to investigate the role of P2X7 in cellular metabolism was analysed using the specific P2X7 receptor antagonist. In a further set of experiments with the sensor system, the inhibition of the effects triggered by Bz-ATP on the HEK-hP2X7 cells was assessed.

Figure 22 shows the inhibitory effect of the P2X7 receptor antagonist on metabolic activity, cellular respiration, and morphology of HEK-hP2X7- and parental HEK293 cells using  $50 \mu\text{M}$  Bz-ATP. All previously observed stimulatory effects on HEK-hP2X7 cells were inhibited by the

P2X7 receptor antagonist, suggesting that P2X7 is important for Bz-ATP-induced intracellular metabolic changes. The inhibition of the Bz-ATP-induced effects observed in the P2X7 overexpressing cells were absent in parental HEK293 cells (Figure 22).



**Figure 22.** Inhibition experiments using HEK-hP2X7- (black column) and parental HEK293 (white column) cells. P2X7 were stimulated by preliminary treatment with 50  $\mu\text{M}$  Bz-ATP, followed by an inhibition of Bz-ATP induced effects with 10  $\mu\text{M}$  of the P2X7 receptor antagonist in the presence of 50  $\mu\text{M}$  Bz-ATP. (Table 4 provides an overview of the inhibition potency). After a wash-out period of at least 4 h after the inhibition step, the cells were again stimulated with 50  $\mu\text{M}$  Bz-ATP to assess regeneration and reactivation processes. Statistical significance between the stimulation effects and inhibition was, for all three sensors,  $*p < 0.05$ ,  $n = 4$ .

*Comparative pharmacology of P2X7 receptor-mediated effects on cellular metabolism, calcium-, and dye influx.*

The P2X7 receptor was activated by Bz-ATP in patch-clamp experiments on a P2X7 receptor-expressing mouse microglia BV2 cell line and was characterised by an  $\text{EC}_{50}$  value of  $197 \pm 2.3 \mu\text{M}$  (mean  $\pm$  SEM,  $n = 5$ ). The P2X7 receptor antagonist was also able to inhibit, with similar affinity, Bz-ATP-induced currents measured in patch-clamp experiments with the mouse microglia cell line, BV2. Bz-ATP induced stable inward currents at a holding potential of -70 millivolt that were blocked by the P2X7 receptor antagonist with an  $\text{IC}_{50}$  of 2.1  $\mu\text{M}$  (95% CI 1.8 - 2.5  $\mu\text{M}$ ,  $n \geq 5$ ) (Figure 23).

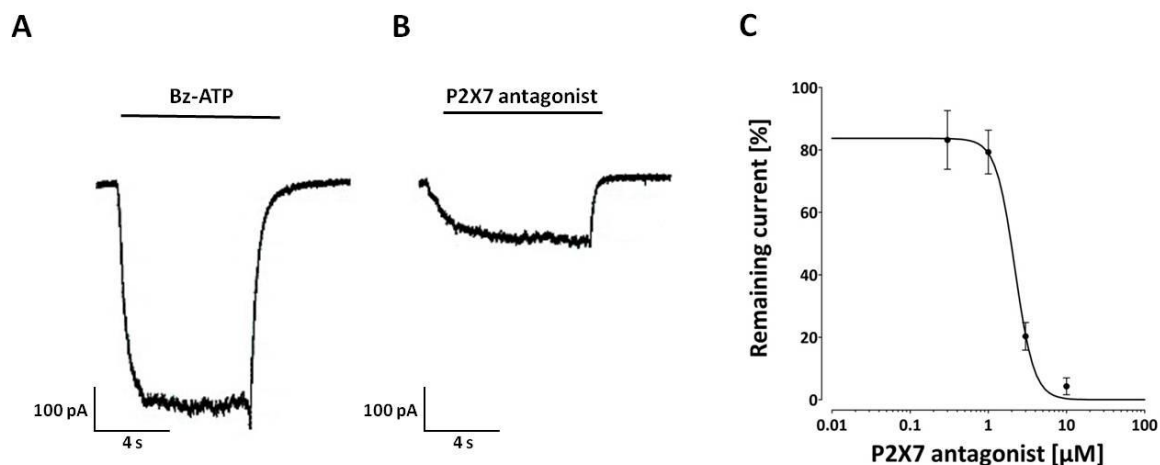


**Figure 23.** Comparison of the raw current signal patterns after stimulation and inhibition of P2X7 expressing mouse microglia BV2 cells. (A) The P2X7 receptor specific patterns of 100  $\mu\text{M}$  Bz-ATP-induced current signals in mouse microglia BV2 cells with an  $\text{EC}_{50}$  of  $197 \pm 2.3 \mu\text{M}$  (mean  $\pm$  SEM,  $n = 5$ ). (B) Indicates the current signal pattern of BV2 cells stimulated with Bz-ATP in the presence of the P2X7 receptor antagonist. (C) Depicts the inhibition curves with the selective P2X7 receptor antagonist on membrane currents in mouse microglia BV2 cells. Bz-ATP was used at 100  $\mu\text{M}$ , which is in the concentration range of the estimated  $\text{EC}_{50}$  values for the agonist. One-hundred  $\mu\text{M}$  Bz-ATP induced a current in mouse microglia BV2 cells that was blocked by the P2X7 receptor antagonist with an  $\text{IC}_{50}$  of 2.1  $\mu\text{M}$  (95% CI 1.8 - 2.5  $\mu\text{M}$ ,  $n \geq 5$ ).

I additionally questioned how closely the P2X7 receptor-mediated effects on cell morphology, extracellular acidification, and cellular respiration are linked to channel function. P2X7 receptors are ion channels permeable to mono- and divalent cations and, upon longer activation, to larger ions such as YoPro1. This dye was used to monitor Bz-ATP and P2X7 receptor antagonist pharmacology in the HEK-hP2X7 cells used in the experiments with the multiparametric cytosensor system. YoPro1 influx into HEK-hP2X7 cells upon stimulation with Bz-ATP for 45 min was measured and was able to antagonise Bz-ATP effects completely with an  $\text{IC}_{50}$  of 11.2 nM (95% CI 9.6 - 13.2 nM, mean of three experiments with  $n = 2$  replicates) (Figure 24).

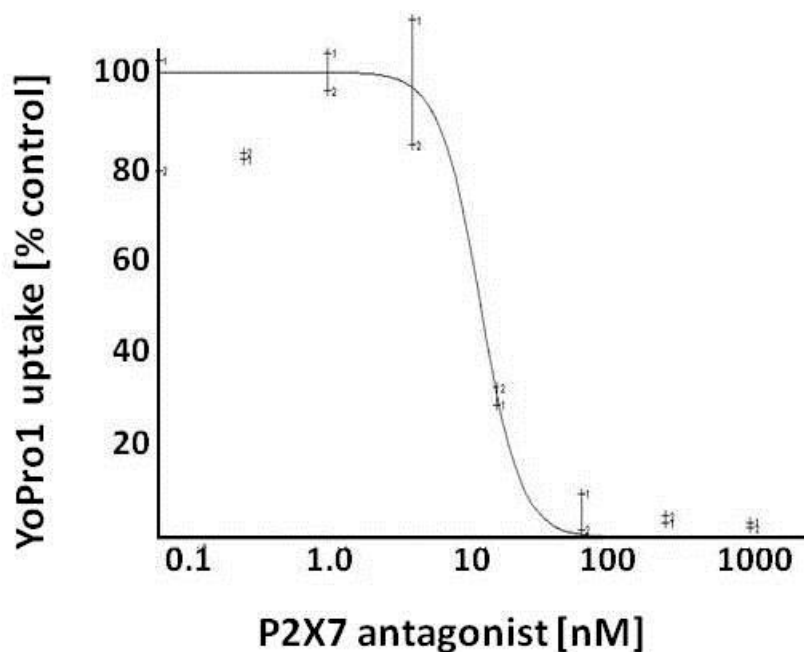


**Figure 24.** YoPro1 dye permeability measurements using ATP as agonist and the selective P2X7 receptor antagonist. Uptake of the YoPro1 dye in human P2X7 overexpressing HEK293 cells was inhibited by the P2X7 receptor antagonist and was characterised by an IC<sub>50</sub> value of 11.2 nM (95% CI 9.6 - 13.2 nM, mean of three experiments with n = 2 replicates; depicted is a representative pattern).

When measuring Ca<sup>2+</sup> influx via P2X7 receptors using a calcium-sensitive fluorescent dye in primary cortical cultures from rat embryonic brains, the P2X7 receptor antagonist inhibited Bz-ATP-induced Ca<sup>2+</sup> influx with an IC<sub>50</sub> of 3.2 μM (95% CI 2.8 - 3.7 μM, n ≥ 4) (Figure 25).

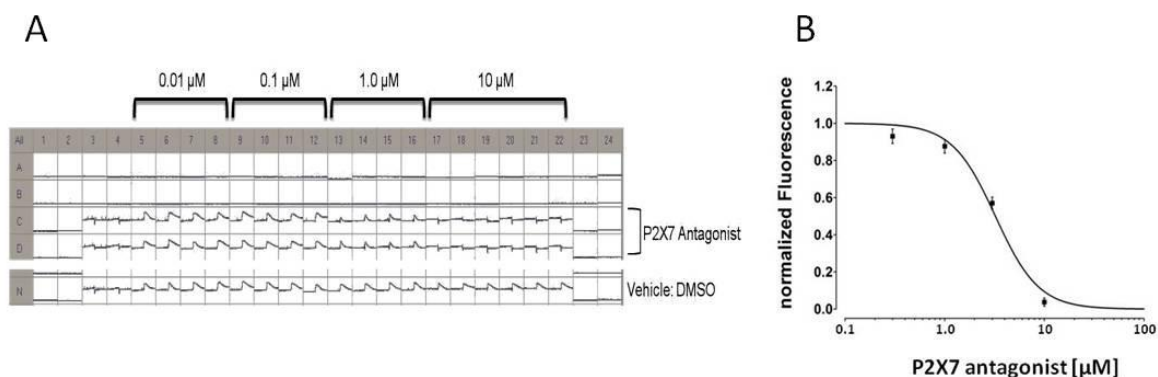


**Figure 25.** Intracellular Ca<sup>2+</sup> increase by Bz-ATP stimulation of P2X7 receptor antagonist in rat cortical cells. (A) Depicted is a section of the 384-well plate and the recorded currents for the P2X7 receptor antagonist and the control (DMSO). (B) The remaining current was measured and showed concentration-dependent effects with an IC<sub>50</sub> of 3.2 μM (95% CI 2.8 - 3.7 μM, n ≥ 4).

All of these experiments, with recombinant cells overexpressing the human P2X7 receptor as well as the rodent P2X7 receptors, showed that the pharmacology of P2X7 receptor-mediated metabolic changes are well in line with the pharmacology of more direct physiological effectors upon receptor activation (Table 4).

**Table 4: Summary of the inhibitory affinity of the P2X7 receptor antagonist**

Assay	Cells	Agonist <sup>a</sup> [ $\mu$ M]	Selective P2X7 receptor antagonist [ $\mu$ M]	IC <sub>50</sub> / % inhibition
<b>H<sub>2</sub>O<sub>2</sub> release</b>	mononuclear blood cells	1`000	0 - 25	<b>3.0 <math>\mu</math>M</b>
<b>YoPro1 uptake</b>	HEK-hP2X7	3`000	$3.8 \times 10^{-5}$ - 10	<b>11.2 nM</b>
<b>Fluo-4-AM</b>	rat cortical	250	0.01 - 10	<b>3.2 <math>\mu</math>M</b>
<b>Patch-clamp</b>	mouse microglia	100	0.3 - 10	<b>2.1 <math>\mu</math>M / 96%<sup>b</sup></b>
<b>Sensor system respiration</b>	HEK-hP2X7	50	10	<b>92%</b>
<b>Sensor system acidification</b>	HEK-hP2X7	50	10	<b>77%</b>
<b>Sensor system impedance</b>	HEK-hP2X7	50	10	<b>77%</b>

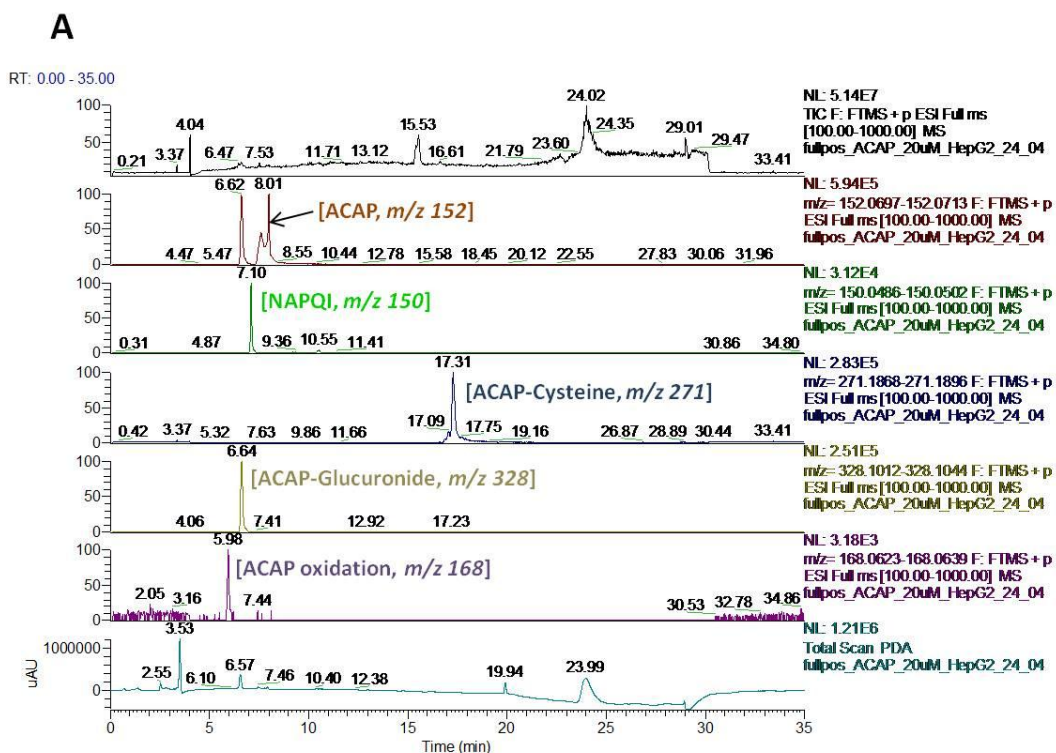
<sup>a</sup> Hydrogen peroxide (H<sub>2</sub>O<sub>2</sub>) release and YoPro1 uptake assays were performed with ATP, all other assays with Bz-ATP; <sup>b</sup> at 10  $\mu$ M selective P2X7 receptor antagonist.

---

### 4.3 Detection of drug-induced liver toxic effects using HepG2 cell

#### *Metabolic activity of HepG2 cells.*

In control experiments, the metabolic activity of HepG2 cells was assessed by means of 19 h incubations with acetaminophen and amiodarone (20  $\mu$ M each). Metabolites were detected using high-resolution liquid chromatography coupled with mass spectrometry in positive ion mode. Acetaminophen incubations with HepG2 cells resulted in the formation of an oxidised metabolite ( $m/z$  168), NAPQI ( $m/z$  150), and two phase II metabolites (a cysteine adduct at  $m/z$  271 and a glucuronic acid conjugate at  $m/z$  328). In incubations with amiodarone, the major metabolite was desethylamiodarone ( $m/z$  618) accompanied by a hydrated- ( $m/z$  648), a dehydrated- ( $m/z$  644) and an oxidised metabolite ( $m/z$  662). Figure 26 and Figure 27 showed the mass spectrometry patterns of acetaminophen and amiodarone, the identified metabolites, and the putative metabolic pathways.



**B**

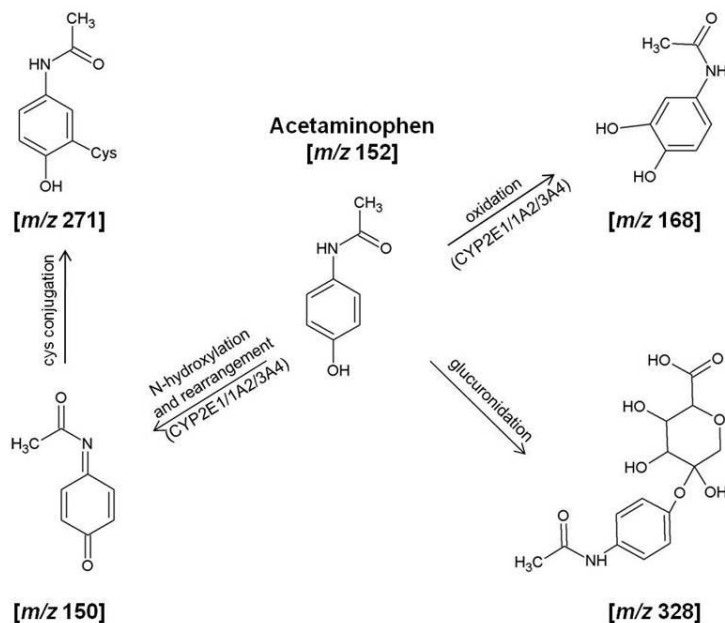


Figure 26. (A) High resolution ion chromatograms in ion positive mode and photodiode array detector pattern (200 - 300 nm) of acetaminophen (ACAP,  $m/z$  152) and its metabolites. Acetaminophen was incubated for 19 h with HepG2 cells. (B) Putative metabolic pathway of the acetaminophen metabolites detected in the 19 h incubation with HepG2 cells.

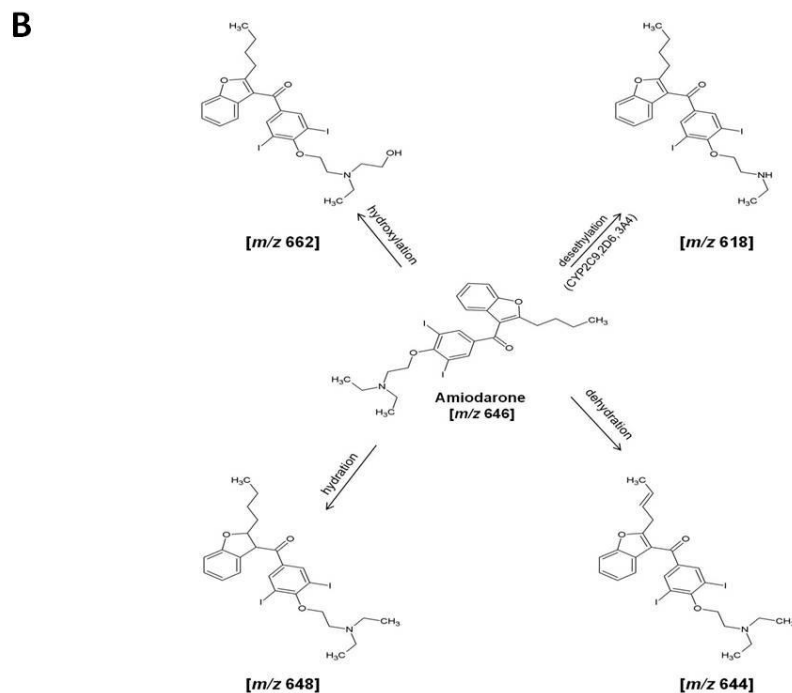
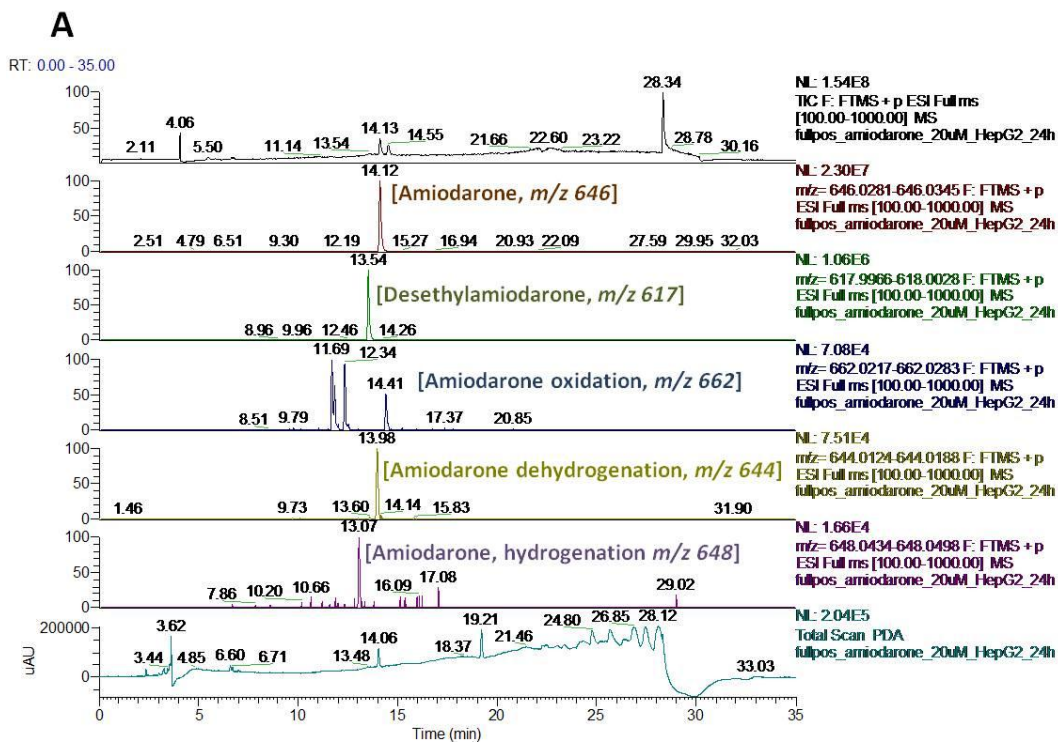


Figure 27. (A) High resolution ion chromatograms in ion positive mode and photodiode array detector (200 - 300 nm) of amiodarone ( $m/z$  646) and its metabolites. Amiodarone was incubated for 19 h with HepG2 cells. (B) Putative metabolic pathway of the amiodarone metabolites detected in the 19 h incubation with HepG2 cells.

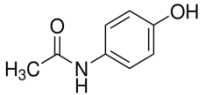
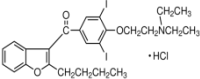
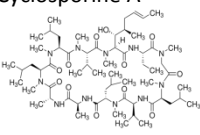
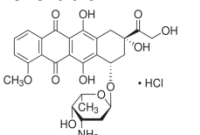
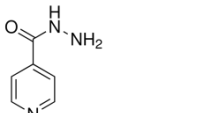
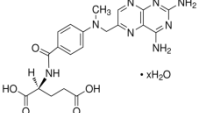
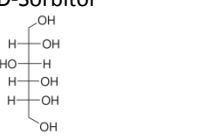
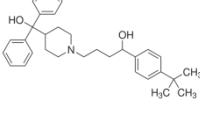
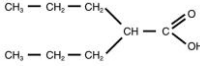


---

*Experimental setup of the multiparametric cytosensor system for analysis of liver toxicological effects.*

Changes in oxygen concentration, extracellular acidification, and cell impedance were monitored in real-time using the multiparametric cytosensor system. The experimental set-up was optimised to achieve maximal sensitivity to physiological alterations (Figure 7B, Table 3). Important assay parameters included the use of an assay medium (Table 3) with a low buffer capacity, which was additionally supplemented with 0.1% (v/v) heat-inactivated foetal bovine serum albumin. Optimal cell density was determined as  $2 \times 10^5$  viable HepG2 cells per chip. Minimal required cell viability, estimated by a trypan blue dye exclusion test, was 90%. The effective volume of the incubation chamber, i.e. the volume of the space between the surface of the sensor chip and the chamber lid, was 5.7  $\mu\text{L}$  and was determined by the distance (200  $\mu\text{m}$ ) between the flow head and the sensor chip surface (Figure 7B). This minimal volume enhances the responsiveness of the system with respect to alterations in pH and oxygen partial pressure. Signals from cell respiration, acidification, and impedance were recorded after an initial stabilisation phase of 3 h. Subsequently, cells were exposed to test compounds for 19 h, followed by a regeneration phase of 2 h to detect cell regeneration. After the experiment, baseline signals of the cell-free cytosensor chips (i.e. 0% reference signal) were recorded after solubilisation of cells using a non-ionic detergent (Triton X-100). Viability of cells was monitored continuously by measurements of cellular impedance. Thus, signals from the three sensor types were recorded relative to initial conditions (100% reference signal) and 0% background signal. Eight marketed drugs were used at, above, and below their clinically relevant plasma concentrations to study hepatotoxic effects *in vitro* (Table 5).

Table 5: Characteristics and toxicological profiles of reference drugs used in the present toxicology project.

Drug	Indication (C <sub>max</sub> , range of therapeutic plasma concentration)	Concentration range in the experiments	Mechanism of toxicity	Reactive metabolites	Liver pathology
Acetaminophen 	NSAID <sup>a</sup> 0.1 mM (129, 130)	0.01 - 10 mM	GSH depletion, mitochondrial toxicity (131-133)	N-acetyl-p- benzoquinone imine (NAPQI), other quinones	Hepatocellular degeneration
Amiodarone 	Antiarrhythmic 2.1 μM (134)	1.0 - 30 μM	ROS formation, mitochondrial toxicity (135-137)	Desethyl- amiodarone	Steatosis, hepatocellular death
Cyclosporine A 	Immunosuppressant 1.5 μM (138)	1.0 - 60 μM	Covalent binding to microsomal proteins, ROS formation, oxidative stress, (133)	Reactive metabolites	Cholestasis
Doxorubicin 	Anticancer 1.9 μM (139)	1.0 - 25 μM	DNA intercalation, ROS formation, oxidative stress, mitochondrial toxicity (140, 141)	Semiquinone radical	Hepatocellular death
Isoniazide 	Antibacterial 0.11 mM (142)	0.1 - 5.0 mM	Oxidative stress, GSH depletion (133, 143-146)	Hydrazine, reactive acetyl species	Steatosis, necrosis, hepatocyte and vasculature damage
Methotrexate 	Anticancer up to 1150 μM; Immunosuppressant 0.4 μM (147, 148)	1.0 - 200 μM	Inhibition of biosynthetic pathways, metabolic stress (149-152)	Polyglutamated methotrexate	Fatty infiltration, fibrosis, cirrhosis
D-Sorbitol 	Laxative 70 μM (153)	0.001 - 5.0 mM	none	none	none
Terfenadine 	Antihistamine 4.5 nM (154)	5.0 - 25 μM;	Modulation of Ca <sup>2+</sup> homeostasis, ROS formation, apoptosis-inducer (155, 156)	unknown	Cholestasis, hepatocellular death
Valproic acid 	Anticonvulsant 0.6 mM (157)	0.5 - 10 mM;	Oxidative stress, altered mitochondrial β-oxidation and oxidative phosphorylation, GSH/NAC <sup>b</sup> depletion (91, 133, 158, 159)	Acyl glucuronides, 2-N-propyl-4- pentenoic acid	Necrosis, steatosis, cholestasis

<sup>a</sup> Non-steroidal anti-inflammatory drug; <sup>b</sup> N-acetylcysteine

### *Effect of D-sorbitol on HepG2 cells.*

D-sorbitol, known to be well tolerated even at high concentrations and non-toxic, was used as a negative control (160). D-sorbitol (Figure 28) showed no relevant effects in the multiparametric cytosensor system at concentrations from 0.001 mM to 5.0 mM. A small but continuous increase in cellular respiration, reaching 110 - 120% of the control values, was detected at all concentrations.

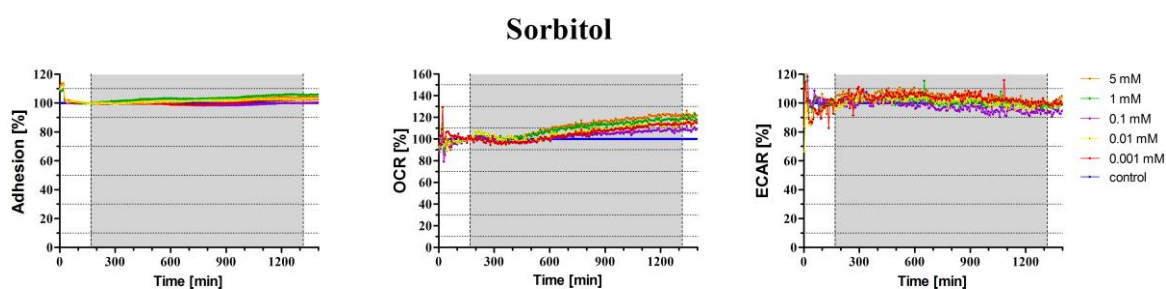


**Figure 28.** Patterns of cytosensor signals upon stimulation of HepG2 cells with D-sorbitol. Cells were incubated with the indicated concentrations of D-sorbitol. Using the multiparametric cytosensor system, three physiological parameters were monitored on-line: cell impedance being an indicator of cell morphology/adhesion, cellular respiration based on oxygen consumption, and metabolic activity resulting in extracellular acidification. The grey areas indicate the initial stabilisation and final regeneration periods, which are carried out in the absence of test compound. Control incubation in the absence of test compound was normalised to 100%. The patterns depict means of  $n \geq 3$  experiments.

### *Effect of acetaminophen on HepG2 cells.*

Acetaminophen was used in a concentration range of 0.01 mM to 10 mM (Figure 29) and induced concentration-dependent effects in the multiparametric cytosensor system at all considered parameters over a 19 h incubation period. The impedance was indicative of shrinking and retraction of cells, reflected by a maximal drop to 80% from baseline values at 10 mM acetaminophen within the first 70 min after addition of the compound. It then remained at around 80% to 90% for the remaining incubation time. Impedance was reversible in the regeneration phase, reaching baseline levels similar to the initial values prior to acetaminophen treatment. Reduction of cell respiration was detected immediately

after acetaminophen application. Maximal reduction was observed at 20 min after drug application reaching 40% of baseline values and was constant until the end of drug treatment. Conversely, at the same time, metabolic activity increased in a concentration-dependent manner up to 130% (10 mM) and remained constant at this level over six hours before it returned to initial baseline levels. These effects were partially reversible during the regeneration phase, reaching values equal to those prior to drug treatment. In the MTT test, cell viability was significantly decreased (Table 6) showing a reduction to 80% and 62% in viability at 1.0 mM and 10 mM acetaminophen, respectively.

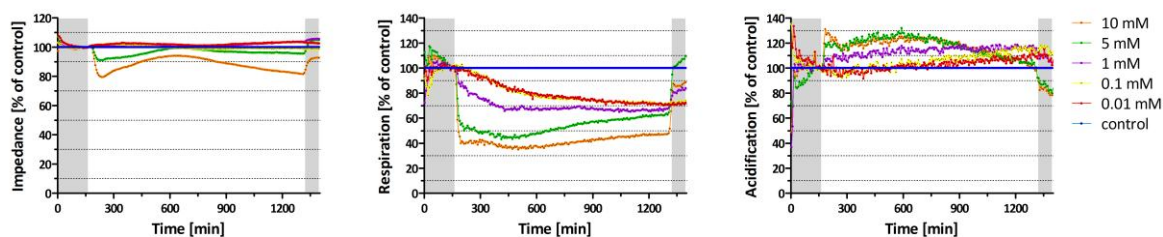


**Figure 29.** Patterns of cytosensor signals upon stimulation of HepG2 cells with acetaminophen. Cells were incubated with the indicated concentrations of acetaminophen. Using the multiparametric cytosensor system, three physiological parameters were monitored on-line: cell impedance being an indicator of cell morphology/adhesion, cellular respiration based on oxygen consumption, and metabolic activity resulting in extracellular acidification. The grey areas indicate the initial stabilisation and final regeneration periods, which are carried out in the absence of a test compound. Control incubation in the absence of test compound was normalised to 100%. The patterns depict means of  $n \geq 3$  experiments.

**Table 6. Cellular viability of HepG2 cells determined after 24 h incubation by the MTT assay. Values are means  $\pm$  SEM (n = 3 of two independent sets of experiments) as compared to untreated control cells (100% viability). Level of significance (Student's t-test as compared to 100% control): \*\* $p \leq 0.01$ , \*\*\* $p \leq 0.001$ .**

Compound	% Viability (statistical significance)	Concentration
Acetaminophen	101.4 $\pm$ 0.7	0.01 mM
	80.3 $\pm$ 0.3 (***)	1.0 mM
	61.8 $\pm$ 0.3 (***)	10 mM
Amiodarone	100.2 $\pm$ 3.2	1.0 $\mu$ M
	95.7 $\pm$ 0.6	10 $\mu$ M
	107.9 $\pm$ 5.9	30 $\mu$ M
Cyclosporine A	87.1 $\pm$ 5.3	1.0 $\mu$ M
	101.0 $\pm$ 0.8	10 $\mu$ M
	81.8 $\pm$ 2.6 (**)	60 $\mu$ M
Doxorubicin	70.2 $\pm$ 3.9 (***)	1.0 $\mu$ M
	61.3 $\pm$ 1.2 (***)	10 $\mu$ M
	53.5 $\pm$ 1.8 (***)	25 $\mu$ M
Isoniazide	97.1 $\pm$ 2.6	0.1 mM
	99.5 $\pm$ 1.8	1.0 mM
	102.9 $\pm$ 0.8	5.0 mM
Methotrexate	79.3 $\pm$ 1.4 (***)	1.0 $\mu$ M
	70.3 $\pm$ 2.5 (***)	50 $\mu$ M
	79.3 $\pm$ 0.8 (***)	200 $\mu$ M
Valproic acid	101.9 $\pm$ 2.0	0.5 mM
	89.0 $\pm$ 1.4 (**)	3.0 mM
	85.2 $\pm$ 1.8 (**)	10 mM
Terfenadine (control for cytotoxicity)	98.9 $\pm$ 6.3	5.0 $\mu$ M
	1.4 $\pm$ 0.2 (***)	25 $\mu$ M

### *Effect of amiodarone on HepG2 cells.*

Amiodarone caused intense changes in the multiparametric cytosensor system experiments (Figure 30). These changes were proportional to the concentrations used, which covered a range of 1.0  $\mu\text{M}$  to 30  $\mu\text{M}$ . Concentrations below 10  $\mu\text{M}$  amiodarone did not influence cellular physiology. However, pronounced effects were observed at concentrations equal to and above 10  $\mu\text{M}$ . Three hours after amiodarone application, cytotoxicity and cell death were evident by a persistent decrease in cell impedance. Dying cells were released from the sensor chip and, at the end of the drug treatment period, only 16% (approx. 32'000 cells) of the initial cell number remained. At concentrations of 10  $\mu\text{M}$  and above, amiodarone affected mitochondrial respiration and metabolic activity non-reversibly. The respiration curve at 30  $\mu\text{M}$  amiodarone described a steep drop until 280 min post-treatment with 30% residual cell respiration, followed by a levelling-off to 15% at the end of the incubation period. The metabolic activity at 15  $\mu\text{M}$  and 30  $\mu\text{M}$  amiodarone increased with a maximal amplitude of 150% at 400 min post-treatment. At 30  $\mu\text{M}$  amiodarone, this boost in metabolic activity changed into a sustained reduction until the end of the drug-treatment, with only 7% residual metabolic activity. In the MTT assay, amiodarone had no statistically significant effect on HepG2 cell viability at all concentrations of the MTT assay (Table 6).

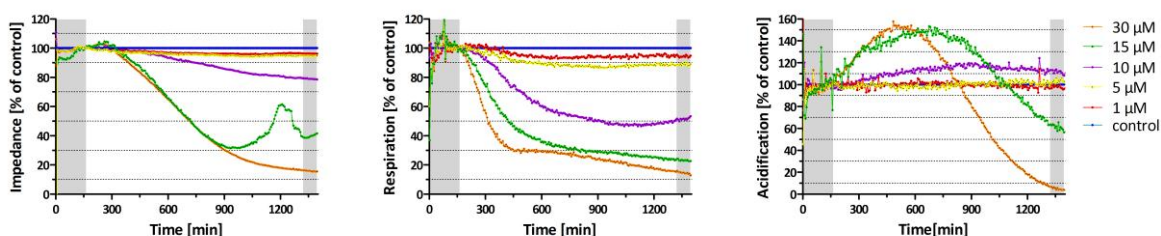


**Figure 30.** Patterns of cytosensor signals upon stimulation of HepG2 cells with amiodarone. Cells were incubated with the indicated concentrations of amiodarone. Using the multiparametric cytosensor system, three physiological parameters were monitored on-line: cell impedance being an indicator of cell morphology/adhesion, cellular respiration based on oxygen consumption, and metabolic activity resulting in extracellular acidification. The grey areas indicate the initial stabilisation and final regeneration periods, which are carried out in the absence of a test compound. Control incubation in the absence of test compound was normalised to 100%. The patterns depict means of  $n \geq 3$  experiments.

### *Effect of cyclosporine A on HepG2 cells.*

Cyclosporine A was analysed at concentrations up to 60  $\mu\text{M}$  and showed no obvious effects with respect to cell impedance (Figure 31). In cell respiration, concentrations below 30  $\mu\text{M}$  showed no obvious effects in the first 400 min of treatment, followed by a small increase in cell respiration to 110% of baseline values. A decrease to 60% was monitored within the first 400 min after application of 30  $\mu\text{M}$  and 60  $\mu\text{M}$  cyclosporine A, followed by a nearly complete recovery of respiratory activity (90%) at the end of the treatment period. The decrease in respiration at 30  $\mu\text{M}$  and 60  $\mu\text{M}$  went in parallel with an increase in metabolic activity up to 110%. Along the time course, the metabolic activity was continually reduced to 90% at the end of the cyclosporine A incubation. The MTT assay showed a statistically significant reduction of 18% in cell viability at the highest concentration of 60  $\mu\text{M}$  (Table 6). No effects were observed in the MTT assay at concentrations below 60  $\mu\text{M}$ .

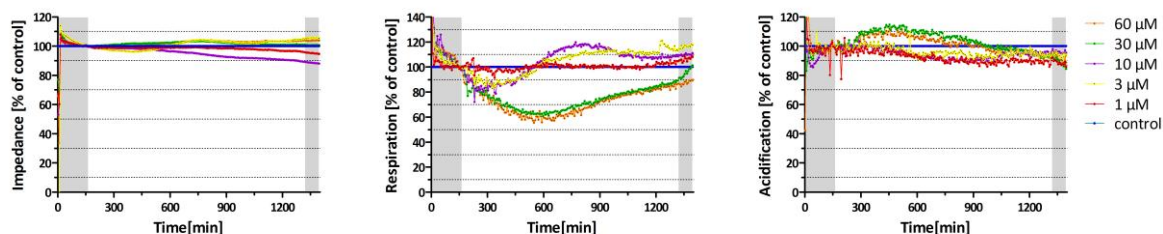


**Figure 31.** Patterns of cytosensor signals upon stimulation of HepG2 cells with cyclosporine A. Cells were incubated with the indicated concentrations of cyclosporine A. Using the multiparametric cytosensor system, three physiological parameters were monitored on-line: cell impedance being an indicator of cell morphology/adhesion, cellular respiration based on oxygen consumption, and metabolic activity resulting in extracellular acidification. The grey areas indicate the initial stabilisation and final regeneration periods, which are carried out in the absence of a test compound. Control incubation in the absence of test compound was normalised to 100%. The patterns depict means of  $n \geq 3$  experiments.

### *Effect of doxorubicin on HepG2 cells.*

Cells treated with up to 25  $\mu\text{M}$  doxorubicin were found to have stable impedance during the experiments (Figure 32). In contrast, mitochondrial respiration was directly affected and

reacted with a sudden, concentration-dependent drop after drug application. At 25  $\mu\text{M}$  doxorubicin, cell respiration diminished to 46% within 230 min, followed by a constant and non-reversible reduction to 30% during the remaining incubation period. Simultaneously, metabolic activity was reduced in a concentration-dependent- and non-reversible manner. Doxorubicin initiated a sustained decrease in metabolic activity at 390 min post-application. At the end of the incubation period, the metabolic activity was in the range of 75% and 90% for doxorubicin concentrations equal to and above 5.0  $\mu\text{M}$  and 1.0  $\mu\text{M}$ , respectively. The 24 h incubations of doxorubicin in the MTT assay indicate an impairment of cell viability (Table 6) showing a 61% and 54% reduction in viability for 10  $\mu\text{M}$  and 25  $\mu\text{M}$  doxorubicin, respectively.

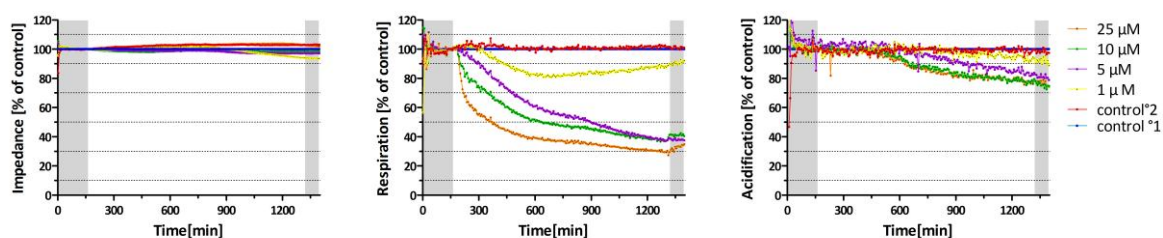


**Figure 32.** Patterns of cytosensor signals upon stimulation of HepG2 cells with doxorubicin. Cells were incubated with the indicated concentrations of doxorubicin. Using the multiparametric cytosensor system, three physiological parameters were monitored on-line: cell impedance being an indicator of cell morphology/adhesion, cellular respiration based on oxygen consumption, and metabolic activity resulting in extracellular acidification. The grey areas indicate the initial stabilisation and final regeneration periods, which are carried out in the absence of a test compound. Control incubation in the absence of test compound was normalised to 100%. The patterns depict means of  $n \geq 3$  experiments.

#### *Effect of isoniazide on HepG2 cells.*

Isoniazide was used in a concentration range of 0.1 mM to 5.0 mM. After applying isoniazide to HepG2 cells, a non-reversible and sustained reduction to 90% in impedance was observed until the end of the incubation period. An initial increase in cell impedance was detected at the highest concentration (5.0 mM), reaching a maximum of 110% at 400 min post-



application (Figure 33). Immediately after drug application, mitochondrial respiration reduced continually during the entire incubation period and remained at levels of 60 - 80% for all concentrations used. Metabolic activity was not affected and remained stable during all experiments. There was also no impact on cell viability as determined by the MTT assay (Table 6), with a viability of 103% at 5.0 mM isoniazide.

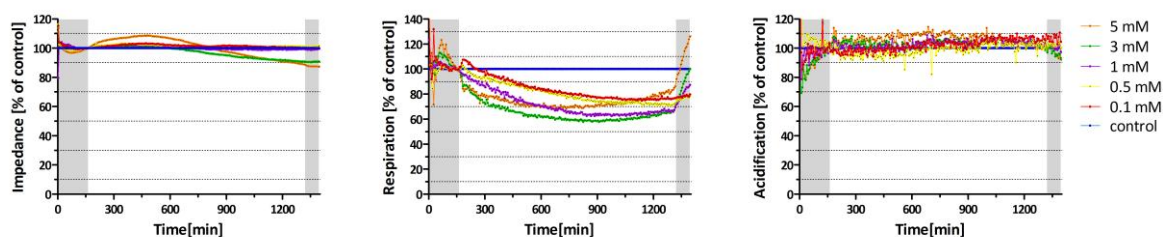


**Figure 33.** Patterns of cytosensor signals upon stimulation of HepG2 cells with isoniazide. Cells were incubated with the indicated concentrations of isoniazide. Using the multiparametric cytosensor system, three physiological parameters were monitored on-line: cell impedance being an indicator of cell morphology/adhesion, cellular respiration based on oxygen consumption, and metabolic activity resulting in extracellular acidification. The grey areas indicate the initial stabilisation and final regeneration periods, which are carried out in the absence of a test compound. Control incubation in the absence of test compound was normalised to 100%. The patterns depict means of  $n \geq 3$  experiments.

#### *Effect of methotrexate on HepG2 cells.*

Methotrexate was investigated at concentrations ranging from 1.0  $\mu\text{M}$  to 200  $\mu\text{M}$ . The two highest concentrations of methotrexate (100  $\mu\text{M}$  and 200  $\mu\text{M}$ ) initiated a reduction of impedance at 80 min post-application, described by a sustained decrease to 86% of baseline values at the end of the incubation (Figure 34). This reduction was not reversible during the regeneration phase, which indicates cell death and was corroborated by observations in the MTT assay, where cellular viability was reduced to 79% at 200  $\mu\text{M}$  (Table 6). The mitochondrial respiration curves at the two highest concentrations described an initial decrease to 78% during the first 320 min after application, followed by a persistent increase, reaching 125% at the end of the incubation. With the exception of the initial decrease,

treatment with 50  $\mu\text{M}$  methotrexate showed similar curves, reaching 145% of the cell respiration signal at the end of the incubation. Metabolic activity was inhibited in a concentration-dependent manner 30 min after drug treatment, with a maximal reduction to 70% at 200  $\mu\text{M}$ , and was subsequently maintained at levels between 60% and 80%. In contrast to cellular respiration, metabolic activity was restored after the removal of the drug, reaching levels of around 90%.

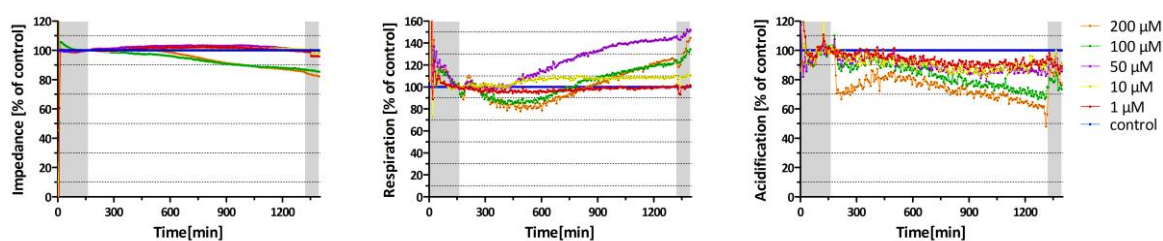


**Figure 34.** Patterns of cytosensor signals upon stimulation of HepG2 cells with methotrexate. Cells were incubated with the indicated concentrations of methotrexate. Using the multiparametric cytosensor system, three physiological parameters were monitored on-line: cell impedance being an indicator of cell morphology/adhesion, cellular respiration based on oxygen consumption, and metabolic activity resulting in extracellular acidification. The grey areas indicate the initial stabilisation and final regeneration periods, which are carried out in the absence of a test compound. Control incubation in the absence of test compound was normalised to 100%. The patterns depict means of  $n \geq 3$  experiments.

#### *Effect of valproic acid on HepG2 cells.*

Valproic acid was used in the concentration range of 0.5 mM to 10 mM. An increase to 112% in cellular impedance was observed during the first six hours of treatment with 10 mM valproic acid (Figure 35). After 640 min of treatment with 3.0 - 10 mM valproic acid, dying cells detached from the sensor chip, indicated by a constant decrease in cell impedance. Half of the initial cell amount ( $1 \times 10^5$  cells) remained on the sensor chip at the end of the incubation period with 10 mM valproic acid. Signals obtained from cell respiration sensors were concentration-dependent. The respiration curve described a sudden, steep drop to 52% at 10 mM valproic acid, followed by a bell-shaped curve with maximal amplitude of

153% at 820 min post-application. At the end of the drug incubation period, cell respiration was 130% at 10 mM valproic acid. Metabolic activity and cell respiration were reciprocally related. Simultaneous to the reduction in cell respiration, the metabolic activity increased to equal extents, reaching levels up to 145%. This amplification levelled off until the end of treatment, with residual metabolic activity of 82% at 10 mM valproic acid. Neither cell respiration nor metabolic activity was reversible in the regeneration phase. The MTT assay indicated a statistically significant trend towards decreased HepG2 cell viability at 10 mM and 1.0 mM, showing 85% and 89% remaining viability, respectively (Table 6).

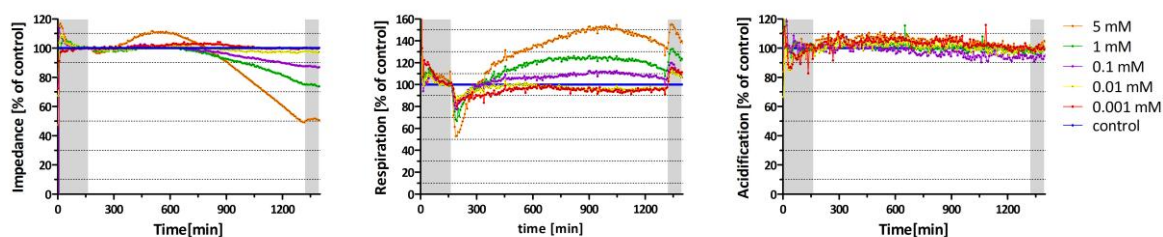


**Figure 35. Patterns of cytosensor signals upon stimulation of HepG2 cells with valproic acid. Cells were incubated with the indicated concentrations of valproic acid. Using the multiparametric cytosensor system, three physiological parameters were monitored on-line: cell impedance being an indicator of cell morphology/adhesion, cellular respiration based on oxygen consumption, and metabolic activity resulting in extracellular acidification. The grey areas indicate the initial stabilisation and final regeneration periods, which are carried out in the absence of a test compound. Control incubation in the absence of test compound was normalised to 100%. The patterns depict means of  $n \geq 3$  experiments.**

---

## 5 DISCUSSION

### 5.1 Real-time identification of P-glycoprotein substrates

Drug interaction studies in pharmaceutical drug research are of great importance when assessing the potential of a drug to generate serious interaction effects with co-administered drugs. Because the amount of medications has increased significantly, especially in adults older than 55 (6), drug-drug interactions plays a pivotal role in the design of new drugs.

The preliminary assessment of P-gp levels in L-MDR1 and parental LLC-PK1 cells indicates a high expression level of P-gp in L-MDR1 cells, and the absence of such in parental LLC-PK1 cells (Figure 10). The level of P-gp in LLC-PK1 cells was possibly below the limit of detection, which was considered low enough to use the parental LLC-PK1 cells as a control cell line in the multiparametric cytosensor system.

In the present project, a multiparametric, chip-based cytosensor system (Figure 7) was used for real-time identification of P-gp substrates in human P-gp overexpressing LLC-PK1 cells (L-MDR1). The results obtained with P-gp overexpressing L-MDR1 cells were compared with those of wild-type LLC-PK1 cells exhibiting only a marginal or no P-gp expression (161). Seven marketed drugs, known to be substrates or non-substrates of P-gp, were used as reference compounds for system validation: caffeine and propranolol are not substrates of P-gp, whereas verapamil, daunorubicin, fexofenadine, quinidine and loperamide are known substrates of the transporter. In contrast to previous studies in which pH microsensors were used for mechanistic studies on P-gp ATPase activation (162), the experiments here included measurements of cellular oxygen consumption and cell adhesion and were focused on efficient identification of P-gp substrates.

---

The multiparametric cytosensor assay was optimised with respect to maximal stimulation amplitudes to allow for sensitive, reliable recording of signals. Important assay parameters included the use of an assay medium with a low buffer capacity supplemented with 2.0% (v/v) foetal bovine serum albumin. Serum proteins reduce non-specific binding of test compounds to surfaces such as the plastic tubing of the microsensor instrument, and they enhance cellular viability in the assay system during incubation times of up to 24 h. Optimal cell densities were in a range of 0.75 to  $1.5 \times 10^5$  attached cells per chip. The design of the actual incubation chamber (i.e. the volume of the 200  $\mu\text{m}$  space between the surface of the sensor chip and the chamber lid) is of critical importance. In the experimental set-up, the effective volume of the incubation chamber was 5.7  $\mu\text{L}$  (Figure 7). Such a minimal volume is needed to monitor the rate of accumulation of metabolic products and the depletion of oxygen in the assay medium. A further reduction of the incubation chamber volume led to cell hypoxia resulting in system instability and a high signal-to-noise ratio for the measured signal. During measurements, the flow of assay medium was periodically interrupted for two minutes. After each measurement period, the incubation chamber was flushed for another two minutes with assay medium before a new measuring cycle was initiated. Prolonged phases of reduced flow of assay medium should be avoided due to the detrimental effects on cell viability and overall system stability, resulted from oxygen depletion (hypoxia). Viability of cells was monitored continuously by measurement of cellular impedance. Deviations in the range of less than  $\pm 20\%$  from initial values over a run time of 1`500 min were considered acceptable and were attributed to cell proliferation or small morphological changes after compound treatment, i.e. shrinking or swelling. Experiments were discontinued as soon as a change in impedance in excess of these limits was recorded.

---

In a first set of experiments, activity of P-gp was monitored in the presence of verapamil (a P-gp substrate (40, 124)) and the negative control caffeine (125). Experiments were initiated as soon as a stable baseline metabolic rate was attained (100% threshold in Figure 12). Extracellular acidifications as well as respiration rates were identified as correlating with P-gp activation (Figure 12, phase 1 of the experiment). Selectivity of the observed P-gp stimulatory effects were demonstrated by inhibition of P-gp activity with elacridar (GF120918), a selective third-generation P-gp inhibitor (163, 164) (Figure 12, phase 3). Elacridar on its own does not stimulate P-gp ATPase activity, but has a slight inhibitory effect on overall metabolic activity of L-MDR1 cells (Figure 12, phase 2). At the end of the experiment (Figure 12), reference 0% signal-levels of the microsensor chip were determined by Triton X-100-mediated removal of attached cells.

Observed acidification rates and respiration rates increased in the presence of increasing concentrations of up to 15  $\mu\text{M}$  verapamil (Figure 13, black symbols) and followed Michaelis-Menten type kinetics. Stimulation of P-gp by verapamil showed saturation at high concentrations and was characterised by a  $K_M$  value of  $0.92 \pm 0.12 \mu\text{M}$  (calculated based on extracellular acidification rates, mean  $\pm$  SEM,  $n = 4$ ) and  $4.9 \pm 2.7 \mu\text{M}$  (calculated based on respiration rates, mean  $\pm$  SEM,  $n = 4$ ). These values are in good agreement with a  $K_M$  value of 1.5  $\mu\text{M}$  reported previously (165) for the stimulation of P-gp for verapamil at low substrate concentrations. It is important to note that, for the first time (to my knowledge) P-gp activation was monitored not only by extracellular acidification (165) but also by stimulation of cellular respiration. In the experimental setup, extracellular acidification rates deliver stronger and more reliable signals as compared to respiration rates:  $V_{\text{max}}$  values for extracellular acidification rates ( $57.4 \pm 1.6\%$  as compared to 0% control, mean  $\pm$  SEM,  $n = 4$ )

---

were twice as high as the corresponding  $V_{\max}$  values for respiration rates ( $25.4 \pm 5.2\%$  as compared to 0% control, mean  $\pm$  SEM,  $n = 4$ ). At substrate concentrations of  $50 \mu\text{M}$  verapamil, a sudden drop in extracellular acidification rates as well as in respiration rates was observed and was attributed to substrate inhibition at high concentrations (162) of the test compound (Figure 13). However, none of the tested verapamil concentrations featured cell impedance deviations from 100% control values by more than  $\pm 13\%$ . In a separate set of control experiments (Figure 13, open symbols), P-gp-deficient LLC-PK1 cells were incubated in the presence of verapamil and did not show any stimulation effects in either extracellular acidification rates or respiration rates. Again, high concentrations of verapamil ( $50 \mu\text{M}$ ) seemed to inhibit cellular metabolic activity, which is related to the limited capacity of the P-gp transporter and a resulting substrate inhibition as described previously (162). P-gp comprises two substrate-binding sites that can translocate slow diffusion compounds. In contrast, fast diffusion compounds (e.g. verapamil) can overrun the capacity of P-gp to translocate the compounds out of the cell and lead to an apparent substrate inhibition with decreasing kinetic parameters for higher concentrations.

The question arises as to whether extracellular acidification rates or respiration rates should be used to monitor P-gp activation. Both parameters can be used to monitor cellular responses upon stimulation of cells using P-gp substrates and are therefore correlated with extracellular acidification rates is predominantly linked to glycolysis whereas respiration rates is indicative of mitochondrial respiration. In the experiments (Figure 12 and Figure 13), extracellular acidification was demonstrated to deliver a three-fold higher signal than oxygen consumption. In addition, baseline respiration rates changed over time during prolonged experimental periods. It is tempting to speculate that overall cellular viability and/or possibly

---

mitochondrial toxicity might be confounding factors that influence cellular respiration in an unpredictable way. In view of the reduced sensitivity as well as the uncertainty associated with the respiration rates parameter, it was decided to quantify P-gp stimulation based on extracellular acidification only, but to monitor respiration rates values as an additional control in parallel with identify cell-permeating compounds affecting mitochondrial respiration.

The chip-based sensor system was also used to identify substrates of P-gp. Representative examples of marketed drugs are shown in Figure 14. Activation of P-gp was expressed as the ratio of acidification rates measured during and immediately before stimulation of L-MDR1 cells (delta extracellular acidification rates). Propranolol, caffeine, quinidine, verapamil, and loperamide were used at a substrate concentration of 10  $\mu\text{M}$ . The substrate concentrations of daunorubicin and fexofenadine had to be reduced to 1.0  $\mu\text{M}$  to avoid cellular toxicity. Propranolol and caffeine, which do not interact with P-gp, were used as negative controls. All P-gp substrates were correctly identified and showed statistically significant differences ( $p < 0.05$ ) in extracellular acidification rates as compared to the negative controls. Cellular impedance and thus cellular viability were not affected by the test compounds in the concentration range used. Absences of cellular toxicity or unspecific stimulatory effects were confirmed in a set of control experiments (Figure 15). None of the test compounds stimulated extracellular acidification rates using the P-gp-deficient LLC-PK1 cell line under the same experimental conditions.



## 5.2 Purinergic P2X7 receptor mediates metabolic changes upon ATP treatment

This project investigated the effects of extracellular ATP on the metabolic activity of cells that overexpress the purinergic P2X7 receptor. I conclude that P2X7 receptors are mediators of these effects, based on the observation that high concentrations of ATP are necessary to induce these metabolic changes and on their inhibition by a selective P2X7 receptor antagonist.

Hydrogen peroxide is a metabolic side product of cell respiration and can be used as a marker for changes in the metabolic activity of cells (126). I measured the hydrogen peroxide released in human mononuclear blood cells upon ATP treatment and found that ATP induced a concentration-dependent increase in H<sub>2</sub>O<sub>2</sub> release with an EC<sub>50</sub> value above 500 μM (Figure 16A), confirming previous reports by Skaper *et al.* (166). In addition, the mass redistribution of HUVEC cells was assessed and showed EC<sub>50</sub> values above 900 μM (Figure 17). Based on the similarity of EC<sub>50</sub> values, I hypothesised the involvement of the P2X7 receptor in mediating the concentration-dependent increase in metabolic activity and morphological changes. To test my hypothesis, I used a specific P2X7 receptor antagonist and showed a strong concentration-dependent inhibition of the ATP-induced hydrogen peroxide release in human mononuclear blood cells (Figure 18). Furthermore, Bz-ATP, a specific agonist for P2X4- and P2X7 receptors (71), was used at a one-tenth concentration (400 μM) as compared to ATP (4`000 μM) and induced equal hydrogen peroxide release at these concentrations from human mononuclear blood cells (Figure 19); further indicating that the increased metabolic activity of the mononuclear blood cells were mediated by P2X7 receptors.

As a validation step, I initially confirmed the functionality of the P2X7 receptors in a recombinant HEK-hP2X7 cell line using the YoPro1 uptake assay and I confirmed the affinity

---

of the antagonist in blocking P2X7 receptors (Figure 24) with an  $IC_{50}$  of 11.2 nM. The experiments with the rodent cells and the YoPro1 uptake experiment were intended to compare and confirm the pharmacology of P2X7 receptors with the classical read-outs traditionally used for studying P2X7.

I subsequently utilised these cells to further investigate the changes in metabolic activity by means of a cell-based, real-time monitoring sensor system, capable of simultaneously recording extracellular acidification as a marker for metabolic activity, oxygen consumption as a measure for cellular respiration, and impedance as a means to assess changes in cell morphology and adhesion. Pfeiffer et al. (128) previously described changes in cell morphology in the presence of P2X7 agonists in cells expressing P2X7 receptors, as P2X7 receptors are co-localised with  $\alpha$ -actin,  $\beta$ -actin, and the  $\beta$ 2-integrin subunit, i.e. factors determining changes in the cytoskeleton components (167). These described morphological changes were detected and confirmed by the measurement of cellular impedance (Figure 20). In addition to this, HEK-hP2X7 cells exhibited concentration-dependent swelling upon treatment with Bz-ATP, possibly reflecting the osmotic influx of water into the cells due to pore dilatation. The estimated potency of Bz-ATP (Figure 21) in terms of cell morphology in this assay was calculated with an  $EC_{50}$  of 9.6  $\mu$ M. The morphological changes detected in parental HEK293 cells were in the range of biologically acceptable deviations, emphasising the hypothesis that P2X7 is the mediator of the detected changes in P2X7 expressing cells.

In addition, cellular respiration was maximally increased at 50  $\mu$ M Bz-ATP to 23% as compared to parental cells. Treatment with 100  $\mu$ M Bz-ATP led to a drop of 23% as compared to parental cells in cellular respiration, indicative for mitochondrial stress (168), whereas metabolic activity was amplified to 24% as compared to parental cells, providing evidence for a role of P2X7 in cellular metabolic activity. The resulting impairment in the

---

generation of ATP via oxidative phosphorylation was compensated to a certain extent by the enhancement of metabolic activity, monitored by an increase in extracellular acidification of up to 23% above the levels derived from control incubations with parental HEK293 cells. The reduction of cellular respiration was probably linked to the formation of reactive oxygen species (166) and activation of the apoptosis cascade (169).

Using the multiparametric cytosensor system, I observed multiple readouts on cellular metabolism simultaneously, enabling a more complete picture to be generated of how ATP affects cellular metabolism through the P2X7 receptor. All effects on cell morphology, mitochondrial respiration, and metabolic activity, as induced by 50  $\mu\text{M}$  Bz-ATP, were inhibited with potencies between 77% and 92% using 10  $\mu\text{M}$  of the P2X7 receptor antagonist (Figure 22). Neither activation nor inhibitory effects were detected in parental HEK293 cells (Figure 22), suggesting that all effects were indeed mediated through the P2X7 receptor.

I investigated how this link between P2X7 receptors and metabolic activity correlates with other functions of these ion channels. In patch-clamp experiments with mouse microglia BV2 cells, which directly measure the flux of small, inorganic ions through these P2X7 channels, Bz-ATP showed distinct effects on the receptor activity ( $\text{EC}_{50} = 197 \mu\text{M}$ ), and the selective P2X7 receptor antagonist had similar affinity ( $\text{IC}_{50} = 2.1 \mu\text{M}$ ), indicating an involvement of the P2X7 receptor in mediating these agonist-induced effects (Figure 23).

I also tested the impact of P2X7 on  $\text{Ca}^{2+}$  influx, and thus cell depolarisation (Figure 25). Primary rat cortical cells were used for these experiments, because P2X-mediated  $\text{Ca}^{2+}$  influx cannot be determined in HEK293 cells, due to the co-activation of endogenously expressed purinergic P2Y receptors (170). However, an experiment with exogenously generated P2X7 activation led to an increased  $\text{Ca}^{2+}$  signal in the cells (171, 172) and was blocked by the P2X7

---

receptor antagonist ( $IC_{50} = 3.2 \mu\text{M}$ ), with similar affinity as derived from patch-clamp experiments.

From a comparison with other functions of P2X7 receptors, such as  $\text{Ca}^{2+}$  influx or depolarisation, it is not possible to deduce clear pathways from ATP-gated channel opening to the activation of cellular metabolism. Both small cations ( $\text{Ca}^{2+}$ ) influx and larger molecules entering the cell upon P2X7-related pore opening triggered further downstream effectors (i.e. interleukin-1 $\beta$  release, apoptosis, etc.)

---

### 5.3 Characterisation of drug-induced liver effects in HepG2 cells

Identifying hepatotoxic effects of potential drug candidates that lead to drug-induced liver injury (DILI) in human remains a challenge. Standard preclinical animal models do not reliably predict human toxicity (animal concordance of 55%) (173).

To improve predictability, specialised animal models can be combined with, for example, *in silico*, *in vitro* (endpoint assays) or toxicogenomic approaches (103). In this context, it was proposed that cytosensor systems be used to monitor reduction in metabolic rates as an indicator of cell death (174). Due to technical limitations, measurements were thereby limited to measuring cellular acidification rates. Only recently have novel, multiparametric sensor chips become available that can be used for the simultaneous determination of cellular impedance as a measure of cell morphology and adherence, oxygen consumption as a measure of mitochondrial respiration, and extracellular acidification as a measure of cellular metabolism, i.e. release of metabolic breakdown products such as lactate and carbonate resulting in a change in extracellular pH (110). In this project, high sensitivity and responsiveness of the multiparametric cytosensor system was achieved by combining an assay medium with low buffer capacity and a minimal inner volume of the perfusion chamber (Figure 7). The system therefore permitted real-time monitoring of physiological changes resulting from toxicological insult over a 24-hour period in human hepatocarcinoma-derived HepG2 cells.

To validate the cytosensor approach, eight different reference drugs known to be hepatotoxic at certain concentrations (Table 5) were selected. They exhibit different hepatotoxic mechanisms and patterns of liver pathology. The drugs are structurally diverse, are used for different clinical indications, and the selection included the intrinsically cytotoxic drugs doxorubicin and methotrexate used to treat cancer. D-sorbitol, known to be

---

non-toxic and well tolerated even at high concentrations, was used as a negative control (160). Assay concentrations were comparable to clinically relevant plasma concentrations, covering a nanomolar to millimolar range.

The test compounds have been reported to have different mechanisms of toxicity (Table 5). Cellular viability was measured by the MTT assay, which responded in a statistically significant manner to the antineoplastic drugs, acetaminophen, cyclosporine A and valproic acid (Table 6). Methotrexate and doxorubicin were used at clinical plasma concentrations as analysed in human cancer treatment. Clinical plasma concentrations of methotrexate and doxorubicin are measured at 1`150  $\mu$ M (147) and at 1.9  $\mu$ M (139), respectively. All other drugs investigated in the MTT viability assay reduced cell viability only at concentrations clearly above the clinically relevant human plasma concentrations. Interestingly, all analysed compounds known to cause DILI in humans also responded with very distinct and characteristic signal patterns in the multiparametric cytosensor assay (Figure 28 to Figure 35). All observed effects were rigidly concentration-dependent. This result was unexpected, because reactive metabolites (and not the parent compound alone) are often suspected sources of adverse effects (Table 5). Thus, in liver tissue, hepatotoxicity is frequently linked to accumulation of the parent drug in combination with its metabolites, initiating pathological effects, and/or an altered cellular defence mechanism, such as the depletion of glutathione (GSH), formation of ROS or the inhibition of metabolising enzymes. In the present study, the human hepatocarcinoma-derived HepG2 cell line was used. As opposed to primary human hepatocytes, HepG2 cells are characterised by a defined but low expression level of cytochrome P450 monooxygenases (113). In contrast, expression levels of most phase II enzymes seem to be normal (175, 176). The results suggest that phase II metabolic enzymes in combination with residual phase I metabolic enzyme (e.g.

cytochrome P450) activity may generate adequate levels of intracellular metabolites to trigger cytotoxic reactions. HepG2 cells therefore seem to be a convenient, stable, economic, and relatively easy to handle alternative to hepatocytes for cytosensor-based toxicological investigations. This view was supported by control experiments where amiodarone and acetaminophen were used to assess the phase I and phase II metabolising enzymes (Figure 26 and Figure 27).

Analysis of the reference drugs in the multiparametric cytosensor system revealed distinct signal patterns that allowed for classification according to six distinct cytotoxic reaction types (Table 7, Figure 37).

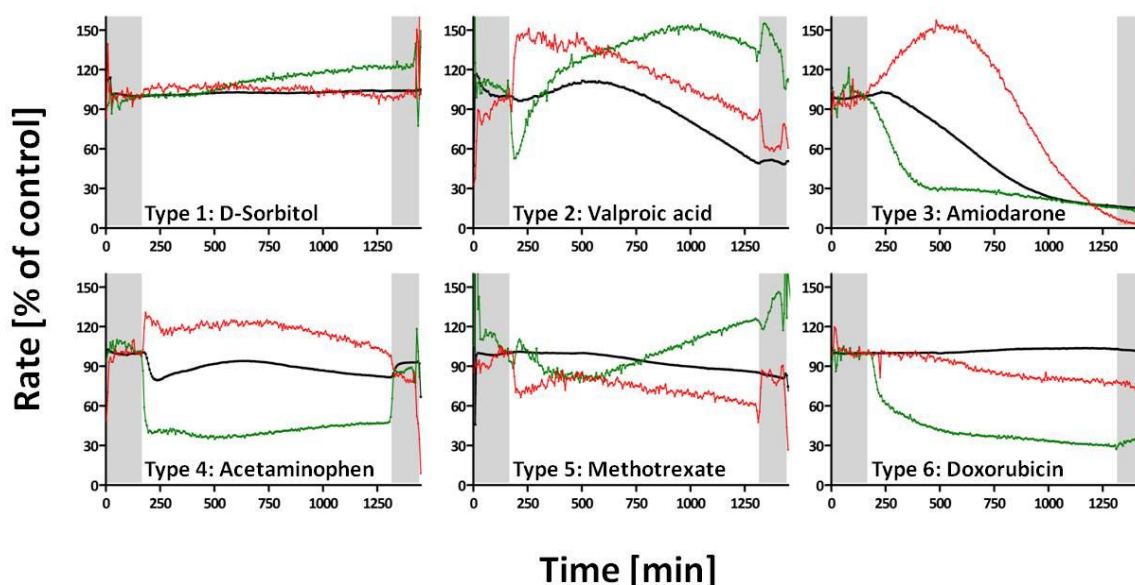


**Figure 36.** Classification of cytotoxic effects based on cytosensor signal patterns. Incubation of HepG2 cells with elevated concentrations of hepatotoxic drugs has an impact on cell morphology/adhesion (impedance, black line), metabolic activity (acidification, red line), and cellular respiration (oxygen consumption, green line). Cellular responses and cytotoxic effects can be classified according to six typical signal patterns (Table 7). Representative examples of experiments are shown in which treatment of HepG2 cells resulted in cytotoxicity and cell death (toxicological effects type 2 and 3) or cellular stress (effects of type 4 to 6). D-sorbitol served as a negative control (no cytotoxicity type 1). Effects are considered reversible if baseline levels of signals are re-established after wash-out of drug (grey areas, absence of test compound). The patterns depict means of  $n \geq 3$  experiments.

**Table 7. Classification of toxic effects based on multiparametric cytosensor signal patterns. Physiological parameters were monitored online in HepG2 cells and included metabolic activity (acidification), respiration (oxygen consumption) and cell morphology and adhesion (increased by swelling of cells or decreased by cell detachment or shrinking). Signals were stable over time (○), increasing in intensity (+) or decreasing (—). Typical signal patterns of representative drugs are shown in Figure 36.**

Type	Classification	Endpoint	Impedance	Acidification	Respiration	Example
1	No toxicity	No effect	○	○	○ / +	D-sorbitol
2	Necrosis-like	Cell death	—	○ / +	+	Valproic acid
3	Apoptosis-like	Cell death	—	○ / +	—	Amiodarone
4	Oxidative stress	Cell stress	○	○ / +	—	Acetaminophen
5	Metabolic stress	Cell stress	○	—	+	Methotrexate
6	Oxidative and metabolic stress	Cell stress	○	—	—	Doxorubicin

Type 1 is represented by D-sorbitol (Figure 36), a well tolerated and safe compound (160), as confirmed in the project. The slight increase in cell respiration of 20% at 5.0 mM during the 24 h of the experiment was attributed to active compensation of the osmotic effect of D-sorbitol on cells.

Type 2 signal patterns are represented by valproic acid (Figure 36). This compound is one of the most widely used antiepileptic drugs, with a black box warning for hepatotoxicity. Oxidative stress, GSH depletion, as well as mitochondrial dysfunctions and necrosis have been associated with valproic acid treatment (159, 177-179). Recently, Ji et al. reported toxicological effects due to valproic acid and its reactive metabolites, suggesting an ability to damage liver cell plasma membranes and resulting in leakage of intracellular enzymes and finally cell death via necrotic or apoptotic pathways (158). These findings were confirmed in the cytosensor assay: an irreversible decrease of 50%, at 10 mM, of the impedance over time, which indicated cell death. This effect was preceded by a short and transient period of



---

water influx resulting in transient cell swelling (i.e. increased impedance), as described recently (180). A sudden drop in respiration was observed after the addition of valproic acid in the first 20 min of incubation, indicating reduced oxidative phosphorylation and hence reduced ATP generation. The reduced cell respiration was compensated by an increase in metabolic activity for a similar time range. The observed reduction of intracellular concentration of ATP led to strong oxidative and metabolic stress and caused an initiation of energy-independent necrotic-like pathways, which was detected in a previous study (181). Consequently, metabolic activity levelled off at 82% over the entire experiment.

Amiodarone was used as a second drug with a black box warning for hepatotoxicity and it is known to generate liver steatosis and hepatocellular death (119). In the multiparametric cytosensor system, the strong tendency of amiodarone to damage cells was confirmed (i.e. irreversible decrease in impedance) and was classified as type 3 (Figure 36), representing drugs causing apoptotic-like cell death. Amiodarone showed the most distinct concentration-dependent cytotoxic behaviour of all drugs analysed in this study. After 9 h of amiodarone treatment (15  $\mu$ M and 30  $\mu$ M), only 50% of the initial cells remained on the sensor chip. Higher concentrations of amiodarone showed almost complete inhibition of cellular respiration (15% of control), correlating with a continuous release of dying cells from the sensor chip. It is interesting to note that these concentrations of amiodarone can also be reached in human plasma (Table 5). Mitochondrial toxicity induced an amplification of metabolic activity as a compensatory but transient means of ATP regeneration. This compensatory mechanism failed after approx. 6 to 8 hours and amplified metabolic stress, as previously described (137) and demonstrated by the steep drop of the acidification curve down to 7%. Amiodarone showed no recovery of signals, thus identifying amiodarone as a

---

potent hazard to liver cells at elevated levels in tissue, without the possibility of regeneration. Furthermore, the observed effects support the previous findings of the production of reactive oxygen species, induced mitochondrial damage, and promoted apoptosis in HepG2 cells (182). It is still unclear whether amiodarone, its postulated reactive metabolite (desethylamiodarone), or both cause toxicity (133). However, the findings showed the significant potential of amiodarone to damage the liver, which was in good agreement with the black box warning of hepatotoxicity on this drug.

In contrast to drugs that induce cell death (i.e. type 2 and type 3 cytotoxicity), several drugs were identified that caused cellular stress only but no changes in cellular impedance. Three out of eight compounds in this study were identified as inducing oxidative stress in HepG2 cells (type 4, acetaminophen, cyclosporine A, and isonidazide). Acetaminophen induces mitochondrial stress upon formation of its reactive metabolites as a consequence of depletion of GSH. Acetaminophen is widely used as an analgesic and antipyretic compound, and is classified as a non-steroidal anti-inflammatory drug. The first hours of the treatment phase showed slight and reversible shrinking of the cells, reflected by reduced impedance values of 70% to 80%, followed by an apparent regeneration period (Figure 36) during which the impedance was maintained at around 80%. This apparent regeneration is most likely linked to the disturbance of mitochondrial  $\text{Ca}^{2+}$  homeostasis (183), characterised by a phenotypic blebbing of the cell surface. Cellular respiration was intensely affected in a concentration-dependent manner and inhibited the respiration to 40% at 10 mM, indicating severe oxidative stress on the cell respiratory system, the formation of toxic benzoquinone metabolites, and the linked depletion of GSH, as previously described (131, 184). The intense impairment of respiration and the consequent deficit of oxidative phosphorylation results in

---

a lack of ATP generation. During such events, cells typically compensate for lack of energy generation by enhancing ATP generation via glycolysis, which is confirmed by the increase in metabolic activity to 130% at 10 mM. During the drug wash-out period, the signals of impedance and cell respiration almost recovered to initial baseline values prior to acetaminophen treatment. Wash-out of the drug reactivated the formation of ATP via oxidative respiration, leading to a decrease in metabolic activity, as the generation of ATP via glycolysis was no longer in demand. A study by Roe et al. (1993) confirmed the formation of the reactive metabolite (NAPQI) and phase 2 conjugation products in HepG2 cells, among others (e.g. benzoquinone) that were also responsible for adverse effects (113). Cyclosporine A showed similar effects (Figure 31) in all physiological parameters. This potent immunosuppressive agent prolongs survival of allergenic transplants by suppressing humoral immunity and, to a greater extent, cell-mediated immune reactions such as allograft rejection and delayed hypersensitivity. Unfortunately, cyclosporine A is associated with toxic effects to several organs, mainly the kidney, but also the liver, which is confirmed in my experiments. Oxidative stress was induced in HepG2 cells, particularly at concentrations equal to and above 30  $\mu$ M followed by a regenerative phase and a slight compensatory amplification of the metabolic activity. It should be noted that the observed effects were apparent at concentrations that were 40 times higher than clinically relevant plasma concentrations of cyclosporine A and therefore of no direct clinical relevance. Additionally, cyclosporine A exemplified the limitations of the HepG2 cells, because the hepatotoxicity of cyclosporine A is accompanied by the ability to inhibit hepatic bile-salt export transporters (e.g. ABCB11) (185). These pumps are responsible for the secretion of bile components into the bile canaliculi. A block of these bile-salt export pumps results in an intracellular accumulation of bile salts and thus cholestasis (119, 186). HepG2 cells are a common *in vitro*

---

model to analyse toxic effects on the liver (187). However, in previous studies, HepG2 cells showed impaired bile-salt transporter levels (188) and therefore HepG2 seems not to be the most appropriate model for studying such specific effects. An alternative to indicate toxicological effects linked with these efflux transporters would be the use of primary hepatocytes.

Isoniazide, another example of a drug that induces oxidative stress, is associated with mild to severe liver toxicity in 2% of patients (189). Its metabolism is characterised by the formation of hydrazine ( $H_2NNH_2$ ) and an additional toxic intermediate, isonicotinic acid. Hydrazine is a well-characterised hepatotoxin (190, 191). Hydrazine can be formed directly by amidohydrolase or indirectly via the isonicotinic acid pathway (N-acetyltransferase) to form acetylhydrazine and then hydrazine. Histopathological observations of isoniazide-induced liver toxicity reveal inflammatory processes and cell death (189). In the experiments (Figure 33), cellular respiration was affected in a concentration-dependent manner and was maximally reduced to 60%, indicative of previously described observations of oxidative stress to cells after isoniazide treatment (143, 144).

Methotrexate is a compound that induces metabolic stress to cells (type 5, Figure 36). This drug is a folic acid antagonist used at high doses in cancer therapy. The intrinsic toxicity of methotrexate was evident in the MTT assay, showing reductions to 70% and 79% of cell viability at 50  $\mu M$  and 200  $\mu M$ , respectively. The mechanism of liver injury is poorly understood (152). The pathological pattern of methotrexate-induced liver injury varies from mild liver enzyme elevations to severe fibrosis and cirrhosis. Methotrexate enters the cell via a folate transporter and is retained within the cell as a polyglutamate (151). The drug inhibits

---

the enzymes required for the synthesis of purines and pyrimidines (192). It additionally blocks the conversion of homocysteine to methionine. High levels of homocysteine cause metabolic stress, with the above-described consequences, i.e. impaired metabolic activity (193, 194). Metabolic stress was clearly observed using the multiparametric sensor system, by a metabolic inhibition to a maximum of 60% of baseline values at 200  $\mu\text{M}$ . The highest concentration (200  $\mu\text{M}$ ) investigated was six-fold below the detected clinical plasma concentrations in humans receiving methotrexate at high doses for anticancer therapy (1`150  $\mu\text{M}$ , Table 5). Therefore methotrexate was a prime example of a drug that is intrinsically toxic, intensely inhibits metabolic activity and induced metabolic stress in HepG2 cells, which was previously described (150). The amplified cellular respiration agreed well with the impaired glycolytic activity, which represents a compensatory mechanism to generate ATP.

Doxorubicin indicates a combined pattern of oxidative and metabolic stress (type 6, Figure 36). Doxorubicin is an anthracycline derivate, commonly used in the treatment of a wide range of cancers, including hematological malignancies, many types of carcinomas, and soft tissue sarcomas. The MTT assay reflects the intrinsic cytotoxicity of the drug (54% viability at 25  $\mu\text{M}$ ), even at concentrations below the human plasma concentrations, which is 1.9  $\mu\text{M}$  (139). The MTT assay at 1.0  $\mu\text{M}$  doxorubicin showed a statistical significant decrease in cell viability of 30% (Table 6) on HepG2 cells after 24 h treatment. During its metabolism, doxorubicin undergoes a one-electron reduction by different oxidoreductases to form a doxorubicin-semiquinone radical (195). The re-oxidation of the radical back to the parent drug leads to the formation of ROS and hydrogen peroxide (196). The reactive species might then cause oxidative stress, lipid peroxidation, damage to proteins and the mitochondrial

---

membrane, oxidation of mitochondrial DNA, as well as the activation of the redox-sensitive mitochondrial permeability transition pore (197). Consequently, the bioenergetics of the cells alters radically (198). I was able to monitor these effects in the cytosensor assay, in that cellular respiration was significantly inhibited ( $IC_{50}$  of  $< 5 \mu M$ ), as a consequence of mitochondrial damage that inhibits cellular respiration. In addition, an inhibition of cellular metabolic activity was observed. These findings are in agreement with previous studies (197). Neither metabolic nor respiratory activities regenerated during the drug wash-out period, indicating irreversible impairment of cell viability, even at clinical relevant concentrations (Table 5).

Using the multiparametric cytosensor system, I was able to monitor alterations in cellular metabolism, respiration and impedance in real-time. These changes were linked to the chemical-induced toxicological effects of the drug or its reactive metabolites. An assessment of reversibility of the effects was used to acquire additional insight into the underlying mechanisms of toxicity. In contrast to the well-established cellular viability (MTT) endpoint assay, the onset of toxic effects was monitored on-line, as opposed to the determination of a physiological endpoint. Based on these results, a Test-Flag-Risk Mitigation strategy (Figure 38) is being introduced; it can be used to extrapolate from an *in vitro* to an *in vivo* situation and to determine risk of cytotoxicity for a given test compound. I propose that signals from the cytosensor system should trigger an alert (flag) that will determine a further course of action and a follow-up strategy. Depending on concentrations used and reversibility of effects, animal experiments will be needed. Such studies can be combined with additional *in vitro* and/or *in vivo* experiments (e.g. enzyme induction or inhibition, drug transporter studies, etc.) to elucidate the mechanism of any adverse effect. Such a Test-Flag-

Risk Mitigation strategy helps reduce the risk of hepatotoxicity and therefore leads to better management of risks associated with DILI. It remains to be elucidated whether this approach can be extended to other organ-specific cell lines that are used to evaluate organ specific toxicity (187).

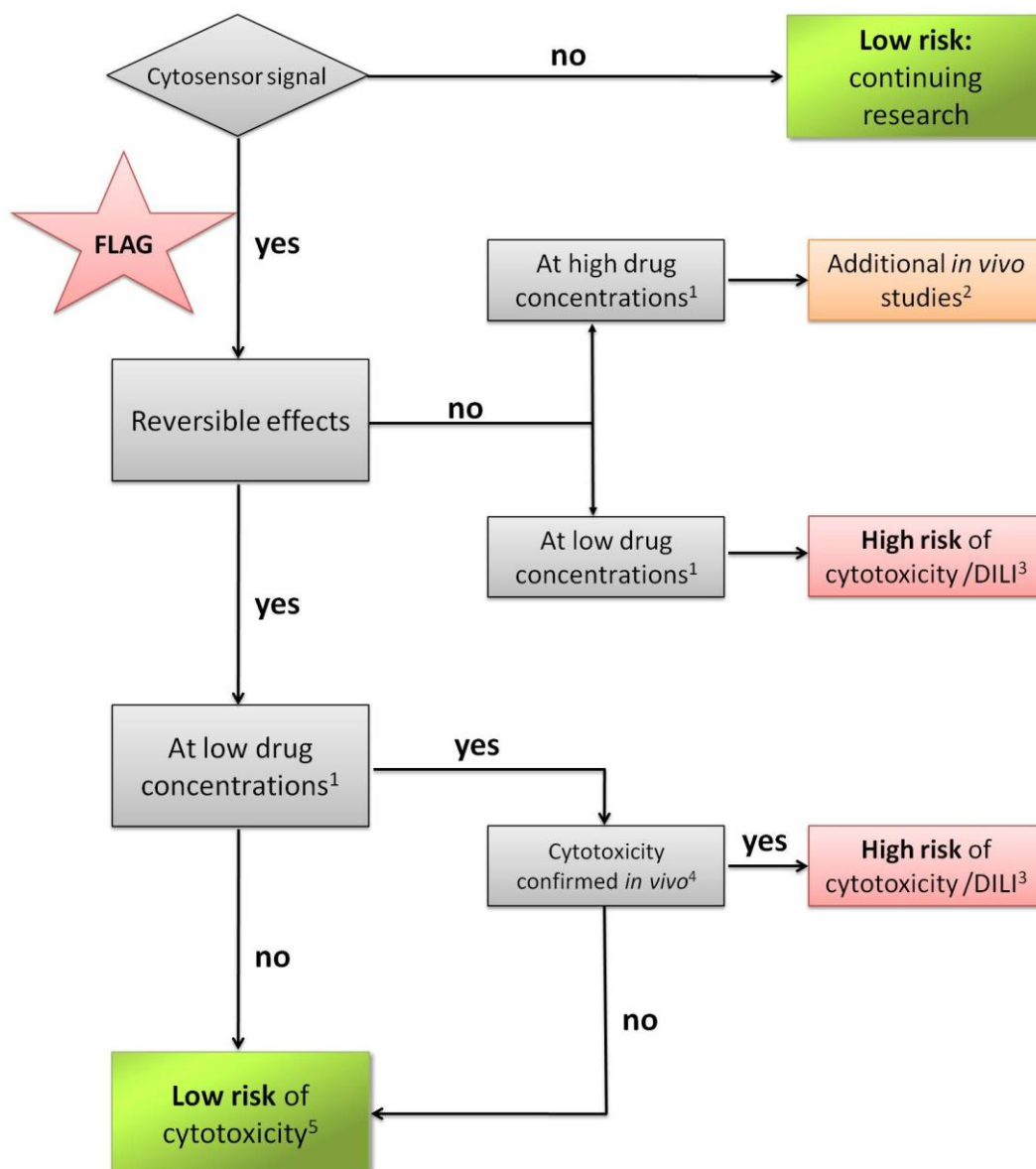


Figure 37. Test-Flag-Risk-Mitigation strategy based on findings in the cytosensor *in vitro* assay. Decisions to be taken during the drug discovery and development process will depend on the mechanism and extent of the observed cytotoxicity relative to the predicted therapeutic drug concentrations (i.e. classification as "low" or "high" drug concentrations). Potential risks uncovered in the multiparametric cytosensor test system will raise a flag and have to be addressed by confirmatory *in vivo* studies. <sup>1</sup>Relative to the awaited plasma concentrations; <sup>2</sup>increase the dose in animal models to elicit the adverse effects from the *in vitro* assay; <sup>3</sup>probably detected also in animal toxicology models and the drug research discontinuation is already decided; <sup>4</sup>further animal studies required for the clarification of the adverse effects and the *in vitro-in vivo* correlation; <sup>5</sup>probably increase the dose in animal studies to classify the drug as 'safe'.

## 6 CONCLUSION

The basic mission of the pharmaceutical industries is to understand disease and to bring safe and effective new drugs to the market. For many reasons, the path to developing new drugs is fulfilled with hurdles and is comparable to the proverbial search for the needle in the haystack. The development of a new drug that fulfils all requirements is long (> 10 years) and very expensive (> 500 million dollars) and has a success rate of only 0.01%.

Therefore, the pharmaceutical industry is looking for new assays to, for example comply with the safety requirements of the authorities, or more specifically to support drug discovery (e.g. discover new drug targets) and drug development (e.g. safety analysis).

Considering this, the general idea of this PhD thesis was to use an *in vitro* technology that can monitor physiological parameters of cells and to develop novel assays that overcome obstacles in drug research.

For the determination of the physiological alterations, I used a non-invasive, label-free multiparametric cytosensor system to monitor simultaneously extracellular acidification, cellular respiration, and cell morphology/adhesion.

Drug-drug interactions and drug resistance are two of the most redoubtable detections in the development of a new drug, because they have a crucial influence on the pharmacodynamic and pharmacokinetic of a drug. A major role of these negative effects was imputed to the ABC-transporters and their famous member, P-gp. P-gp is found in many endothelial cells of the body, where it acts as a barrier to molecules, including drugs. In this case, efficient *in vitro* screening methods have been developed and used frequently in drug development. However, these assays are not necessarily reflecting the real *in vivo* situation and evince several limitations in the reliable identification of substrates of the P-gp



---

transporter. Utilising the properties of the P-gp transporter to hydrolyse ATP for the translocation of substrates, I was able to identify substrates for P-gp transporters by measuring the regeneration of the hydrolysed ATP in living cells expressing P-gp at high levels. The ATP regeneration process is linked to the excretion of acidifying metabolic breakdown products and increased oxygen consumption, and this was clearly observed using the multiparametric cytosensor system. Concentrations of compounds used in the experiments with the multiparametric cytosensor system showed great sensitivity, and this provides the opportunity to reduce concentrations of test compounds to more physiological relevant concentrations. Confirmatory experiments with cells lacking an expression of P-gp showed a clear absence of any effects detected with cells overexpressing P-gp. The effects were concentration-dependent and followed protein kinetic behaviour. The estimated protein kinetic parameters were in good agreement with previously published data. Summarising the results of the P-gp project it was possible to develop a novel, label-free and non-invasive technology to identify reliably P-gp substrates in living cells. The P-gp project serves as a proof-of-concept project and the extension of the validated application to other ATP-dependent transporters can be investigate.

Another project was the characterisation of a potential new drug target, i.e. the purinergic P2X7 receptor, using the multiparametric cytosensor system. The effects of intracellular ATP are well described, but little is known about the effects of extracellular ATP, particular when the extracellular concentrations of ATP rise due to pathological circumstances. I analysed these effects and was able to link the detected physiological changes to the P2X7 receptor. The study identifies a leading role of the purinergic P2X7 receptor in mediating downstream signalling and thereby changes in cellular metabolism at non-physiologically high levels of extracellular ATP.

In summary, I discovered the role of P2X7 receptors in coupling extracellular ATP with yet to be elucidated intracellular metabolic pathways. Further experiments are necessary to investigate the specificity of the receptors involved in this link between extracellular ATP and metabolic activity and in what normal or pathological situations this coupling plays a role. Extracellular ATP has been shown to play a role in inflammation and apoptosis, and there are models of this relationship, between extracellular ATP and metabolic activity, that already exist, with both processes highly linked to metabolism. It is readily conceivable that P2X7 receptor-mediated modulation of cellular metabolism contributes to some of the observed downstream effects, such as cytokine release, at least to some degree.

In the third project, I used the multiparametric cytosensor system to identify adverse effects in liver cells upon exposure to drugs known to exhibit the potential to injure the liver. I used an established and characterised liver cell line (HepG2) and proved the possibility of using this cell line, despite its limitations in metabolic activity and expression of drug transporters.

A panel of eight marketed drugs was used to develop a novel cytosensor-based *in vitro* toxicological assay. Reference drugs in my study were classified as either non-toxic (D-sorbitol), intrinsically toxic (antineoplastic drugs) or potentially toxic under conditions of exaggerated exposure resulting from, for example, intentional intoxication, drug-drug interactions or disease-induced physiological alterations. Drugs were tested using concentrations equal to, above, and below the clinically relevant plasma concentrations. Real-time monitoring of drug-induced physiological effects in HepG2 cells revealed characteristic signal patterns. Mechanistic insight into the action of these compounds was used to predict detrimental events such as cell stress, cell death, cytotoxicity, or DILI in humans. In addition, information was obtained on the reversibility of the observed effects. All identified alterations were rigidly concentration-dependent. My findings suggest that

cytosensor-based toxicological investigations may provide early indications of potential mechanisms of hepatotoxicity, which might be followed up by studies in experimental animal models. The early indications of potential mechanisms of hepatotoxicity, together with the Test-Flag-Risk Mitigation strategy, may therefore guide the design of specific follow-up studies in experimental animals.

Based on the capabilities of the multiparametric cytosensor system, it was possible to develop successful three new, supportive assays for different areas of the pharmaceutical research (i.e. preclinical, toxicology, and pharmacology) and the system therefore exceeded the expectations of the author of this PhD thesis. Based on the knowledge derived from the PhD thesis projects, it is possible to implement the multiparametric cytosensor system in laboratories for these specific disciplines and probably to extend its use to similar or different applications.

## 7 ABSTRACT

The basic mission of the pharmaceutical industry is to understand disease and to bring safe and effective drugs to patients. Starting with the drug discovery process, for any particular disease a first step involves selecting a disease-specific target, then finding a suitable assay to determine the activity of molecules in relation to the selected target. This path is difficult and, lacking proper technology, is similar to the proverbial search for the needle in a haystack. However, once a molecule emerges as a successful candidate in the drug discovery process, it enters into drug development. The drug development process provides safety data prior to "first-in-man" trials. Drug discovery and development are extended, expensive, and inefficient processes with a success rate of only 0.01%. Placing these difficulties into perspective, it remains the desire of the pharmaceutical industry to develop novel, economical, reliable *in vitro* technologies to meet the above challenges.

In this PhD thesis, a multiparametric cytosensor system was used for real-time identification of physiological parameters in living cells, and to meet the above-mentioned challenges in drug research. This technology allows us to simultaneously monitor extracellular acidification (pH changes), cellular respiration (oxygen consumption), and cellular morphology and adhesion (impedance measurements).

All work done by a cell and all of the activities of life in general necessitate energy, commonly in the form of adenosine triphosphate (ATP). The regeneration of the consumed ATP leads to increased oxygen consumption and an excretion of acidifying side products (lactate and carbon dioxide), which can be monitored and used to deduce changes in physiological pathways.

---

The first project of this thesis explored the influence of the P-glycoprotein (ABCB1) transporter on drug-drug-interactions, drug resistance, as well as drug absorption and distribution, all of which are important factors to be considered during the development of new drugs. Thus, the early identification and the exclusion of compounds that show a high affinity to P-glycoprotein can help to select drug candidates. The aim of this first project was to use the multiparametric cytosensor system for the label-free identification of P-glycoprotein substrates in living cells by monitoring extracellular acidification and cellular respiration upon stimulation with substrates of P-glycoprotein. Using L-MDR1 cells, a human P-glycoprotein-expressing cell line, the influence of P-glycoprotein activity was determined for seven different compounds, demonstrating the applicability of the system for P-glycoprotein substrate identification. Effects were concentration dependent, as shown for the P-glycoprotein substrate verapamil, and were associated with cellular acidification and respiration. P-glycoprotein ATPase activation by verapamil was able to be described by a Michaelis-Menten type kinetics profile showing saturation at high substrate concentrations. Control experiments using a P-glycoprotein inhibitor indicated that the observed effects were related to P-glycoprotein ATPase activity. In contrast, wild-type LLC-PK1 cells that did not express P-glycoprotein were not responsive to stimulation with different P-glycoprotein substrates. Summarising these findings, the microsensor system used is a generic system suitable for the identification of P-glycoprotein substrates. In contrast to other biochemical P-glycoprotein assays, activation of the drug efflux pump can be monitored on-line and label-free in living cells in order to identify P-glycoprotein substrates and to study the molecular mechanisms of ATP-dependent active transport.

The second project of this thesis explored the pharmacology of the purinergic P2X7 receptor and its influence on changes in metabolic activity after ATP treatment. The purinergic P2X7

---

receptor plays a prominent role in cell metabolism and possibly determines downstream effects based on its interactions with extracellular ATP. Adenosine triphosphate, a key agent in physiology, provides energy in numerous reactions and acts as a neurotransmitter. Extracellular ATP concentrations are known to rise under pathological conditions, thereby triggering immune system responses that lead to pro-inflammatory states and immune modulation, to the extent of initiating cell death. These adverse effects have been linked to the purinergic P2X7 receptor, which triggers downstream signalling when levels of extracellular ATP are high. The purinergic P2X7 receptor is also involved in modulating cellular responses that include membrane depolarisation, secondary messenger activation,  $\text{Ca}^{2+}$  influx, and activation of the mitogen-activated protein kinase pathway. Moreover, it features a unique ability to form a large, non-selective pore, allowing molecules up to 900 Daltons to enter the cell, with potentially deleterious consequences. In addition, the P2X7 receptor purportedly regulates many metabolic processes inside the cell, while little is known of how extracellular ATP triggers these P2X7-mediated metabolic effects. In this study, the stimulatory effects of exogenously applied ATP on metabolic activity and the associated morphological changes in cells in relation to the P2X7 receptor were explored using the multiparametric cytosensor system for a deeper view inside the cell.

Analysis of cell physiological parameters revealed that ATP-induced metabolic stimulation was detectable. Furthermore, based on signal patterns of the multiparametric cytosensor system, it was possible to detect ATP-induced oxidative stress to cells. Experiments with rodent brain cells that express P2X7 receptors demonstrated similar activation effects. Exploring and elucidating the evident relationship between the P2X7 receptor and extracellular ATP concentrations leads to the hypothesis that high levels of ATP reflect a pathological state and lead to an increase in metabolic activity in the cell.

The third project of this thesis explored liver toxicology and used the multiparametric cytosensor system to detect these adverse effects. The liver plays a pivotal role in the biotransformation and detoxification of drugs and is consequently vulnerable to potential injury as a consequence of significant drug exposure. Drug-induced liver injury (DILI) is of considerable concern in drug discovery and development, placing emphasis on the need for predictive *in vitro* technologies that identify potential hepatotoxic side effects of drugs. A label-free, real-time, multiparametric cytosensor system has therefore been established for *in vitro* assessment of drug-induced toxicity. The system is based on monitoring cellular respiration, metabolic activity, cell morphology, and adhesion of human hepatocarcinoma-derived HepG2 cells. The read-out derived from the multiparametric cytosensor system has been optimised and permits sensitive, reliable, and simultaneous recording of cell physiological signals, such as metabolic activity, cellular respiration and morphological changes, and cell adhesion upon exposure to a drug.

Analysis of eight prototypic reference drugs revealed distinct patterns of drug-induced physiological signals. Effects proved to be rigidly concentration-dependent. Based on signal patterns and reversibility of the observed effects, compounds were able to be classified as triggering mechanisms of oxidative or metabolic stress or as leading to cell death (necrosis-like and apoptosis-like). A test-flag-risk mitigation strategy is proposed to address potential risks for drug-induced hepatotoxicity.

Concluding all three projects, the general concept of monitoring the physiological parameters of cells with an *in vitro* technology to overcome obstacles in drug research has clearly been shown to be viable. It was possible to develop a successful, novel assay for reliable, real-time, label-free identification of potential drug-drug interactions based on the identification of P-glycoprotein transporter substrates. Furthermore, the pharmacology of

the purinergic P2X7 receptor after application of extracellular ATP was characterised and, finally and importantly, drug-induced liver effects were detected by on-line monitoring of liver HepG2 cells exposed to drugs.



## 8 BIBLIOGRAPHY

1. Campillos, M, Kuhn, M, Gavin, AC, Jensen, LJ & Bork, P: Drug target identification using side-effect similarity. *Science*, 321: 263-6, 2008.
2. Blake, DA, Junyi Ma, MD & Jia-Qiang, H: Identifying Cardiotoxic Compounds. *Genetic Engineering & Biotechnology News*, 29, 2009.
3. Adams, CP & Brantner, VV: Estimating the cost of new drug development: is it really 802 million dollars? *Health Aff (Millwood)*, 25: 420-8, 2006.
4. DiMasi, JA: The value of improving the productivity of the drug development process: faster times and better decisions. *Pharmacoeconomics*, 20 Suppl 3: 1-10, 2002.
5. Stratmann, HG: Bad Medicine: When Medical Research Goes Wrong. *Analog Science Ficton and Fact*, CXXX, 2010.
6. Qato, DM, Alexander, GC, Conti, RM, Johnson, M, Schumm, P & Lindau, ST: Use of Prescription and Over-the-counter Medications and Dietary Supplements Among Older Adults in the United States. *JAMA: The Journal of the American Medical Association*, 300: 2867-2878, 2008.
7. Haider, SI, Johnell, K, Thorslund, M & Fastbom, J: Trends in polypharmacy and potential drug-drug interactions across educational groups in elderly patients in Sweden for the period 1992 - 2002. *Int J Clin Pharmacol Ther*, 45: 643-53, 2007.
8. Haider, SI, Johnell, K, Weitoft, GR, Thorslund, M & Fastbom, J: The influence of educational level on polypharmacy and inappropriate drug use: a register-based study of more than 600,000 older people. *J Am Geriatr Soc*, 57: 62-9, 2009.
9. Muller, F & Fromm, MF: Transporter-mediated drug-drug interactions. *Pharmacogenomics*, 12: 1017-37, 2011.
10. Ho, RH & Kim, RB: Transporters and drug therapy: implications for drug disposition and disease. *Clin Pharmacol Ther*, 78: 260-77, 2005.
11. Shitara, Y, Sato, H & Sugiyama, Y: Evaluation of drug-drug interaction in the hepatobiliary and renal transport of drugs. *Annu Rev Pharmacol Toxicol*, 45: 689-723, 2005.
12. Stieger, B, Fattinger, K, Madon, J, Kullak-Ublick, GA & Meier, PJ: Drug- and estrogen-induced cholestasis through inhibition of the hepatocellular bile salt export pump (Bsep) of rat liver. *Gastroenterology*, 118: 422-30, 2000.
13. Hamman, MA, Bruce, MA, Haehner-Daniels, BD & Hall, SD: The effect of rifampin administration on the disposition of fexofenadine. *Clin Pharmacol Ther*, 69: 114-21, 2001.
14. Greiner, B, Eichelbaum, M, Fritz, P, Kreichgauer, HP, von Richter, O, Zundler, J & Kroemer, HK: The role of intestinal P-glycoprotein in the interaction of digoxin and rifampin. *J Clin Invest*, 104: 147-53, 1999.
15. Cvetkovic, M, Leake, B, Fromm, MF, Wilkinson, GR & Kim, RB: OATP and P-glycoprotein transporters mediate the cellular uptake and excretion of fexofenadine. *Drug Metab Dispos*, 27: 866-71, 1999.
16. Vaidyanathan, S, Camenisch, G, Schuetz, H, Reynolds, C, Yeh, CM, Bizot, MN, Dieterich, HA, Howard, D & Dole, WP: Pharmacokinetics of the oral direct renin inhibitor aliskiren in combination with digoxin, atorvastatin, and ketoconazole in healthy subjects: the

- role of P-glycoprotein in the disposition of aliskiren. *J Clin Pharmacol*, 48: 1323-38, 2008.
17. Thiebaut, F, Tsuruo, T, Hamada, H, Gottesman, MM, Pastan, I & Willingham, MC: Cellular localization of the multidrug-resistance gene product P-glycoprotein in normal human tissues. *Proc Natl Acad Sci U S A*, 84: 7735-8, 1987.
  18. Drescher, S, Glaeser, H, Murdter, T, Hitzl, M, Eichelbaum, M & Fromm, MF: P-glycoprotein-mediated intestinal and biliary digoxin transport in humans. *Clin Pharmacol Ther*, 73: 223-31, 2003.
  19. Fromm, MF, Kim, RB, Stein, CM, Wilkinson, GR & Roden, DM: Inhibition of P-glycoprotein-mediated drug transport: A unifying mechanism to explain the interaction between digoxin and quinidine [see comments]. *Circulation*, 99: 552-7, 1999.
  20. Eberl, S, Renner, B, Neubert, A, Reisig, M, Bachmakov, I, Konig, J, Dorje, F, Murdter, TE, Ackermann, A, Dormann, H, Gassmann, KG, Hahn, EG, Zierhut, S, Brune, K & Fromm, MF: Role of p-glycoprotein inhibition for drug interactions: evidence from in vitro and pharmacoepidemiological studies. *Clin Pharmacokinet*, 46: 1039-49, 2007.
  21. Chu, XY, Bleasby, K, Yabut, J, Cai, X, Chan, GH, Hafey, MJ, Xu, S, Bergman, AJ, Braun, MP, Dean, DC & Evers, R: Transport of the dipeptidyl peptidase-4 inhibitor sitagliptin by human organic anion transporter 3, organic anion transporting polypeptide 4C1, and multidrug resistance P-glycoprotein. *J Pharmacol Exp Ther*, 321: 673-83, 2007.
  22. Marques-Santos, LF, Bernardo, RR, de Paula, EF & Rumjanek, VM: Cyclosporin A and trifluoperazine, two resistance-modulating agents, increase ivermectin neurotoxicity in mice. *Pharmacol Toxicol*, 84: 125-9, 1999.
  23. Schinkel, AH, Smit, JJ, van Tellingen, O, Beijnen, JH, Wagenaar, E, van Deemter, L, Mol, CA, van der Valk, MA, Robanus-Maandag, EC, te Riele, HP & et al.: Disruption of the mouse *mdr1a* P-glycoprotein gene leads to a deficiency in the blood-brain barrier and to increased sensitivity to drugs. *Cell*, 77: 491-502, 1994.
  24. Center\_for\_Drug\_Evaluation\_and\_Research: Guidance for Industry - Drug Interaction Studies. Silver Spring, MD, US, FDA\_U.S.\_Food\_and\_Drug\_Administration, 2012.
  25. Mertsch, K & Maass, J: Blood-Brain Barrier Penetration and Drug Development from an Industrial Point of View. *Current Medicinal Chemistry*, 2: 15, 2002.
  26. Lespine, A, Dupuy, J, Orlowski, S, Nagy, T, Glavinas, H, Krajcsi, P & Alvinerie, M: Interaction of ivermectin with multidrug resistance proteins (MRP1, 2 and 3). *Chem Biol Interact*, 159: 169-79, 2006.
  27. Jones, PM & George, AM: The ABC transporter structure and mechanism: perspectives on recent research. *Cell Mol Life Sci*, 61: 682-99, 2004.
  28. Gottesman, MM & Ambudkar, SV: Overview: ABC transporters and human disease. *J Bioenerg Biomembr*, 33: 453-8, 2001.
  29. Litman, T, Druley, TE, Stein, WD & Bates, SE: From MDR to MXR: new understanding of multidrug resistance systems, their properties and clinical significance. *Cell Mol Life Sci*, 58: 931-59, 2001.
  30. McKeegan, KS, Borges-Walmsley, MI & Walmsley, AR: The structure and function of drug pumps: an update. *Trends Microbiol*, 11: 21-9, 2003.
  31. Borges-Walmsley, MI, McKeegan, KS & Walmsley, AR: Structure and function of efflux pumps that confer resistance to drugs. *Biochem J*, 376: 313-38, 2003.
  32. Raviv, Y, Pollard, HB, Bruggemann, EP, Pastan, I & Gottesman, MM: Photosensitized labeling of a functional multidrug transporter in living drug-resistant tumor cells. *J Biol Chem*, 265: 3975-80, 1990.

33. Urbatsch, IL, Sankaran, B, Bhagat, S & Senior, AE: Both P-glycoprotein nucleotide-binding sites are catalytically active. *J Biol Chem*, 270: 26956-61, 1995.
34. Szakacs, G, Paterson, JK, Ludwig, JA, Booth-Genthe, C & Gottesman, MM: Targeting multidrug resistance in cancer. *Nat Rev Drug Discov*, 5: 219-34, 2006.
35. Sauna, ZE & Ambudkar, SV: Characterization of the catalytic cycle of ATP hydrolysis by human P-glycoprotein. The two ATP hydrolysis events in a single catalytic cycle are kinetically similar but affect different functional outcomes. *J Biol Chem*, 276: 11653-61, 2001.
36. Aanismaa, P, Gatlik-Landwojtowicz, E & Seelig, A: P-glycoprotein senses its substrates and the lateral membrane packing density: consequences for the catalytic cycle. *Biochemistry*, 47: 10197-207, 2008.
37. Ambudkar, SV, Cardarelli, CO, Pashinsky, I & Stein, WD: Relation between the turnover number for vinblastine transport and for vinblastine-stimulated ATP hydrolysis by human P-glycoprotein. *J Biol Chem*, 272: 21160-6, 1997.
38. Omote, H & Al-Shawi, MK: A novel electron paramagnetic resonance approach to determine the mechanism of drug transport by P-glycoprotein. *J Biol Chem*, 277: 45688-94, 2002.
39. Schinkel, AH, Wagenaar, E, van Deemter, L, Mol, CA & Borst, P: Absence of the mdr1a P-Glycoprotein in mice affects tissue distribution and pharmacokinetics of dexamethasone, digoxin, and cyclosporin A. *J Clin Invest*, 96: 1698-705, 1995.
40. Schwab, D, Fischer, H, Tabatabaei, A, Poli, S & Huwyler, J: Comparison of in vitro P-glycoprotein screening assays: recommendations for their use in drug discovery. *J Med Chem*, 46: 1716-25, 2003.
41. Eytan, GD, Regev, R, Oren, G, Hurwitz, CD & Assaraf, YG: Efficiency of P-glycoprotein-mediated exclusion of rhodamine dyes from multidrug-resistant cells is determined by their passive transmembrane movement rate. *Eur J Biochem*, 248: 104-12, 1997.
42. Tiberghien, F & Loor, F: Ranking of P-glycoprotein substrates and inhibitors by a calcein-AM fluorometry screening assay. *Anticancer Drugs*, 7: 568-78, 1996.
43. Braun, A, Hammerle, S, Suda, K, Rothen-Rutishauser, B, Gunthert, M, Kramer, SD & Wunderli-Allenspach, H: Cell cultures as tools in biopharmacy. *Eur J Pharm Sci*, 11 Suppl 2: S51-60, 2000.
44. Sarkadi, B, Price, EM, Boucher, RC, Germann, UA & Scarborough, GA: Expression of the human multidrug resistance cDNA in insect cells generates a high activity drug-stimulated membrane ATPase. *J Biol Chem*, 267: 4854-8, 1992.
45. Madsen, U, Krogsgaard-Larsen, P & Liljefors, T: *Textbook of Drug Design and Discovery.*, Washington, DC 2002.
46. FDA\_U.S.\_Food\_and\_Drug\_Administration: NME Drug and New Biologic Approvals. Silver Spring, MD, US, U.S. Dept of Health, 2011.
47. Miska, D: Biotech's twentieth birthday blues. *Nat Rev Drug Discov*, 2: 231-3, 2003.
48. Glassman, RH & Sun, AY: Biotechnology: identifying advances from the hype. *Nat Rev Drug Discov*, 3: 177-83, 2004.
49. Lindsay, MA: Target discovery. *Nat Rev Drug Discov*, 2: 831-8, 2003.
50. Knowles, J & Gromo, G: A guide to drug discovery: Target selection in drug discovery. *Nat Rev Drug Discov*, 2: 63-9, 2003.
51. Sams-Dodd, F: Target-based drug discovery: is something wrong? *Drug Discov Today*, 10: 139-47, 2005.
52. Schmidt, RF & Thews, G: *Human Physiology*, Berlin Heidelberg New York Paris Tokyo, Springer Verlag 1989.

53. Alberts, B, Johnson, A & Lewis, J: *Molecular Biology of the Cell*, New York, US, Garland Science 2002.
54. Schliwa, M: *Molecular Motors*, Weinheim, Germany, Wiley-VCH Verlag GmbH & Co. KGaA 2002.
55. Voet, D & Voet, JG: *Biochemie*, Hoboken NJ, Wiley VCH 1994.
56. Alberts, B, D., B & Johnson, A: *Lehrbuch der Molekularen Zellbiologie*, Hoboken NJ, Wiley-VCH 1999.
57. Beis, I & Newsholme, EA: The contents of adenine nucleotides, phosphagens and some glycolytic intermediates in resting muscles from vertebrates and invertebrates. *Biochem J*, 152: 23-32, 1975.
58. Burnstock, G: Historical review: ATP as a neurotransmitter. *Trends Pharmacol Sci*, 27: 166-76, 2006.
59. Volonte, C, Amadio, S, Cavaliere, F, D'Ambrosi, N, Vacca, F & Bernardi, G: Extracellular ATP and neurodegeneration. *Curr Drug Targets CNS Neurol Disord*, 2: 403-12, 2003.
60. Bardoni, R, Goldstein, PA, Lee, CJ, Gu, JG & MacDermott, AB: ATP P2X receptors mediate fast synaptic transmission in the dorsal horn of the rat spinal cord. *J Neurosci*, 17: 5297-304, 1997.
61. Pankratov, Y, Lalo, U, Verkhratsky, A & North, RA: Vesicular release of ATP at central synapses. *Pflugers Arch*, 452: 589-97, 2006.
62. Eltzschig, HK, Eckle, T, Mager, A, Kuper, N, Karcher, C, Weissmuller, T, Boengler, K, Schulz, R, Robson, SC & Colgan, SP: ATP release from activated neutrophils occurs via connexin 43 and modulates adenosine-dependent endothelial cell function. *Circ Res*, 99: 1100-8, 2006.
63. Sharnez, R, Lathia, J, Kahlenberg, D, Prabhu, S & Dekleva, M: In situ monitoring of soil dissolution dynamics: a rapid and simple method for determining worst-case soils for cleaning validation. *PDA J Pharm Sci Technol*, 58: 203-14, 2004.
64. Billingsley, KG, Stern, LE, Lowy, AM, Kahlenberg, MS & Thomas, CR, Jr.: Uncommon anal neoplasms. *Surg Oncol Clin N Am*, 13: 375-88, 2004.
65. Rousseau, DL, Jr., Petrelli, NJ & Kahlenberg, MS: Overview of anal cancer for the surgeon. *Surg Oncol Clin N Am*, 13: 249-62, 2004.
66. Yoon, MJ, Lee, HJ, Kim, JH & Kim, DK: Extracellular ATP induces apoptotic signaling in human monocyte leukemic cells, HL-60 and F-36P. *Arch Pharm Res*, 29: 1032-41, 2006.
67. Cosentino, S, Banfi, C, Burbiel, JC, Luo, H, Tremoli, E & Abbracchio, MP: Cardiomyocyte death induced by ischemic/hypoxic stress is differentially affected by distinct purinergic P2 receptors. *J Cell Mol Med*, 2011.
68. Dawicki, DD, Chatterjee, D, Wyche, J & Rounds, S: Extracellular ATP and adenosine cause apoptosis of pulmonary artery endothelial cells. *Am J Physiol*, 273: L485-94, 1997.
69. Chessell, IP, Michel, AD & Humphrey, PP: Effects of antagonists at the human recombinant P2X7 receptor. *Br J Pharmacol*, 124: 1314-20, 1998.
70. Arbeloa, J, Perez-Samartin, A, Gottlieb, M & Matute, C: P2X7 receptor blockade prevents ATP excitotoxicity in neurons and reduces brain damage after ischemia. *Neurobiol Dis*, 45: 954-61, 2012.
71. Coddou, C, Yan, Z, Obsil, T, Huidobro-Toro, JP & Stojilkovic, SS: Activation and regulation of purinergic P2X receptor channels. *Pharmacol Rev*, 63: 641-83, 2011.
72. Ralevic, V & Burnstock, G: Receptors for purines and pyrimidines. *Pharmacol Rev*, 50: 413-92, 1998.

73. Ferrari, D, Pizzirani, C, Adinolfi, E, Lemoli, RM, Curti, A, Idzko, M, Panther, E & Di Virgilio, F: The P2X7 receptor: a key player in IL-1 processing and release. *J Immunol*, 176: 3877-83, 2006.
74. Armstrong, JN, Brust, TB, Lewis, RG & MacVicar, BA: Activation of presynaptic P2X7-like receptors depresses mossy fiber-CA3 synaptic transmission through p38 mitogen-activated protein kinase. *J Neurosci*, 22: 5938-45, 2002.
75. Surprenant, A: Functional properties of native and cloned P2X receptors. *Ciba Found Symp*, 198: 208-19; discussion 219-22, 1996.
76. Buisman, HP, Steinberg, TH, Fischbarg, J, Silverstein, SC, Vogelzang, SA, Ince, C, Ypey, DL & Leijh, PC: Extracellular ATP induces a large nonselective conductance in macrophage plasma membranes. *Proc Natl Acad Sci U S A*, 85: 7988-92, 1988.
77. Ferrari, D, Chiozzi, P, Falzoni, S, Dal Susino, M, Collo, G, Buell, G & Di Virgilio, F: ATP-mediated cytotoxicity in microglial cells. *Neuropharmacology*, 36: 1295-301, 1997.
78. Labasi, JM, Petrushova, N, Donovan, C, McCurdy, S, Lira, P, Payette, MM, Brissette, W, Wicks, JR, Audoly, L & Gabel, CA: Absence of the P2X7 receptor alters leukocyte function and attenuates an inflammatory response. *J Immunol*, 168: 6436-45, 2002.
79. Donnelly-Roberts, DL, Namovic, MT, Faltynek, CR & Jarvis, MF: Mitogen-activated protein kinase and caspase signaling pathways are required for P2X7 receptor (P2X7R)-induced pore formation in human THP-1 cells. *J Pharmacol Exp Ther*, 308: 1053-61, 2004.
80. North, RA: Molecular Physiology of P2X Receptors. *Physiological Reviews*, 82: 1013-1067, 2002.
81. Chiozzi, P, Sanz, JM, Ferrari, D, Falzoni, S, Aleotti, A, Buell, GN, Collo, G & Di Virgilio, F: Spontaneous cell fusion in macrophage cultures expressing high levels of the P2Z/P2X7 receptor. *J Cell Biol*, 138: 697-706, 1997.
82. Surprenant, A, Rassendren, F, Kawashima, E, North, RA & Buell, G: The cytolytic P2Z receptor for extracellular ATP identified as a P2X receptor (P2X7). *Science*, 272: 735-8, 1996.
83. Egan, TM, Samways, DS & Li, Z: Biophysics of P2X receptors. *Pflugers Arch*, 452: 501-12, 2006.
84. Ferrari, D, Chiozzi, P, Falzoni, S, Hanau, S & Di Virgilio, F: Purinergic modulation of interleukin-1 beta release from microglial cells stimulated with bacterial endotoxin. *J Exp Med*, 185: 579-82, 1997.
85. Smith, DA & Schmid, EF: Drug withdrawals and the lessons within. *Curr Opin Drug Discov Devel*, 9: 38-46, 2006.
86. Davies, DM: Pheochromocytoma and adverse drug reactions. *Adverse Drug React Acute Poisoning Rev*, 6: 91-110, 1987.
87. Pirmohamed, M, Breckenridge, AM, Kitteringham, NR & Park, BK: Adverse drug reactions. *BMJ*, 316: 1295-8, 1998.
88. Graham, DJ, Green, L, Senior, JR & Nourjah, P: Troglitazone-induced liver failure: a case study. *Am J Med*, 114: 299-306, 2003.
89. Watkins, PB & Whitcomb, RW: Hepatic dysfunction associated with troglitazone. *N Engl J Med*, 338: 916-7, 1998.
90. David, S & Hamilton, JP: Drug-induced Liver Injury. *US Gastroenterol Hepatol Rev*, 6: 73-80, 2010.
91. Fromenty, B & Pessayre, D: Inhibition of mitochondrial beta-oxidation as a mechanism of hepatotoxicity. *Pharmacol Ther*, 67: 101-54, 1995.

92. Jaeschke, H, Gores, GJ, Cederbaum, AI, Hinson, JA, Pessayre, D & Lemasters, JJ: Mechanisms of Hepatotoxicity. *Toxicological Sciences*, 65: 166-176, 2002.
93. Berson, A, Renault, S, Letteron, P, Robin, MA, Fromenty, B, Fau, D, Le Bot, MA, Riche, C, Durand-Schneider, AM, Feldmann, G & Pessayre, D: Uncoupling of rat and human mitochondria: a possible explanation for tacrine-induced liver dysfunction. *Gastroenterology*, 110: 1878-90, 1996.
94. Setzer, B, Lebrecht, D & Walker, UA: Pyrimidine nucleoside depletion sensitizes to the mitochondrial hepatotoxicity of the reverse transcriptase inhibitor stavudine. *Am J Pathol*, 172: 681-90, 2008.
95. Lee, AU & Farrell, GC: Mechanism of azathioprine-induced injury to hepatocytes: roles of glutathione depletion and mitochondrial injury. *J Hepatol*, 35: 756-64, 2001.
96. Leist, M, Single, B, Castoldi, AF, Kuhnle, S & Nicotera, P: Intracellular adenosine triphosphate (ATP) concentration: a switch in the decision between apoptosis and necrosis. *J Exp Med*, 185: 1481-6, 1997.
97. Weinshilboum, R: Inheritance and drug response. *N Engl J Med*, 348: 529-37, 2003.
98. Guengerich, FP: Cytochrome P450s and other enzymes in drug metabolism and toxicity. *AAPS J*, 8: E101-11, 2006.
99. Guengerich, FP: Common and uncommon cytochrome P450 reactions related to metabolism and chemical toxicity. *Chem Res Toxicol*, 14: 611-50, 2001.
100. Zimmerman, HJ & Maddrey, WC: Acetaminophen (paracetamol) hepatotoxicity with regular intake of alcohol: analysis of instances of therapeutic misadventure. *Hepatology*, 22: 767-73, 1995.
101. Liss, G & Lewis, JH: Drug-induced liver injury: what was new in 2008? *Expert Opin Drug Metab Toxicol*, 5: 843-60, 2009.
102. Liss, G, Rattan, S & Lewis, JH: Predicting and preventing acute drug-induced liver injury: what's new in 2010? *Expert Opin Drug Metab Toxicol*, 6: 1047-61, 2010.
103. Liu, Z, Shi, Q, Ding, D, Kelly, R, Fang, H & Tong, W: Translating clinical findings into knowledge in drug safety evaluation--drug induced liver injury prediction system (DILIPS). *PLoS Comput Biol*, 7: e1002310, 2011.
104. Twiner, MJ, Hirst, M, Valenciano, A, Zacharewski, TR & Dixon, SJ: N,N-Dimethylformamide modulates acid extrusion from murine hepatoma cells. *Toxicol Appl Pharmacol*, 153: 143-51, 1998.
105. Löffler, G: *Physiologische Chemie. Lehrbuch der medizinischen Biochemie und Pathobiochemie für Studierende und Ärzte*, Berlin Heidelberg New York Paris Tokyo, Springer Verlag 1990.
106. Porter, RK & Brand, MD: Mitochondrial proton conductance and H<sup>+</sup>/O ratio are independent of electron transport rate in isolated hepatocytes. *Biochem J*, 310 ( Pt 2): 379-82, 1995.
107. Rich, PR: The molecular machinery of Keilin's respiratory chain. *Biochem Soc Trans*, 31: 1095-105, 2003.
108. Thedinga, E, Kob, A, Holst, H, Keuer, A, Drechsler, S, Niendorf, R, Baumann, W, Freund, I, Lehmann, M & Ehret, R: Online monitoring of cell metabolism for studying pharmacodynamic effects. *Toxicol Appl Pharmacol*, 220: 33-44, 2007.
109. Ehret, R, Baumann, W, Brischwein, M, Schwinde, A & Wolf, B: On-line control of cellular adhesion with impedance measurements using interdigitated electrode structures. *Med Biol Eng Comput*, 36: 365-70, 1998.

110. Seeland, S, Treiber, A, Hafner, M & Huwyler, J: On-line identification of P-glycoprotein substrates by monitoring of extracellular acidification and respiration rates in living cells. *Biochim Biophys Acta*, 1808: 1827-31, 2011.
111. Guillouzo, A, Corlu, A, Aninat, C, Glaise, D, Morel, F & Guguen-Guillouzo, C: The human hepatoma HepaRG cells: a highly differentiated model for studies of liver metabolism and toxicity of xenobiotics. *Chem Biol Interact*, 168: 66-73, 2007.
112. Wilkening, S, Stahl, F & Bader, A: Comparison of primary human hepatocytes and hepatoma cell line Hepg2 with regard to their biotransformation properties. *Drug Metab Dispos*, 31: 1035-42, 2003.
113. Roe, AL, Snawder, JE, Benson, RW, Roberts, DW & Casciano, DA: HepG2 cells: an in vitro model for P450-dependent metabolism of acetaminophen. *Biochem Biophys Res Commun*, 190: 15-9, 1993.
114. Fabre, G, Julian, B, Saint-Aubert, B, Joyeux, H & Berger, Y: Evidence for CYP3A-mediated N-deethylation of amiodarone in human liver microsomal fractions. *Drug Metab Dispos*, 21: 978-85, 1993.
115. Trivier, JM, Libersa, C, Belloc, C & Lhermitte, M: Amiodarone N-deethylation in human liver microsomes: involvement of cytochrome P450 3A enzymes (first report). *Life Sci*, 52: PL91-6, 1993.
116. Wilson, DE & Chosewood, LC: *Biosafety in Microbiological and Biomedical Laboratories 5th Edition*, CreateSpace 2009.
117. Hoffman, MM, Wei, LY & Roepe, PD: Are altered pH<sub>i</sub> and membrane potential in hu MDR 1 transfectants sufficient to cause MDR protein-mediated multidrug resistance? *J Gen Physiol*, 108: 295-313, 1996.
118. Polli, JW, Wring, SA, Humphreys, JE, Huang, L, Morgan, JB, Webster, LO & Serabjit-Singh, CS: Rational use of in vitro P-glycoprotein assays in drug discovery. *J Pharmacol Exp Ther*, 299: 620-8, 2001.
119. Van Summeren, A, Renes, J, Bouwman, FG, Noben, J-P, van Delft, JHM, Kleinjans, JCS & Mariman, ECM: Proteomics Investigations of Drug-Induced Hepatotoxicity in HepG2 Cells. *Toxicological Sciences*, 120: 109-122, 2011.
120. Michel, AD, Chessell, IP, Hibell, AD, Simon, J & Humphrey, PP: Identification and characterization of an endogenous P2X7 (P2Z) receptor in CHO-K1 cells. *Br J Pharmacol*, 125: 1194-201, 1998.
121. Rassendren, F, Buell, GN, Virginio, C, Collo, G, North, RA & Surprenant, A: The permeabilizing ATP receptor, P2X7. Cloning and expression of a human cDNA. *J Biol Chem*, 272: 5482-6, 1997.
122. Hamill, OP, Marty, A, Neher, E, Sakmann, B & Sigworth, FJ: Improved patch-clamp techniques for high-resolution current recording from cells and cell-free membrane patches. *Pflugers Arch*, 391: 85-100, 1981.
123. Farmer, SR, Wan, KM, Ben-Ze'ev, A & Penman, S: Regulation of actin mRNA levels and translation responds to changes in cell configuration. *Mol Cell Biol*, 3: 182-9, 1983.
124. Spoelstra, EC, Westerhoff, HV, Pinedo, HM, Dekker, H & Lankelma, J: The multidrug-resistance-reverser verapamil interferes with cellular P-glycoprotein-mediated pumping of daunorubicin as a non-competing substrate. *Eur J Biochem*, 221: 363-73, 1994.
125. Smetanova, L, Stetinova, V, Kholova, D, Kvetina, J, Smetana, J & Svoboda, Z: Caco-2 cells and Biopharmaceutics Classification System (BCS) for prediction of transepithelial transport of xenobiotics (model drug: caffeine). *Neuro Endocrinol Lett*, 30 Suppl 1: 101-5, 2009.

126. Giorgio, M, Trinei, M, Migliaccio, E & Pelicci, PG: Hydrogen peroxide: a metabolic by-product or a common mediator of ageing signals? *Nat Rev Mol Cell Biol*, 8: 722-8, 2007.
127. Baraldi, PG, del Carmen Nunez, M, Morelli, A, Falzoni, S, Di Virgilio, F & Romagnoli, R: Synthesis and biological activity of N-arylpiperazine-modified analogues of KN-62, a potent antagonist of the purinergic P2X7 receptor. *J Med Chem*, 46: 1318-29, 2003.
128. Pfeiffer, ZA, Aga, M, Prabhu, U, Watters, JJ, Hall, DJ & Bertics, PJ: The nucleotide receptor P2X7 mediates actin reorganization and membrane blebbing in RAW 264.7 macrophages via p38 MAP kinase and Rho. *J Leukoc Biol*, 75: 1173-82, 2004.
129. el-Azab, G, Youssef, MK, Higashi, Y, Murakami, T & Yata, N: Acetaminophen plasma level after oral administration in liver cirrhotic patients suffering from schistosomal infection. *Int J Clin Pharmacol Ther*, 34: 299-303, 1996.
130. Stocker, ME & Montgomery, JE: Serum paracetamol concentrations in adult volunteers following rectal administration. *British Journal of Anaesthesia*, 87: 638-640, 2001.
131. Kumari, A & Kakkar, P: Lupeol protects against acetaminophen-induced oxidative stress and cell death in rat primary hepatocytes. *Food Chem Toxicol*, 2012.
132. Leung, L, Kalgutkar, AS & Obach, RS: Metabolic activation in drug-induced liver injury. *Drug Metab Rev*, 2011.
133. Zhou, S, Chan, E, Duan, W, Huang, M & Chen, YZ: Drug bioactivation, covalent binding to target proteins and toxicity relevance. *Drug Metab Rev*, 37: 41-213, 2005.
134. Meng, X, Mojaverian, P, Doedee, M, Lin, E, Weinryb, I, Chiang, ST & Kowey, PR: Bioavailability of amiodarone tablets administered with and without food in healthy subjects. *Am J Cardiol*, 87: 432-5, 2001.
135. Fromenty, B, Fisch, C, Berson, A, Letteron, P, Larrey, D & Pessayre, D: Dual effect of amiodarone on mitochondrial respiration. Initial protonophoric uncoupling effect followed by inhibition of the respiratory chain at the levels of complex I and complex II. *J Pharmacol Exp Ther*, 255: 1377-84, 1990.
136. Fromenty, B, Fisch, C, Labbe, G, Degott, C, Deschamps, D, Berson, A, Letteron, P & Pessayre, D: Amiodarone inhibits the mitochondrial beta-oxidation of fatty acids and produces microvesicular steatosis of the liver in mice. *J Pharmacol Exp Ther*, 255: 1371-6, 1990.
137. Kim, IY, Kang, YJ, Yoon, MJ, Kim, EH, Kim, SU, Kwon, TK, Kim, IA & Choi, KS: Amiodarone sensitizes human glioma cells but not astrocytes to TRAIL-induced apoptosis via CHOP-mediated DR5 upregulation. *Neuro Oncol*, 13: 267-79, 2011.
138. Grant, D, Kneteman, N, Tchervenkov, J, Roy, A, Murphy, G, Tan, A, Hendricks, L, Guilbault, N & Levy, G: Peak cyclosporine levels (C<sub>max</sub>) correlate with freedom from liver graft rejection: results of a prospective, randomized comparison of neoral and sandimmune for liver transplantation (NOF-8). *Transplantation*, 67: 1133-7, 1999.
139. Speth, PA, van Hoesel, QG & Haanen, C: Clinical pharmacokinetics of doxorubicin. *Clin Pharmacokinet*, 15: 15-31, 1988.
140. King, PD & Perry, MC: Hepatotoxicity of Chemotherapy. *The Oncologist*, 6: 162-176, 2001.
141. Ye, N, Qin, J, Liu, X, Shi, W & Lin, B: Characterizing doxorubicin-induced apoptosis in HepG2 cells using an integrated microfluidic device. *Electrophoresis*, 28: 1146-53, 2007.
142. McIlleron, H, Wash, P, Burger, A, Norman, J, Folb, PI & Smith, P: Determinants of rifampin, isoniazid, pyrazinamide, and ethambutol pharmacokinetics in a cohort of tuberculosis patients. *Antimicrob Agents Chemother*, 50: 1170-7, 2006.



143. Bhadauria, S, Singh, G, Sinha, N & Srivastava, S: Isoniazid induces oxidative stress, mitochondrial dysfunction and apoptosis in Hep G2 cells. *Cell Mol Biol (Noisy-le-grand)*, 53: 102-14, 2007.
144. Bhadauria, S, Mishra, R, Kanchan, R, Tripathi, C, Srivastava, A, Tiwari, A & Sharma, S: Isoniazid-induced apoptosis in HepG2 cells: generation of oxidative stress and Bcl-2 down-regulation. *Toxicol Mech Methods*, 20: 242-51, 2010.
145. Chowdhury, A, Santra, A, Bhattacharjee, K, Ghatak, S, Saha, DR & Dhali, GK: Mitochondrial oxidative stress and permeability transition in isoniazid and rifampicin induced liver injury in mice. *J Hepatol*, 45: 117-26, 2006.
146. Woo, J, Chan, CH, Walubo, A & Chan, KK: Hydrazine--a possible cause of isoniazid--induced hepatic necrosis. *J Med*, 23: 51-9, 1992.
147. Comandone, A, Passera, R, Boglione, A, Tagini, V, Ferrari, S & Cattel, L: High dose methotrexate in adult patients with osteosarcoma: clinical and pharmacokinetic results. *Acta Oncol*, 44: 406-11, 2005.
148. Shiozawa, K, Tanaka, Y, Yoshihara, R, Imura, S, Murata, M, Yamane, T, Miura, Y, Hashiramoto, A & Shiozawa, S: Serum levels and pharmacodynamics of methotrexate and its metabolite 7-hydroxy methotrexate in Japanese patients with rheumatoid arthritis treated with 2-mg capsule of methotrexate three times per week. *Mod Rheumatol*, 15: 405-9, 2005.
149. Cetin, A, Kaynar, L, Kocyigit, I, Hacioglu, SK, Saraymen, R, Ozturk, A, Sari, I & Sagdic, O: Role of grape seed extract on methotrexate induced oxidative stress in rat liver. *Am J Chin Med*, 36: 861-72, 2008.
150. Kaminskas, E & Nussey, AC: Effects of Methotrexate and of Environmental Factors on Glycolysis and Metabolic Energy State In Cultured Ehrlich Ascites Carcinoma Cells. *Cancer Research*, 38: 2989-2996, 1978.
151. Kevat, S, Ahern, M & Hall, P: Hepatotoxicity of methotrexate in rheumatic diseases. *Med Toxicol Adverse Drug Exp*, 3: 197-208, 1988.
152. West, SG: Methotrexate hepatotoxicity. *Rheum Dis Clin North Am*, 23: 883-915, 1997.
153. Hubinont, C, Sener, A & Malaisse, WJ: Sorbitol content of plasma and erythrocytes during induced short-term hyperglycemia. *Clin Biochem*, 14: 19-20, 1981.
154. Clifford, CP, Adams, DA, Murray, S, Taylor, GW, Wilkins, MR, Boobis, AR & Davies, DS: The cardiac effects of terfenadine after inhibition of its metabolism by grapefruit juice. *Eur J Clin Pharmacol*, 52: 311-5, 1997.
155. Nicolau-Galmes, F, Asumendi, A, Alonso-Tejerina, E, Perez-Yarza, G, Jangi, SM, Gardeazabal, J, Arroyo-Berdugo, Y, Careaga, JM, Diaz-Ramon, JL, Apraiz, A & Boyano, MD: Terfenadine induces apoptosis and autophagy in melanoma cells through ROS-dependent and -independent mechanisms. *Apoptosis*, 16: 1253-67, 2011.
156. Jangi, SM, Ruiz-Larrea, MB, Nicolau-Galmes, F, Andollo, N, Arroyo-Berdugo, Y, Ortega-Martinez, I, Diaz-Perez, JL & Boyano, MD: Terfenadine-induced apoptosis in human melanoma cells is mediated through Ca<sup>2+</sup> homeostasis modulation and tyrosine kinase activity, independently of H1 histamine receptors. *Carcinogenesis*, 29: 500-9, 2008.
157. Fisher, C & Broderick, W: Sodium valproate or valproate semisodium: is there a difference in the treatment of bipolar disorder? *Psychiatric Bulletin*, 27: 446-448, 2003.
158. Ji, Q, Shi, X, Lin, R, Mao, Y, Zhai, X, Lin, Q & Zhang, J: Participation of lipid transport and fatty acid metabolism in valproate sodium-induced hepatotoxicity in HepG2 cells. *Toxicol In Vitro*, 24: 1086-91, 2010.

159. Tong, V, Teng, XW, Chang, TK & Abbott, FS: Valproic acid II: effects on oxidative stress, mitochondrial membrane potential, and cytotoxicity in glutathione-depleted rat hepatocytes. *Toxicol Sci*, 86: 436-43, 2005.
160. Lederle, FA: Epidemiology of constipation in elderly patients. Drug utilisation and cost-containment strategies. *Drugs Aging*, 6: 465-9, 1995.
161. Takara, K, Tsujimoto, M, Kokufu, M, Ohnishi, N & Yokoyama, T: Up-regulation of MDR1 function and expression by cisplatin in LLC-PK1 cells. *Biol Pharm Bull*, 26: 205-9, 2003.
162. Gatlik-Landwojtowicz, E, Aanismaa, P & Seelig, A: Quantification and characterization of P-glycoprotein-substrate interactions. *Biochemistry*, 45: 3020-32, 2006.
163. Hyafil, F, Vergely, C, Du Vignaud, P & Grand-Perret, T: In vitro and in vivo reversal of multidrug resistance by GF120918, an acridonecarboxamide derivative. *Cancer Res*, 53: 4595-602, 1993.
164. Martin, C, Berridge, G, Mistry, P, Higgins, C, Charlton, P & Callaghan, R: The molecular interaction of the high affinity reversal agent XR9576 with P-glycoprotein. *Br J Pharmacol*, 128: 403-11, 1999.
165. Landwojtowicz, E, Nervi, P & Seelig, A: Real-time monitoring of P-glycoprotein activation in living cells. *Biochemistry*, 41: 8050-7, 2002.
166. Skaper, SD, Facci, L, Culbert, AA, Evans, NA, Chessell, I, Davis, JB & Richardson, JC: P2X(7) receptors on microglial cells mediate injury to cortical neurons in vitro. *Glia*, 54: 234-42, 2006.
167. Kim, M, Jiang, LH, Wilson, HL, North, RA & Surprenant, A: Proteomic and functional evidence for a P2X7 receptor signalling complex. *EMBO J*, 20: 6347-58, 2001.
168. Gandelman, M, Peluffo, H, Beckman, JS, Cassina, P & Barbeito, L: Extracellular ATP and the P2X7 receptor in astrocyte-mediated motor neuron death: implications for amyotrophic lateral sclerosis. *J Neuroinflammation*, 7: 33, 2010.
169. Hillman, KA, Harada, H, Chan, CM, Townsend-Nicholson, A, Moss, SE, Miyamoto, K, Suketa, Y, Burnstock, G, Unwin, RJ & Dunn, PM: Chicken DT40 cells stably transfected with the rat P2X7 receptor ion channel: a system suitable for the study of purine receptor-mediated cell death. *Biochem Pharmacol*, 66: 415-24, 2003.
170. He, M-L, Zemkova, H, Koshimizu, T-a, Tomic, M & Stojilkovic, SS: Intracellular calcium measurements as a method in studies on activity of purinergic P2X receptor channels. *American Journal of Physiology - Cell Physiology*, 285: C467-C479, 2003.
171. Takenouchi, T, Ogihara, K, Sato, M & Kitani, H: Inhibitory effects of U73122 and U73343 on Ca<sup>2+</sup> influx and pore formation induced by the activation of P2X7 nucleotide receptors in mouse microglial cell line. *Biochim Biophys Acta*, 1726: 177-86, 2005.
172. Donnelly-Roberts, DL, Namovic, MT, Han, P & Jarvis, MF: Mammalian P2X7 receptor pharmacology: comparison of recombinant mouse, rat and human P2X7 receptors. *Br J Pharmacol*, 157: 1203-14, 2009.
173. Olson, H, Betton, G, Robinson, D, Thomas, K, Monro, A, Kolaja, G, Lilly, P, Sanders, J, Sipes, G, Bracken, W, Dorato, M, Van Deun, K, Smith, P, Berger, B & Heller, A: Concordance of the toxicity of pharmaceuticals in humans and in animals. *Regul Toxicol Pharmacol*, 32: 56-67, 2000.
174. Cao, CJ, Mioduszewski, RJ, Menking, DE, Valdes, JJ, Cortes, VI, Eldefrawi, ME & Eldefrawi, AT: Validation of the cytosensor for in vitro cytotoxicity studies. *Toxicol In Vitro*, 11: 285-93, 1997.

175. Westerink, WM & Schoonen, WG: Cytochrome P450 enzyme levels in HepG2 cells and cryopreserved primary human hepatocytes and their induction in HepG2 cells. *Toxicol In Vitro*, 21: 1581-91, 2007.
176. Westerink, WM & Schoonen, WG: Phase II enzyme levels in HepG2 cells and cryopreserved primary human hepatocytes and their induction in HepG2 cells. *Toxicol In Vitro*, 21: 1592-602, 2007.
177. Kiang, TKL, Teng, XW, Karagiozov, S, Surendradoss, J, Chang, TKH & Abbott, FS: Role of Oxidative Metabolism in the Effect of Valproic Acid on Markers of Cell Viability, Necrosis, and Oxidative Stress in Sandwich-Cultured Rat Hepatocytes. *Toxicological Sciences*, 118: 501-509, 2010.
178. Tong, V, Teng, XW, Karagiozov, S, Chang, TK & Abbott, FS: Valproic acid glucuronidation is associated with increases in 15-F2t-isoprostane in rats. *Free Radic Biol Med*, 38: 1471-83, 2005.
179. Tong, V, Teng, XW, Chang, TK & Abbott, FS: Valproic acid I: time course of lipid peroxidation biomarkers, liver toxicity, and valproic acid metabolite levels in rats. *Toxicol Sci*, 86: 427-35, 2005.
180. Noch, E & Khalili, K: Molecular mechanisms of necrosis in glioblastoma: the role of glutamate excitotoxicity. *Cancer Biol Ther*, 8: 1791-7, 2009.
181. Bown, CD, Wang, JF & Young, LT: Increased expression of endoplasmic reticulum stress proteins following chronic valproate treatment of rat C6 glioma cells. *Neuropharmacology*, 39: 2162-9, 2000.
182. Zahno, A, Brecht, K, Morand, R, Maseneni, S, Torok, M, Lindinger, PW & Krahenbuhl, S: The role of CYP3A4 in amiodarone-associated toxicity on HepG2 cells. *Biochem Pharmacol*, 81: 432-41, 2011.
183. Moore, M, Thor, H, Moore, G, Nelson, S, Moldeus, P & Orrenius, S: The toxicity of acetaminophen and N-acetyl-p-benzoquinone imine in isolated hepatocytes is associated with thiol depletion and increased cytosolic Ca<sup>2+</sup>. *J Biol Chem*, 260: 13035-40, 1985.
184. Kumari, A & Kakkar, P: Lupeol prevents acetaminophen-induced in vivo hepatotoxicity by altering the Bax/Bcl-2- and oxidative stress-mediated mitochondrial signaling cascade. *Life Sci*, 2012.
185. Kullak-Ublick, GA, Stieger, B, Hagenbuch, B & Meier, PJ: Hepatic transport of bile salts. *Semin Liver Dis*, 20: 273-92, 2000.
186. Bohme, M, Muller, M, Leier, I, Jedlitschky, G & Keppler, D: Cholestasis caused by inhibition of the adenosine triphosphate-dependent bile salt transport in rat liver. *Gastroenterology*, 107: 255-65, 1994.
187. Lin, Z & Will, Y: Evaluation of drugs with specific organ toxicities in organ-specific cell lines. *Toxicol Sci*, 126: 114-27, 2012.
188. Cooper, AD, Craig, WY, Taniguchi, T & Everson, GT: Characteristics and regulation of bile salt synthesis and secretion by human hepatoma HepG2 cells. *Hepatology*, 20: 1522-31, 1994.
189. Sarich, TC, Adams, SP, Petricca, G & Wright, JM: Inhibition of Isoniazid-Induced Hepatotoxicity in Rabbits by Pretreatment with an Amidase Inhibitor. *Journal of Pharmacology and Experimental Therapeutics*, 289: 695-702, 1999.
190. Gent, WL, Seifart, HI, Parkin, DP, Donald, PR & Lamprecht, JH: Factors in hydrazine formation from isoniazid by paediatric and adult tuberculosis patients. *Eur J Clin Pharmacol*, 43: 131-6, 1992.

- 
191. Patrick, RL & Back, KC: Pathology and Toxicology of Repeated Doses of Hydrazine and 1,1-Dimethyl Hydrazine in Monkeys and Rats. *Ind Med Surg*, 34: 430-5, 1965.
  192. Aithal, GP: Hepatotoxicity related to antirheumatic drugs. *Nat Rev Rheumatol*, 7: 139-50, 2011.
  193. Basseri, S & Austin, RC: ER stress and lipogenesis: a slippery slope toward hepatic steatosis. *Dev Cell*, 15: 795-6, 2008.
  194. Mato, JM & Lu, SC: Homocysteine, the bad thiol. *Hepatology*, 41: 976-9, 2005.
  195. Minotti, G: Reactions of adriamycin with microsomal iron and lipids. *Free Radic Res Commun*, 7: 143-8, 1989.
  196. Minotti, G, Recalcati, S, Mordente, A, Liberi, G, Calafiore, AM, Mancuso, C, Preziosi, P & Cairo, G: The secondary alcohol metabolite of doxorubicin irreversibly inactivates aconitase/iron regulatory protein-1 in cytosolic fractions from human myocardium. *FASEB J*, 12: 541-52, 1998.
  197. Sarda, VA, Pereira, SL & Oliveira, PJ: Drug-induced mitochondrial dysfunction in cardiac and skeletal muscle injury. *Expert Opin Drug Saf*, 7: 129-46, 2008.
  198. Zhou, S, Starkov, A, Froberg, MK, Leino, RL & Wallace, KB: Cumulative and irreversible cardiac mitochondrial dysfunction induced by doxorubicin. *Cancer Res*, 61: 771-7, 2001.

---

## 9 PUBLICATIONS ARISING FROM THIS THESIS

### Publications

Seeland, S, Treiber, A, Hafner, M & Huwyler, J: On-line identification of P-glycoprotein substrates by monitoring of extracellular acidification and respiration rates in living cells. *Biochim Biophys Acta*, 1808: 1827-31, 2011.

Seeland, S, Toeroek, M, Kettiger, H, Treiber, A, Hafner, M & Huwyler, J: A cell-based, multiparametric sensor approach characterises drug-induced cytotoxicity in human liver HepG2 cells. *Toxicological Sciences*, 2012 (submitted for publication).

Seeland, S, Murphy, M, Mosbacher, J, Treiber, A, Giller, J, Kiss, A, Sube, R, Hafner, M & Huwyler, J: Purinergic P2X7 receptor mediates effects of extracellular ATP on cell metabolism. *Pharmacological Research*, 2012 (submitted for publication).

### Poster presentation and award

Seeland, S, Flueeli, A, Treiber, A, Huwyler, J & Hafner, M: Poster: Identification of P-Glycoprotein Substrates by Real-Time Monitoring of Living Cells. *MipTec - European Drug Discovery Event*. Basel 2010, P0113. Poster Prize, 3<sup>rd</sup> prize.

### Communications

Talk: Bionas cytosensor: A reliable and predictive system for the identification of cellular processes. *DMPK Seminar, Actelion Pharmaceutical Ltd, Allschwil, Switzerland*. Allschwil 2009.

Talk: Online identification of P-glycoprotein substrates in living cells by monitoring of extracellular acidification and respiration. *Annual Research Meeting, Department of Pharmaceutical Science, University of Basel*. Basel 2011.

Talk: Identification of P-glycoprotein Substrates by real-time monitoring of living cells. *DMPK Seminar, Actelion Pharmaceutical Ltd, Allschwil, Switzerland*. Allschwil 2011.

## 10 ACKNOWLEDGEMENTS

I would like to thank Dr. Martine Clozel and Dr. Alexander Treiber for granting me the opportunity to do my PhD thesis in the preclinical department at Actelion Pharmaceuticals Ltd, Allschwil, Switzerland. I am grateful for scientific supervision, support, excellent review of my PhD thesis and fruitful discussions during these interesting and challenging projects.

I would like to thank Prof. Dr. Mathias Hafner for being the first supervisor of my PhD thesis. I would like to thank him and Prof. Dr. Jörg Huwyler for being my thesis advisory committee members, for their excellent scientific discussions and interest in my project, and I would also like to thank Prof. Dr. Gert Fricker for joining my doctoral examination committee as an expert.

I am grateful to my laboratory colleagues Sibylle Fläschel, Markus Schäuble, Tommaso Miraval, Ali Selimi and Dr. Thomas Pfeifer for making the laboratory such an enjoyable place to work.

Further, I gratefully acknowledge the support of Dr. Michael Török, Helene Kettiger, Dr. Johannes Mosbacher, Dr. Mark Murphy, Andrea Kiss, Romain Sube, Jasmin Giller, Dr. Christopher Kohl, and Dr. Jérôme Segrestaa for their outstanding assistance and advice in various instances.

Many thanks to Mark Inglin for his excellent editorial assistance.

I would also like to thank Andreas Flüeli for the opportunity to supervise his traineeship and Bachelor thesis (University for Applied Sciences, MuttENZ, Switzerland), which was part of my PhD thesis.

Finally, my biggest thanks go to my wife, Christina Nadine, to my three boys, Lucas Maximilian, Elias Phillip and Johannes Benedikt, and last but not least to my parents for their enormous support, encouragement, and overall patience with me. Thank you for make my life so colourful.